AD-A149 844 MERGING OF NON-CONCENTRIC FIREBALLS(U) MISSION RESEARCH 1/1
CORP SANTA BARBARA CA K COSNER 01 DEC 83 MRC-R-806
DNA-TR-83-49 DNA001-83-C-0127

UNCLASSIFIED F/G 18/3 NL

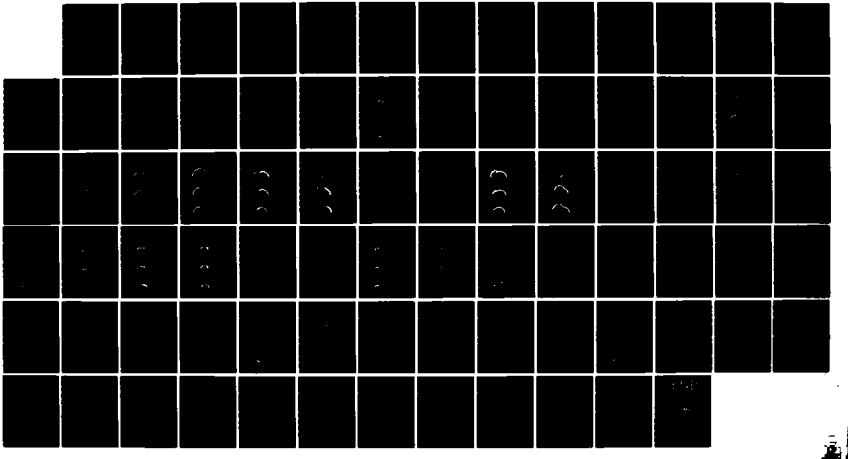

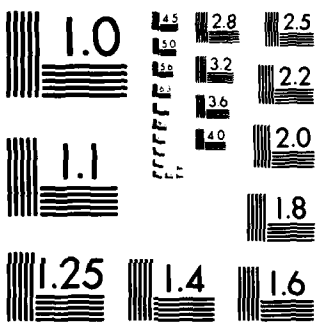

AD-E 301586

(12)

DNA-TR-83-49

MERGING OF NON-CONCENTRIC FIREBALLS

Kenneth Cosner
Mission Research Corporation
P.O. Drawer 719
Santa Barbara, California 93102

1 December 1983

Technical Report

CONTRACT No. DNA 001-83-C-0127

THIS WORK WAS SPONSORED BY THE DEFENSE NUCLEAR AGENCY
UNDER RDT&E RMSS CODE B322083466 S99QMXBI00014 H2590D.

Prepared for
Director
DEFENSE NUCLEAR AGENCY
Washington, DC 20305

Destroy this report when it is no longer needed. Do not return to sender.

PLEASE NOTIFY THE DEFENSE NUCLEAR AGENCY, ATTN: STTI, WASHINGTON, D.C. 20305, IF YOUR ADDRESS IS INCORRECT, IF YOU WISH TO BE DELETED FROM THE DISTRIBUTION LIST, OR IF THE ADDRESSEE IS NO LONGER EMPLOYED BY YOUR ORGANIZATION.

UNCLASSIFIED

SECURITY CLASSIFICATION OF THIS PAGE (When Data Entered)

REPORT DOCUMENTATION PAGE		READ INSTRUCTIONS BEFORE COMPLETING FORM
1. REPORT NUMBER DNA-TR-83-49	2. GOVT ACCESSION NO. AD-A149844	3. RECIPIENT'S CATALOG NUMBER
4. TITLE (and Subtitle) MERGING OF NON-CONCENTRIC FIREBALLS		5. TYPE OF REPORT & PERIOD COVERED Technical Report 6. PERFORMING ORG. REPORT NUMBER MRC-R-806
7. AUTHOR(s) Kenneth Cosner		8. CONTRACT OR GRANT NUMBER(s) DNA 001-83-C-0127
9. PERFORMING ORGANIZATION NAME AND ADDRESS Mission Research Corporation P.O. Drawer 719 Santa Barbara, California 93102		10. PROGRAM ELEMENT, PROJECT, TASK AREA & WORK UNIT NUMBERS Task S99QMXBI-00014
11. CONTROLLING OFFICE NAME AND ADDRESS Director Defense Nuclear Agency Washington, DC 20305		12. REPORT DATE 1 December 1983 13. NUMBER OF PAGES 78
14. MONITORING AGENCY NAME & ADDRESS(if different from Controlling Office)		15. SECURITY CLASS (of this report) UNCLASSIFIED 15a. DECLASSIFICATION/DOWNGRADING SCHEDULE N/A since UNCLASSIFIED

16. DISTRIBUTION STATEMENT (of this Report)

Approved for public release, distribution unlimited, 15 May 1984.

17. DISTRIBUTION STATEMENT (of the abstract entered in Block 20, if different from Report)

18. SUPPLEMENTARY NOTES

This work was sponsored by the Defense Nuclear Agency under RDT&E RMSS Code B322083466 S99QMXBI00014 H2590D.

19. KEY WORDS (Continue on reverse side if necessary and identify by block number)

Radiation-coupled Hydrodynamics
MICE
Fireball
Multiburst
C/LAMP

20. ABSTRACT (Continue on reverse side if necessary and identify by block number)

The MICE radiation hydrodynamics code was used to study low altitude multiple non-concentric megaton bursts to study effects dependent upon burst separation.

DD FORM 1 JAN 73 1473 EDITION OF 1 NOV 65 IS OBSOLETE

UNCLASSIFIED

SECURITY CLASSIFICATION OF THIS PAGE (When Data Entered)

TABLE OF CONTENTS

LIST OF ILLUSTRATIONS

LIST OF ILLUSTRATIONS (Continued)

LIST OF ILLUSTRATIONS (Continued)

LIST OF ILLUSTRATIONS (Continued)

LIST OF ILLUSTRATIONS (Concluded)

SECTION I
INTRODUCTION

One of the goals of the C/LAMP project is to provide a good mode of multiple burst phenomenology. In order to do this, it is necessary to have a corresponding data base. While there have been several calculations of concentric bursts (References 1, 2, 3) and low yield nonconcentric bursts (Reference 4), little has been done for other multiple burst configurations.

The goal of the calculations described in this report is to expand the data base with calculations of non-concentric bursts with a higher yield than past calculations (1 megaton), spanning the regime in which the fireballs are expected to merge, in order to determine the thermal yield as a function of burst separation.

SECTION II
CALCULATION

In the current calculations MICE was run in its low altitude mode using 2-D cylindrical geometry in which radiation and hydrodynamic effects were followed and equilibrium chemistry was used. Hydrodynamic calculations were done using an implicit continuous Eulerian grid.

Radiation used two approximations with one always dominant in any given region. In regions of large optical depth, a diffusion approximation was used, while in regions of small optical depth a free streaming approximation was used. Both approximations are discussed in detail in Reference 1.

Finally, in order to simplify the analysis by removing effects which have nothing to do with multiple bursts, the ground was removed and the atmosphere was allowed to continue smoothly to negative altitudes, thus removing reflected shocks.

The first burst, which was used in all of the calculations, was at an altitude of 2 km and, like all of the bursts studied, was of a generic 1 megaton explosion consisting of 250 kilotons of debris kinetic energy and 750 kilotons of X-ray deposition energy. In order to save time, the development through 0.995 seconds was obtained from a calculation done in 1982 and described in Reference 1. Since that calculation included a ground, it was regridded at 0.995 seconds (before the shock reached the ground) so as to remove the ground.

In all of the calculations, the second detonation occurred 4 seconds after the first and was identical to the first except for location. In this report, all times for calculations involving two bursts are measured from the time of the second burst. The desired separation was achieved by displacing the second bursts directly below the first. Whenever possible, The various calculations will be distinguished by Δz, the separation distance from the first burst.

SECTION III
RESULTS

In all of the cases studied except the concentric case (Δz = 0), asymmetries eventually developed due to the interaction of the fireballs. The density gradient was so steep at the burst point for the cases of Δz = 0.6 km and Δz = 0.7 km, that the initial x-ray deposition was noticeably asymmetric causing an initial temperature distribution that was also asymmetric, as can be seen in Figure 1. Bursts with larger Δz had a relatively constant x-ray deposition, but still eventually developed asymmetries. These asymmetries were due to the variation of shock propagation speeds between the top and bottom of the new fireball when that fireball became sufficiently large that there was a significant variation in density due to the first fireball.

Figure 2 shows the fractional thermal yield of the second burst at 10 seconds as a function of separation distance. As can be seen, the radiated energy varies dramatically with separation. For example, at a separation of 0.6 km, the thermal yield is over 50% greater than that of a single burst - for the concentric case, almost twice. For a separation of 1.2 km, the radiative yield is essentially the same as that radiated by a single burst. As can be seen from the power curves in Figures 3 and 4, quantities related to the radiated power, such as the power output at second maximum, varied much more slowly. And, in fact, these were often within the uncertainty of MICE. Past comparisons with RADFLO calculations have indicated that MICE is better at predicting thermal yield, than the radiated power of any given instant.

Figure 5 shows the thermal yield $\int_0^t P(t')\,dt'$, where P is the power radiated. The fireballs from the multiple bursts radiated more energy at later times than did the single burst. This was due to the larger dimensions of the combined fireball, which increased the average optical depth. In addition, in all cases the majority of the thermal yield came from the merged fireball. In all of the non-concentric cases studied, complete fireball merging occurred between 0.2 and 0.5 seconds - approximately the time of second thermal maximum.

Figure 6 shows the early rise for some selected cases. As expected, all of the dual bursts had larger vertical extents than the single burst case. For bursts with $\Delta z \geq 1.0$ km, the passage of the shock from the second burst caused the first fireball to form a torus and increased the altitude of the top of the combined fireball.

Figures 7 through 54 show the detailed evolution of the six non-concentric dual bursts. The three quantities which are plotted are the density, temperature, and the specific power loss due to radiative cooling. The last quantity is defined as the power loss per gram of material due to radiation escaping the grid. The power less per gram is quite sharply peaked, especially when the fireball is opaque. This sharp gradient can be used to measure the fireball size.

As expected, the fireballs tend to remain spherical during their expansion phase as long as the density of the air through which they are expanding does not vary much over the region of the fireball.

Figures 7 through 12 show the situation at 0.01 seconds, long before merging. At this time, the fireballs are very symmetrical. Even those bursts with small Δz, which started out with unsymmetrical x-ray deposition have become more spherical at this time than they were earlier or will be later.

Figures 13 through 18 show the fireballs at 0.1 seconds, immediately before merging and second thermal maximum. The plots of density (Figures 13 and 14) show how the shocks of the bursts with the smaller Δz have advanced significantly farther into the first fireball than those with larger Δz. In none of the cases could the fireballs be said to have completely merged. The plots for the case with Δz = 0.6 km are done with a different scale than the others.

Figures 19 through 21 show the fireballs at 0.3 seconds. By this time some of the fireball have completely merged. This is also approximately the time of second thermal maximum. If the time at which merging is completed is defined as the time when the shock of the second fireball reaches the far side of the first, then it appears that the fireballs at Δz = 0.6 and 0.7 km have merged, while the one at Δz = 0.8 has almost merged. Fireballs with greater separation are well on their way to completing merging but certainly have not finished the process yet. All of this is most clearly seen in the temperature plots.

During the second thermal maximum -- between approximately 0.3 and 0.5 seconds -- a cooling wave propagates back through the combined fireball. Afterwards, the hottest region is at the position of greatest optical depth -- well within the area originally occupied by the first fireball.

Figures 25 through 30 show the fireballs at 1.0 second. Again, the temperature plots (Figures 27-28) give the best picture of merging. These plots show that by this time all of the fireballs have merged. The cooling plots (Figures 29-30) show that for separation distances greater than 1.0 km, there is a torus forming in the region originally occupied by the first fireball. This is presumably due to the passage of the shock from the second burst. The region occupied by the second fireball shows no sign of torus formation. At this time, the density plots (Figures 25-26) show the relative positions of the shocks. The shock from the second burst has the appearance of coming from the combined fireball, although it has traveled farther from the new fireball than from the old. The first shock may appear to be distorted, but this is due to a distortion of the contours arising from the nonuniformity of the ambient atmosphere and is not a real effect.

Figures 31 through 36 show the situation at 2.0 seconds. The toruses for those cases with Δz of at least 1.0 km have become more obvious and can be distinguished on all three plots -- density, temperature, and radiative cooling.

As Figures 37 through 42 show, the shock toruses for the cases with Δz of at least 1.0 km are well developed by 5.0 seconds. At this time, the shock from the first burst has left the grid. Since the aim of this investigation is to study the fireball, no attempt was made to follow the shock.

Figures 43 through 48 show the situation at 10.0 seconds. At this time, the shock from the second burst has also left the grid. Those fireballs with $\Delta z < 1.0$ km and the lower portions of the fireballs with greater separation are showing the early stages of formation of a rise torus.

Figures 49 through 54 show the fireballs at 20.0 seconds. At this time, all of the fireballs are rising and have formed toruses. It is interesting to note that at 20 seconds, the combined fireballs whose top is at the highest altitude are those which started out with the second burst at the lowest altitude -- thus giving the largest Δz. This was mentioned earlier in this report and is due to the shock from the second burst raising the top of the fireball of the first.

Since in all of the cases studied, the second burst was underneath the first, two toruses are not seen as is the case for some of the dual bursts studied in Reference 4.

COMPARISONS WITH OTHER CALCULATIONS

Taking advantage of the fact that both of the bursts had the same yield, then if a scaled separation distance is defined as $\Delta z/Y^{1/3}$, and scaled separation times as $\Delta t/Y^{1/3}$, then one of the calculations of Reference 4 falls between the current calculations as shown in Table 1.

Table 1. Thermal yields from equal non-concentric bursts.

Y	Δz	Δt(sec)	$\Delta z/Y^{1/3}$	$\Delta t/Y^{1/3}$	Fractional Thermal Yield
1 MT	1200	4.0	120	0.40	0.37
1 MT	1100	4.0	110	0.40	0.40
1 MT	1000	4.0	100	0.40	0.46
5 KT*	150	0.8	88	0.47	0.54
1 MT	800	4.0	80	0.40	0.60
1 MT	700	4.0	70	0.40	0.62
1 MT	600	4.0	60	0.40	0.66

* The 5 KT calculation, in which the second burst was displaced below the first, is from Reference 4.

SECTION IV
CONCLUSIONS

As expected, fractional thermal yield at 10 seconds varies dramatically as a function of separation distance. For $\Delta z \geq 1.2$ km the yield is essentially that of a single burst for the 1 megaton case studied in this investigation.

Also as expected, the initial energy deposition due to X-rays was asymmetric when the second burst occurred in a region of rapidly varying density. In this investigation, this ocurred for Δz near 0.6 km.

Combined fireballs tend to emit more energy at later times. This is due to the larger dimensions of the combined fireball, which in turn increases the average optical depth. In addition, in almost all of the cases studied, the majority of the energy is radiated from the combined fireball. Even for those cases when Δz is large enough that the amount of radiated energy is the same as that from a single burst, a significant fraction of the energy is emitted after the fireballs have merged.

For Δz greater than 1.0 km, the passage of the shock from the second burst causes the first fireball to form a torus and increases the altitude of the top of the combined fireball. No shock torusing effect is evident for the cases utilizing smaller Δz.

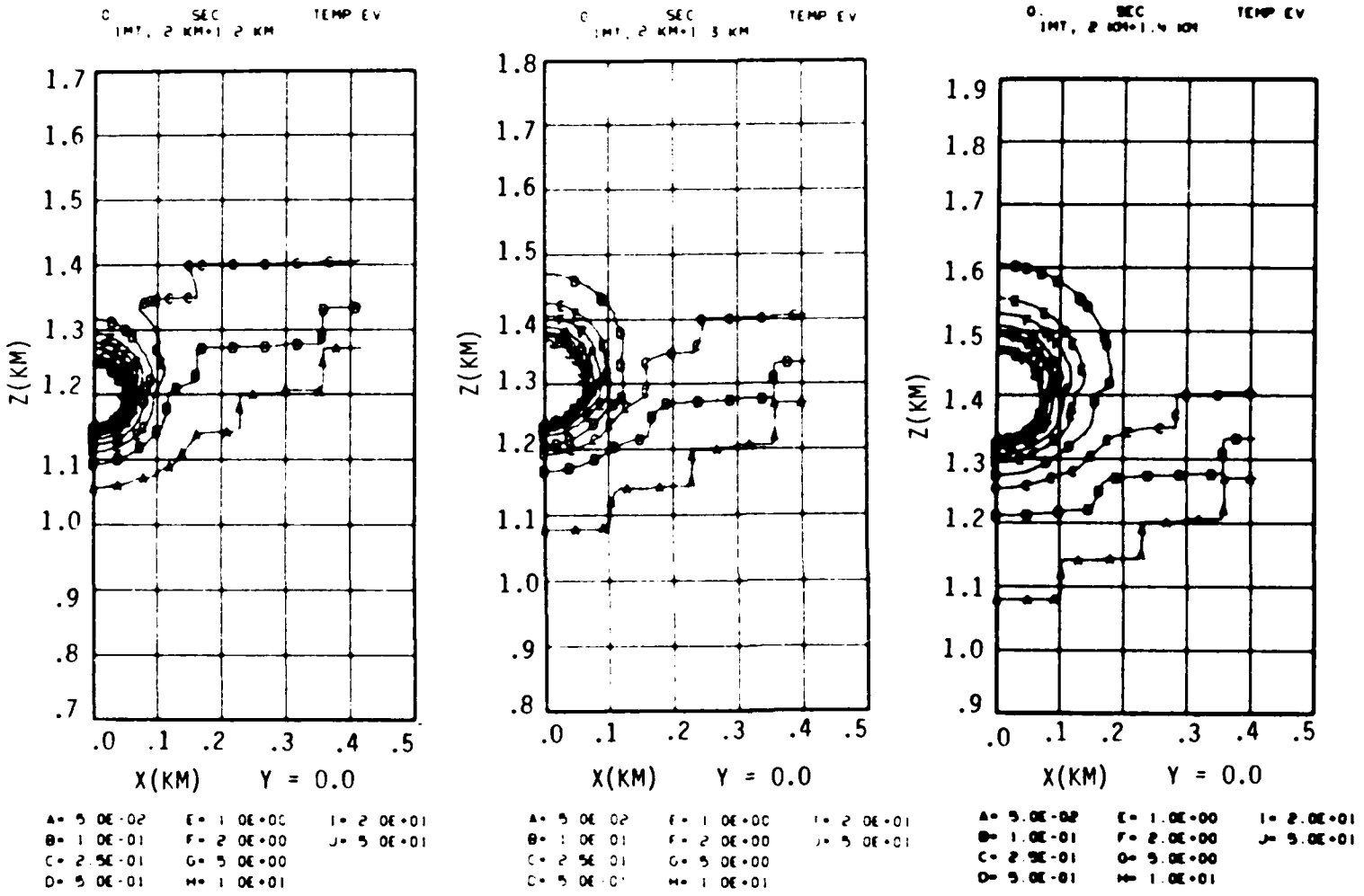

Figure 1. Distribution of temperature immediately after X-ray deposition for Δz = 0.8, 0.7, and 0.6 km showing the asymmetry. The scales are the same for all three.

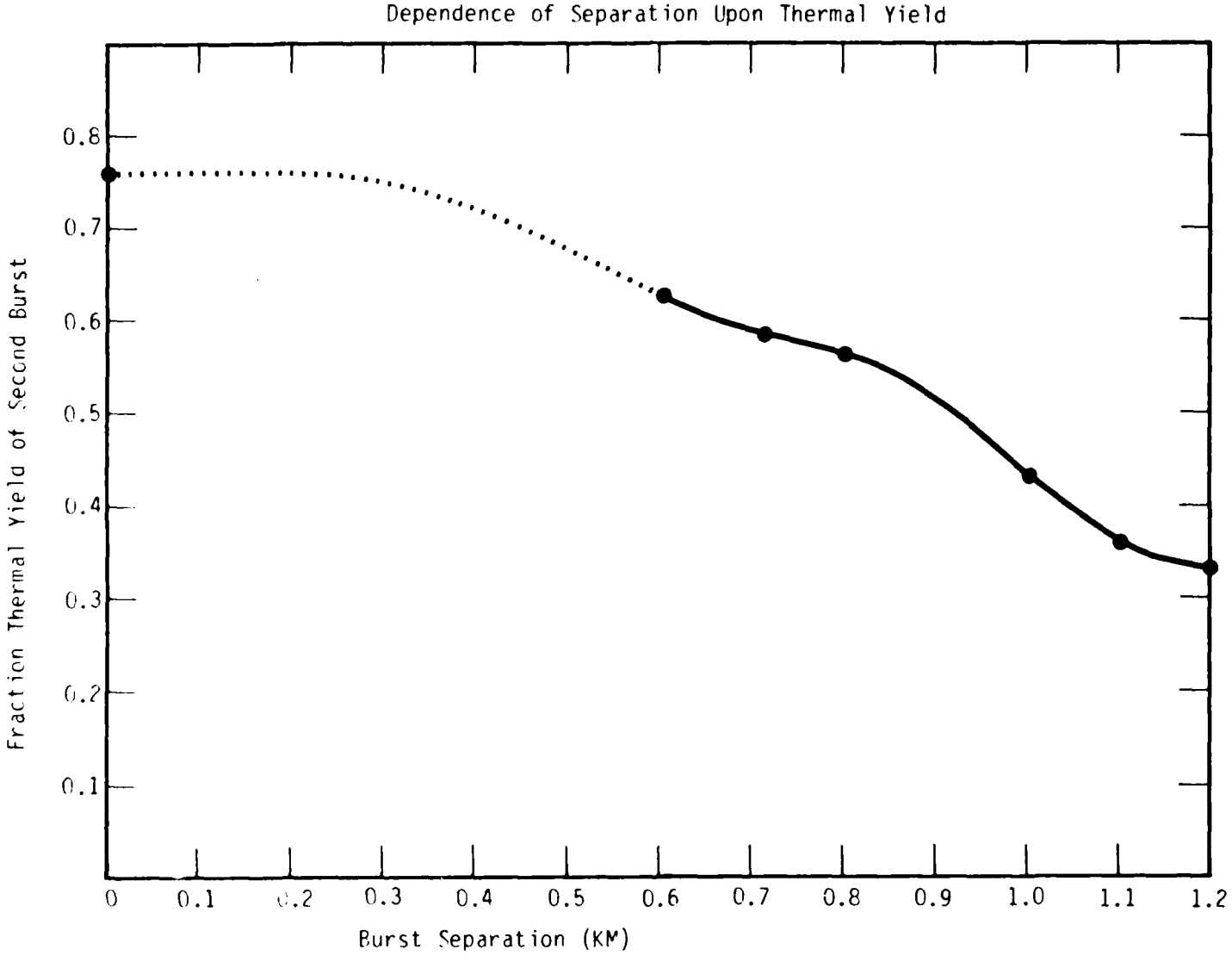

Figure 2. Fraction of the yield of one burst, in the form of thermal radiation by 10 seconds, as a function of burst separation.

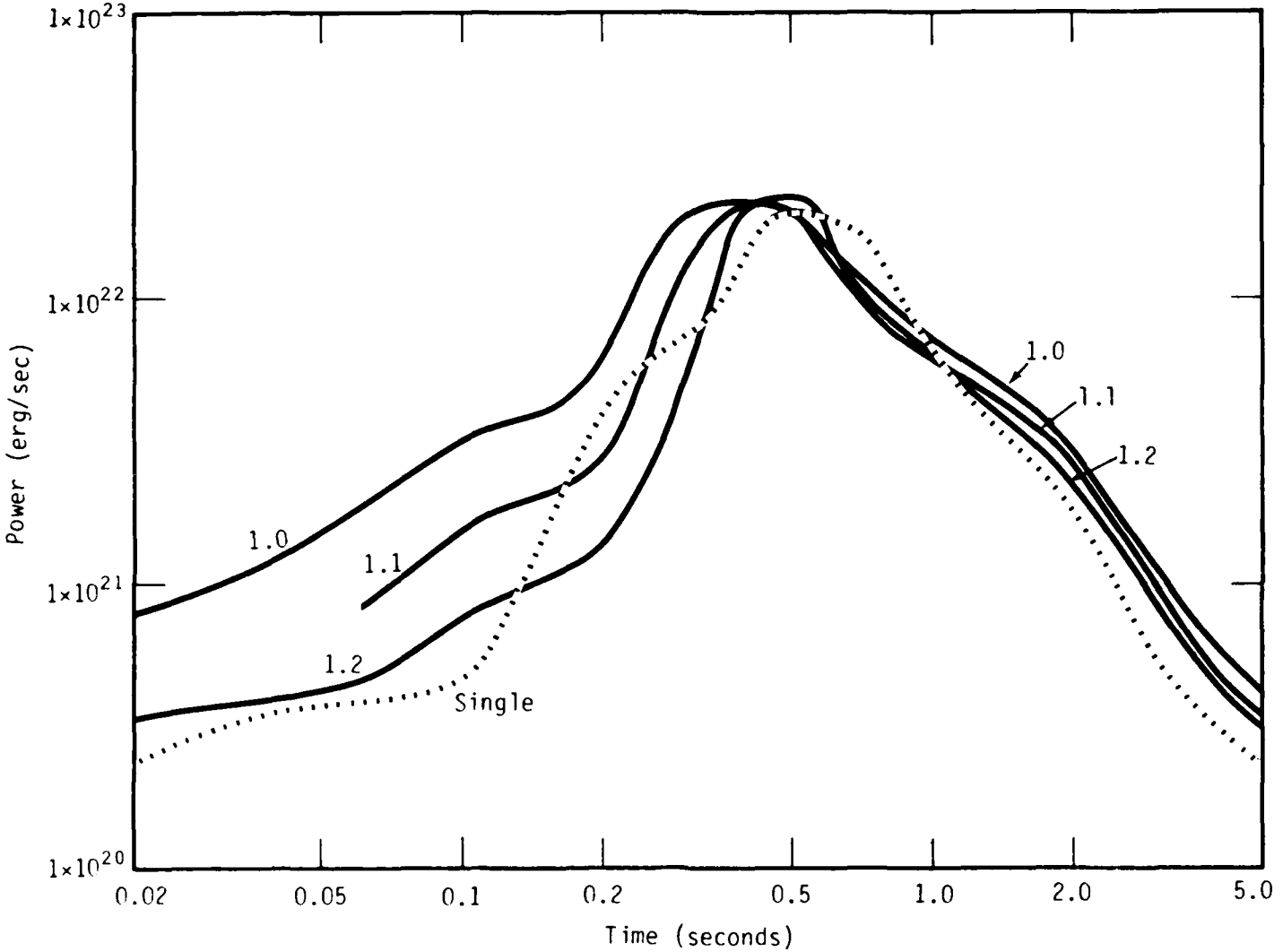

Figure 3. Power curves for Δz = 1.2, 1.1, and 1.0 km (solid lines), and a single burst (dotted line).

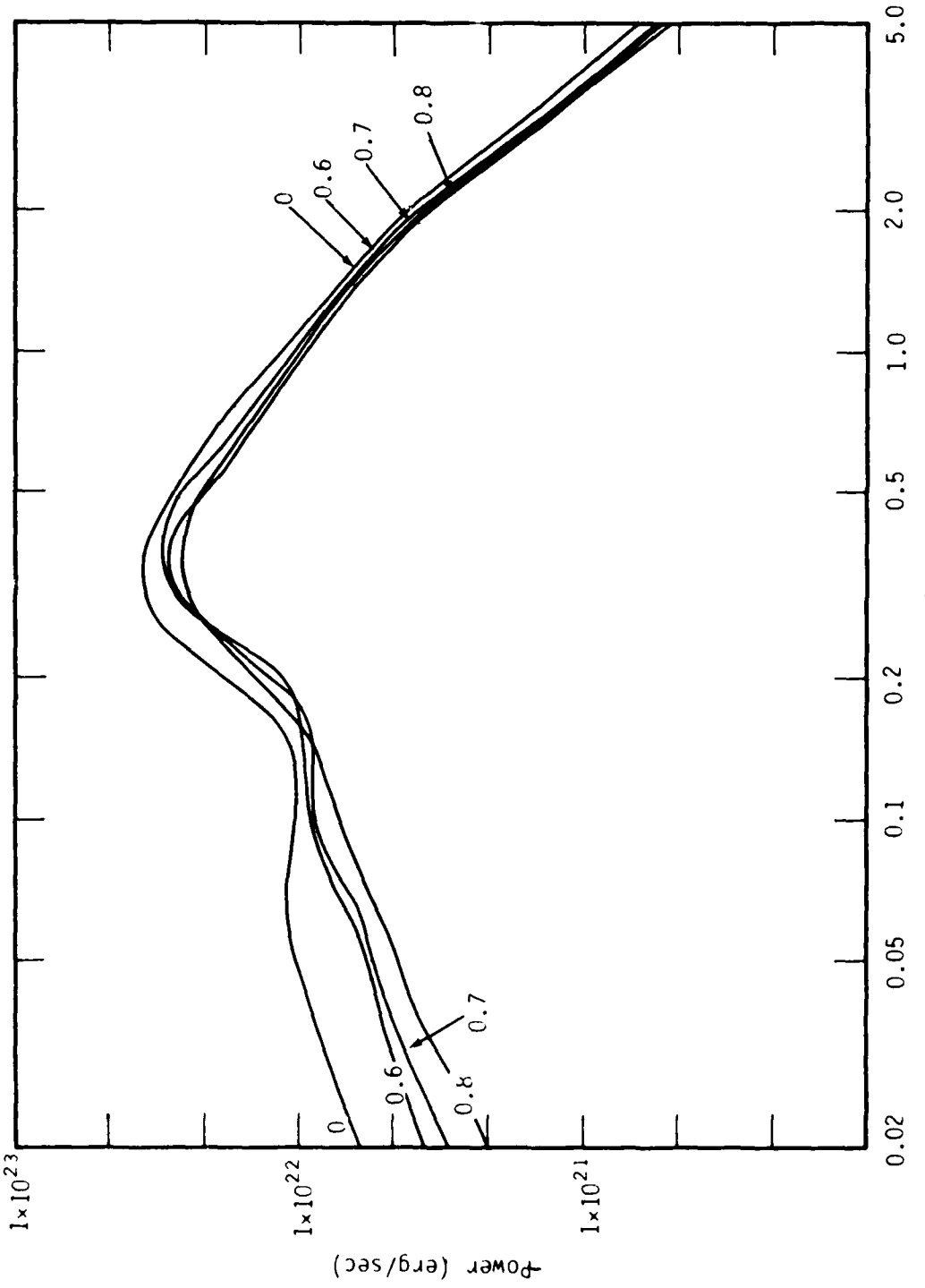

Figure 4. Power curves for Δz = 0, 0.6, 0.7, and 0.8 km.

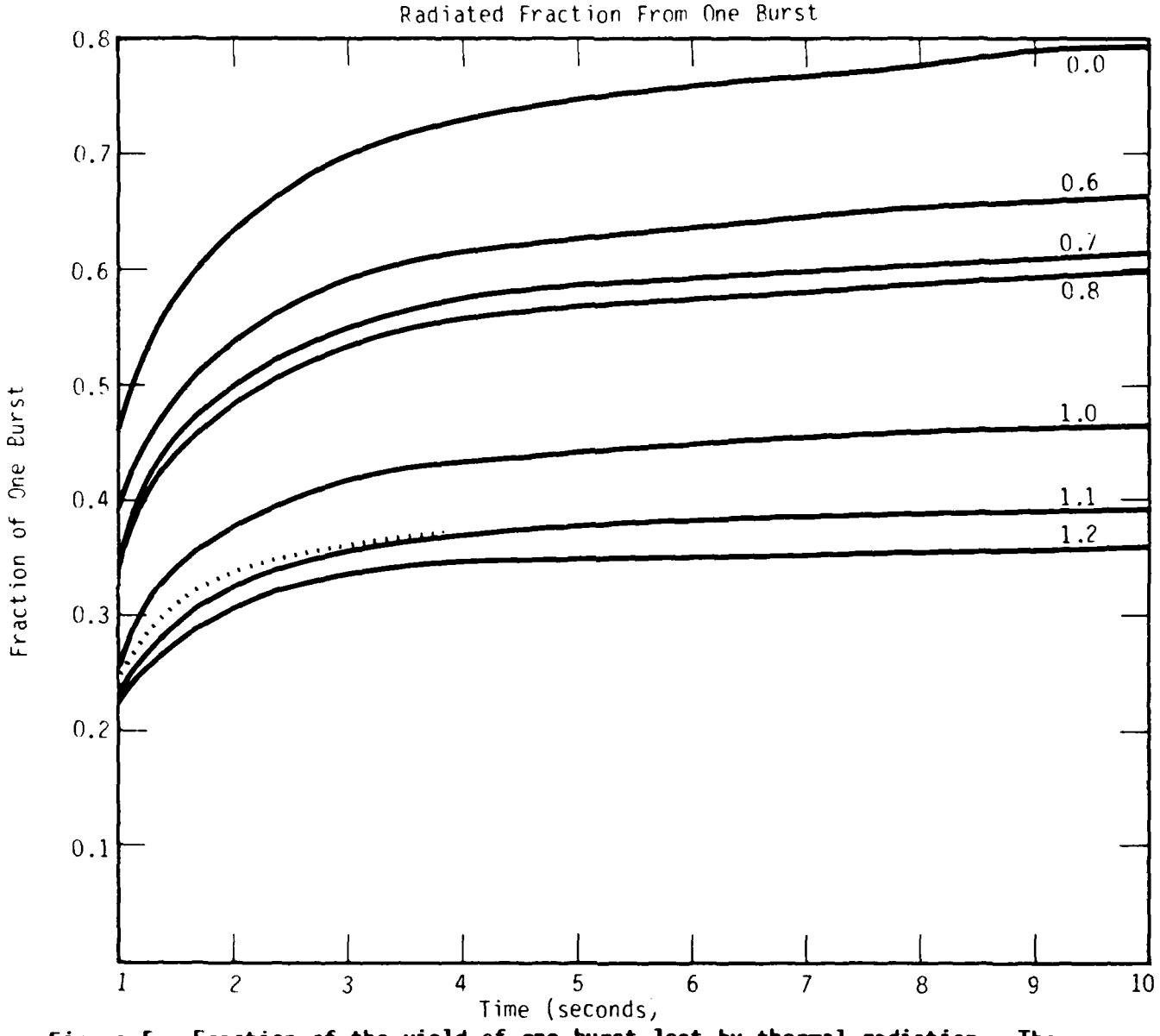

Figure 5. Fraction of the yield of one burst lost by thermal radiation. The labels indicate the value of Δz. Dotted line shows single burst case.

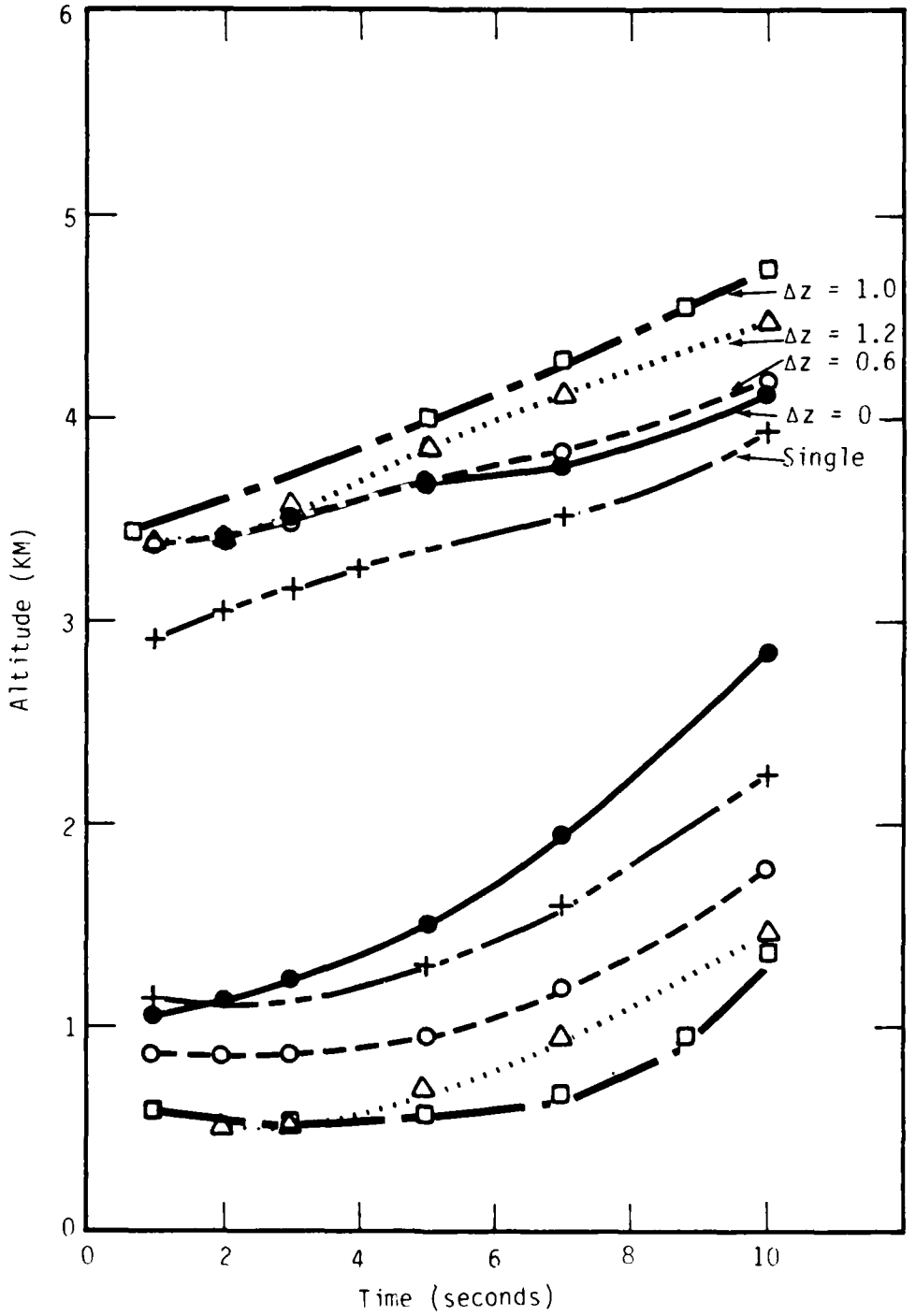

Figure 6. Uppermost and lowermost positions which are cooling due to radiation.

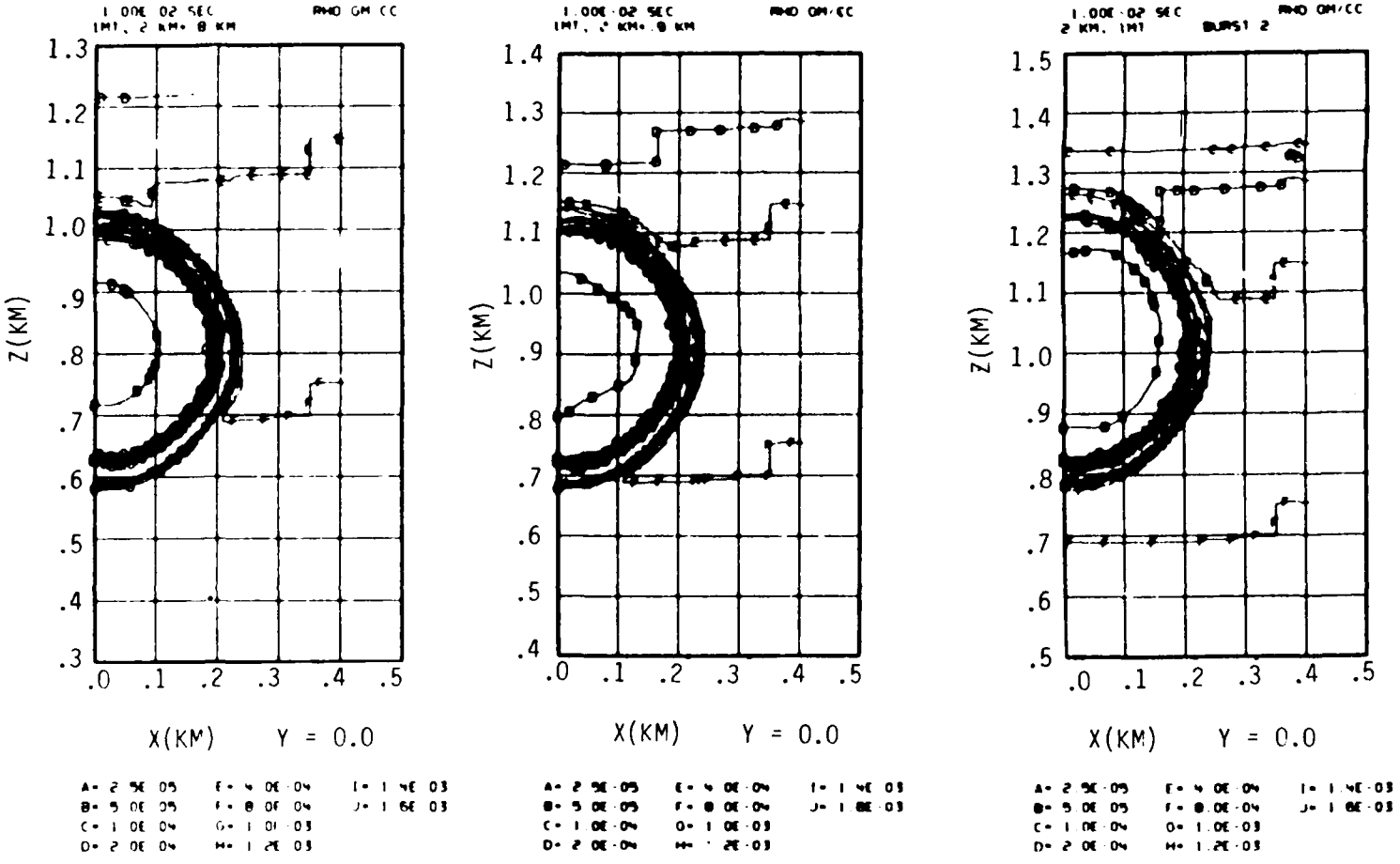

Figure 7. Distribution of density at 0.01 seconds for Δz = 1.2, 1.1, and 1.0 km from left to right.

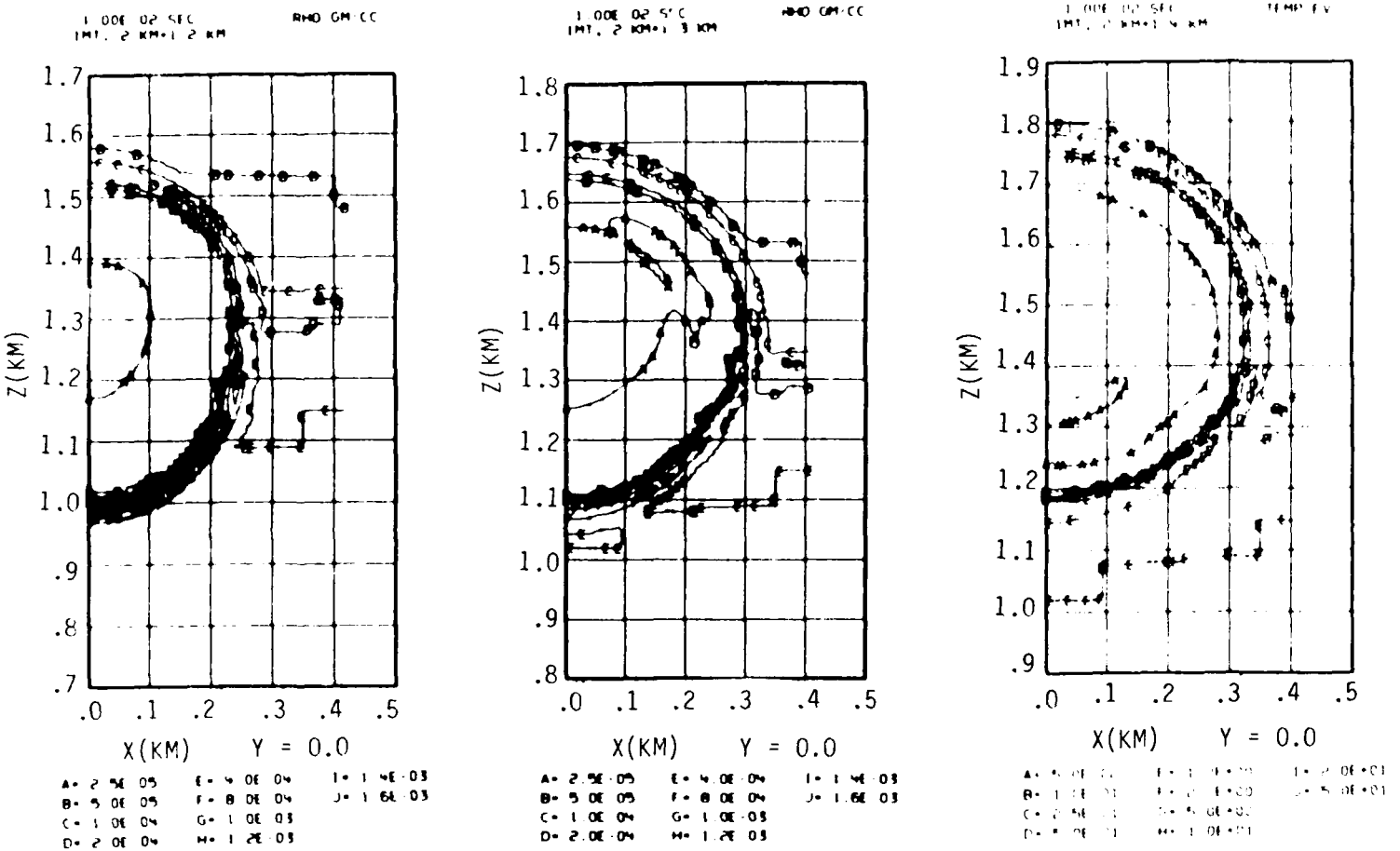

Figure 8. Distribution of density at 0.01 seconds for Δz = 0.8, 0.7, and 0.6 km from left to right.

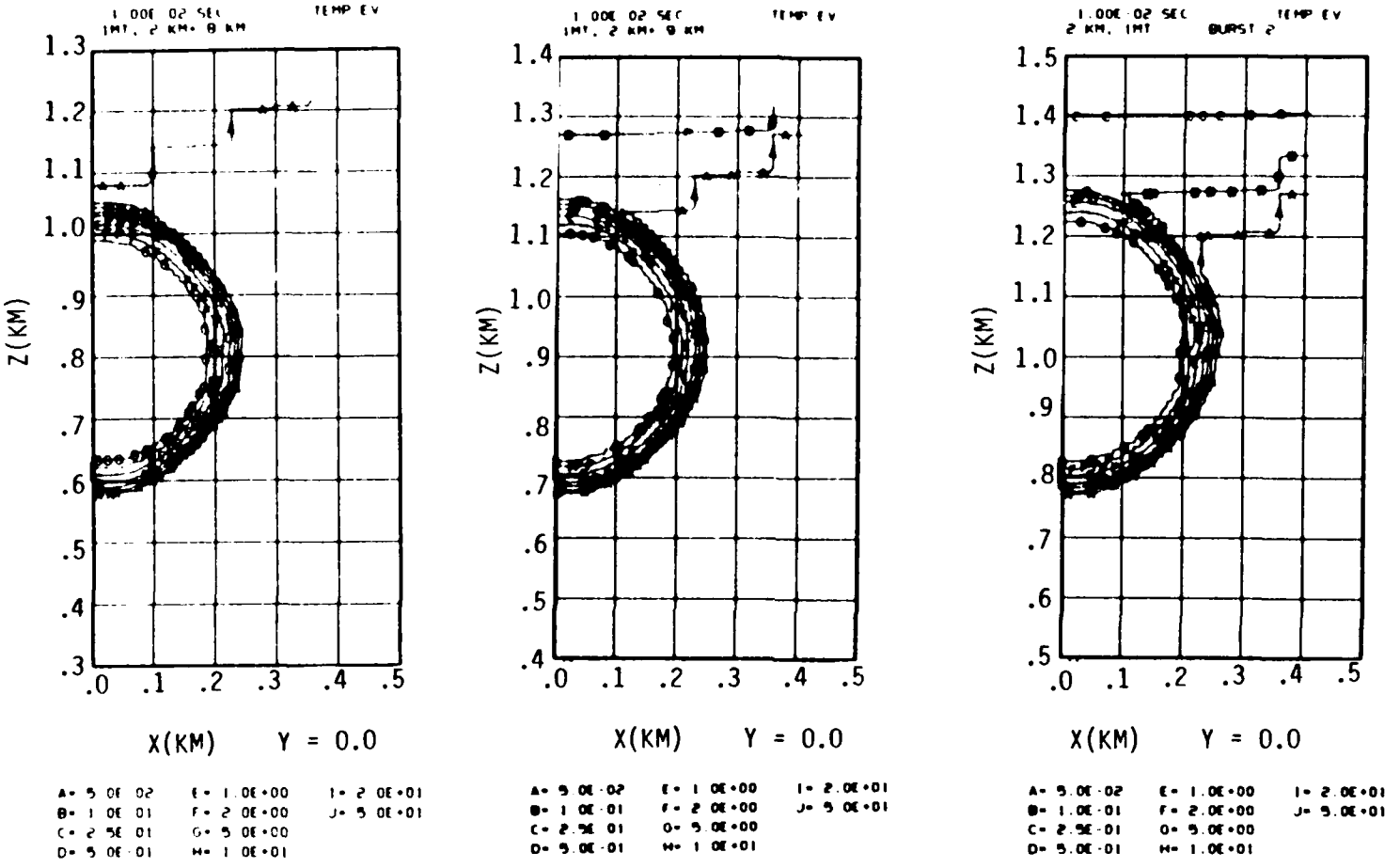

Figure 9. Distribution of temperature at 0.01 seconds for Δz = 1.2, 1.1, and 1.0 from left to right.

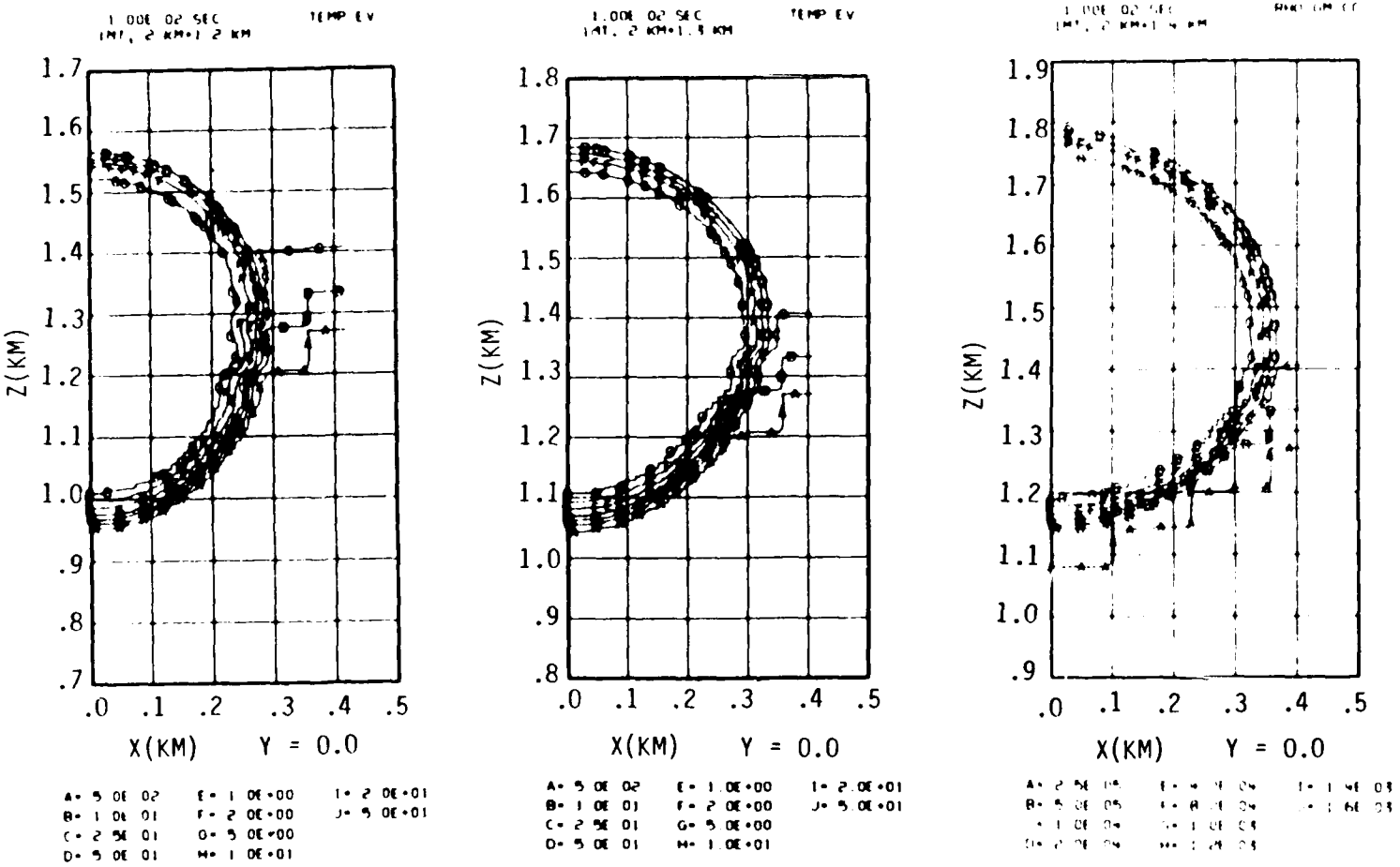

Figure 10. Distribution of temperature at 0.01 seconds for Δz = 0.8, 0.7, and 0.6 km from left to right.

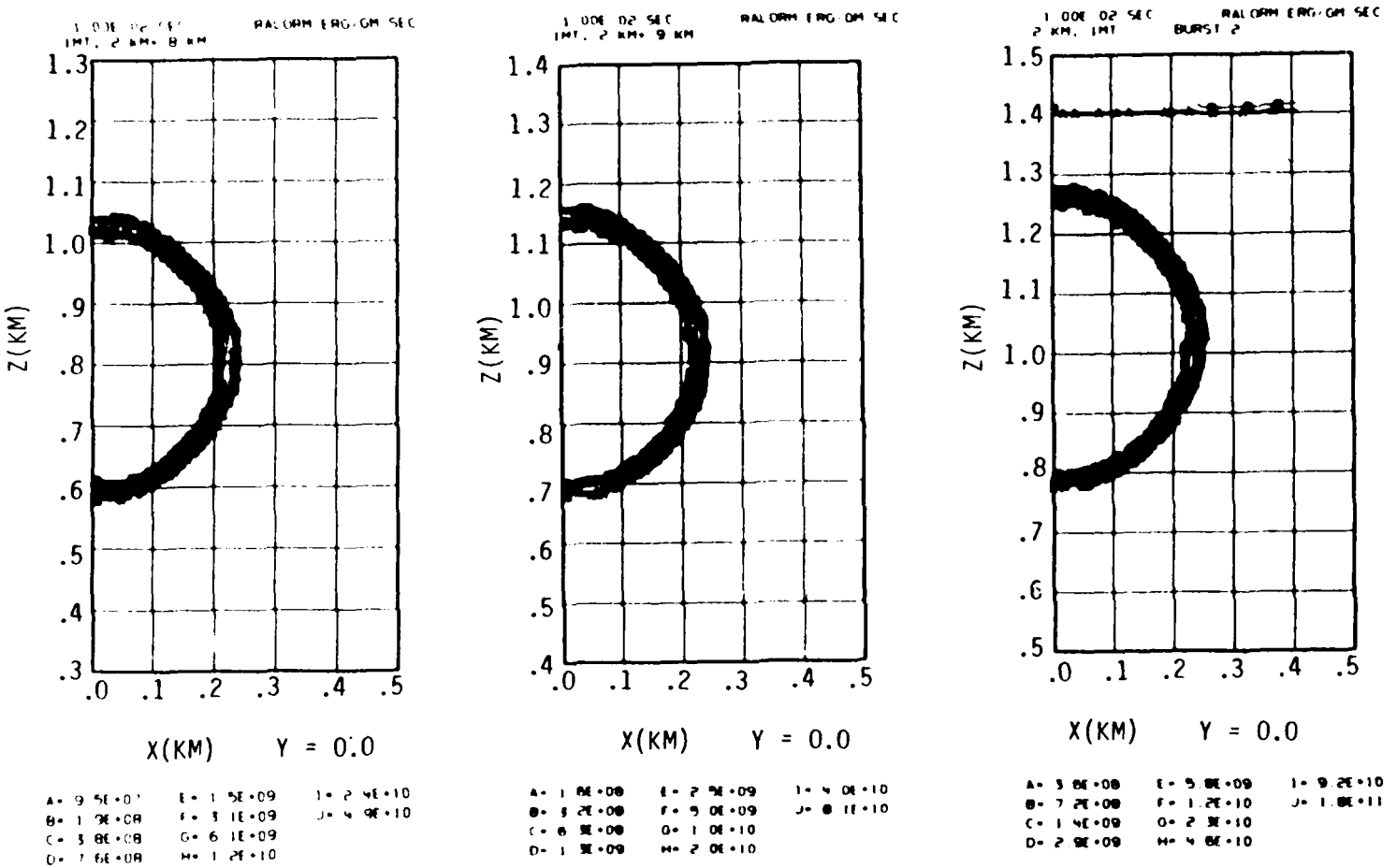

Figure 11. Distribution of cooling at 0.01 seconds due to escaping radiation for Δz = 1.2, 1.1, and 1.0 km from left to right.

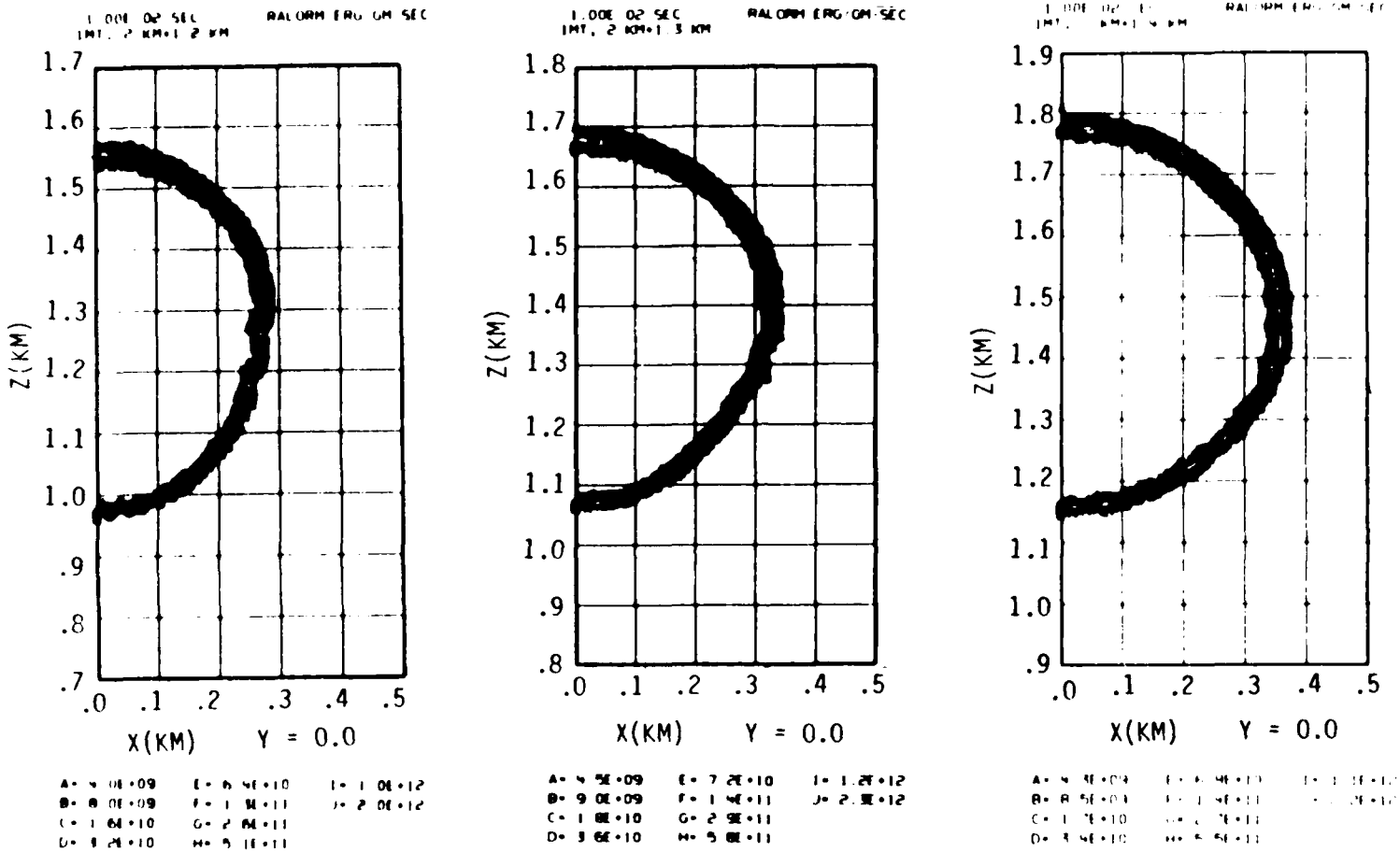

Figure 12. Distribution of cooling due to escaping radiation at 0.01 seconds for Δz = 0.8, 0.7, and 0.6 km from left to right.

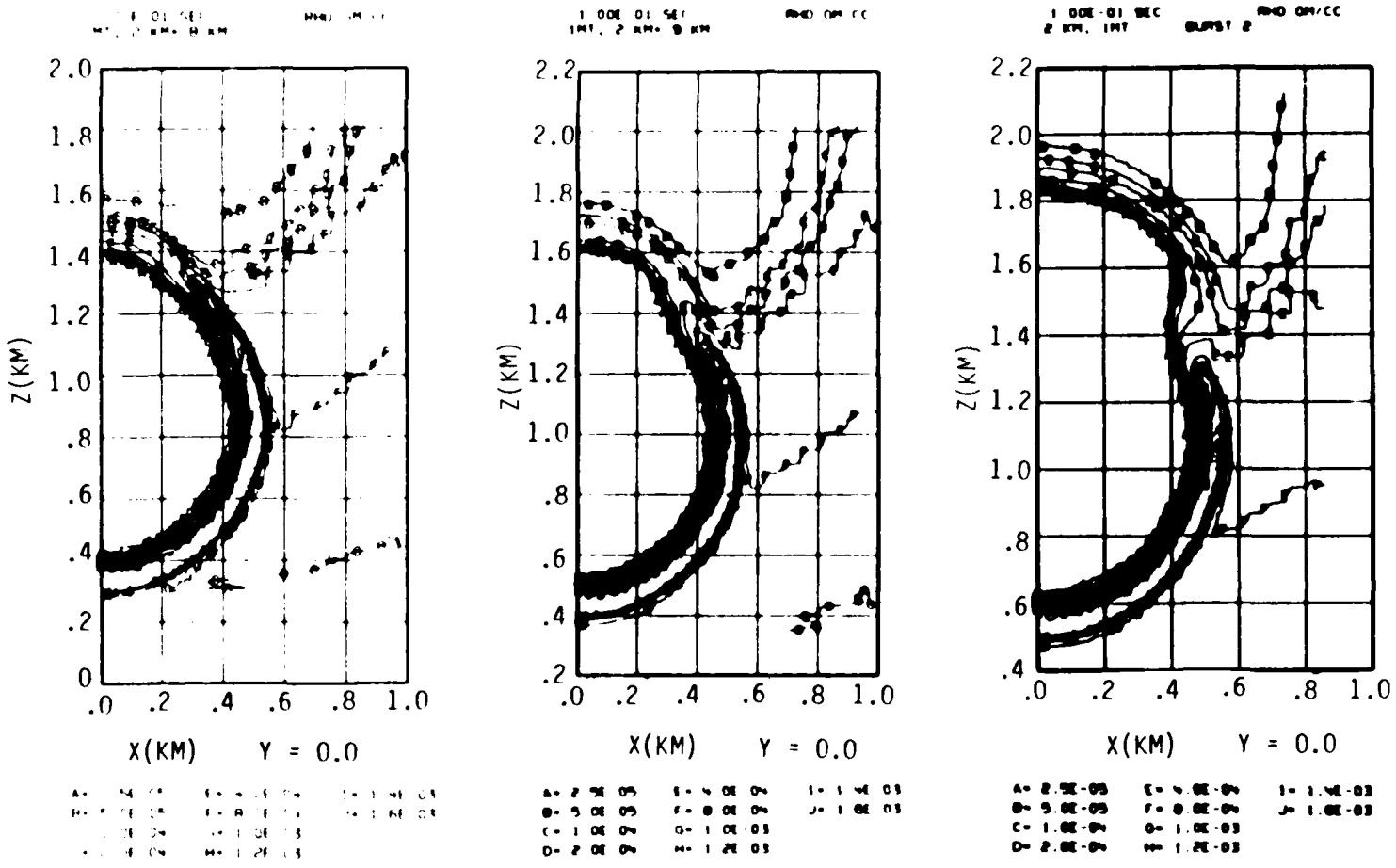

Figure 13. Distribution of density at 0.1 seconds for Δz = 1.2, 1.1, and 1.0 km from left to right.

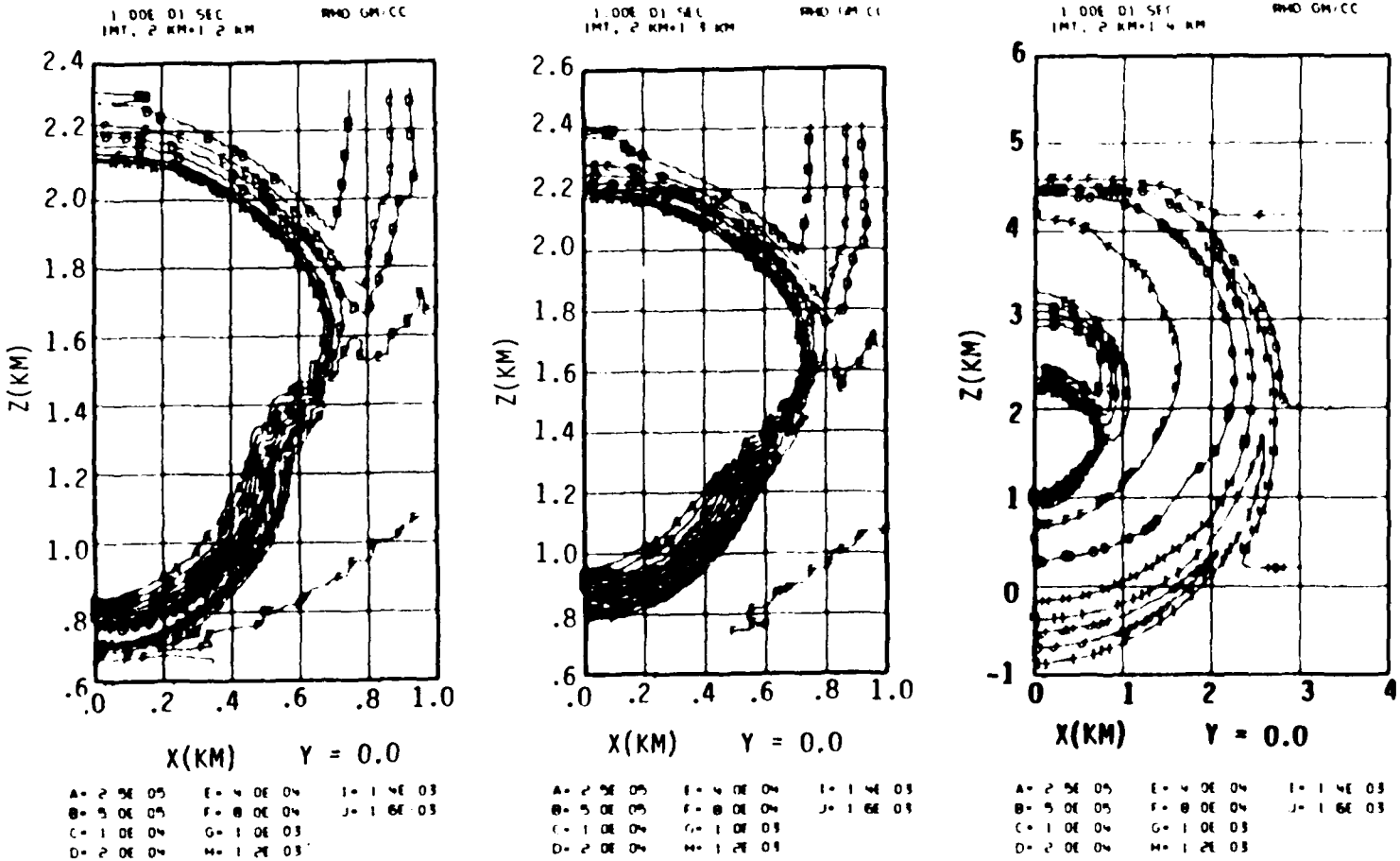

Figure 14. Distribution of density of 0.1 seconds for Δz = 0.8, 0.7, and 0.6 km from left to right.

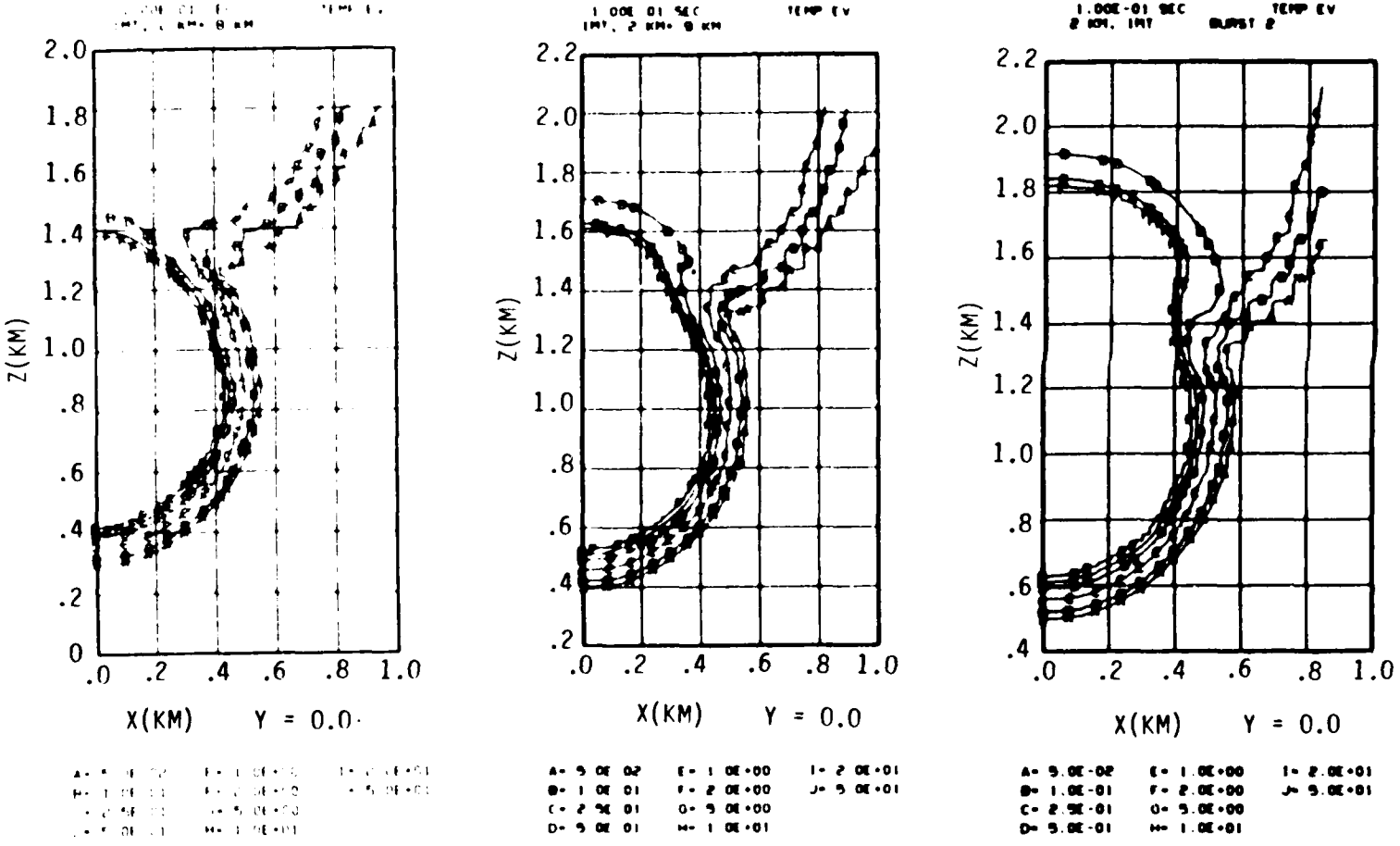

Figure 15. Distribution of temperature at 0.1 seconds for Δz = 1.2, 1.1, and 1.0 km from left to right.

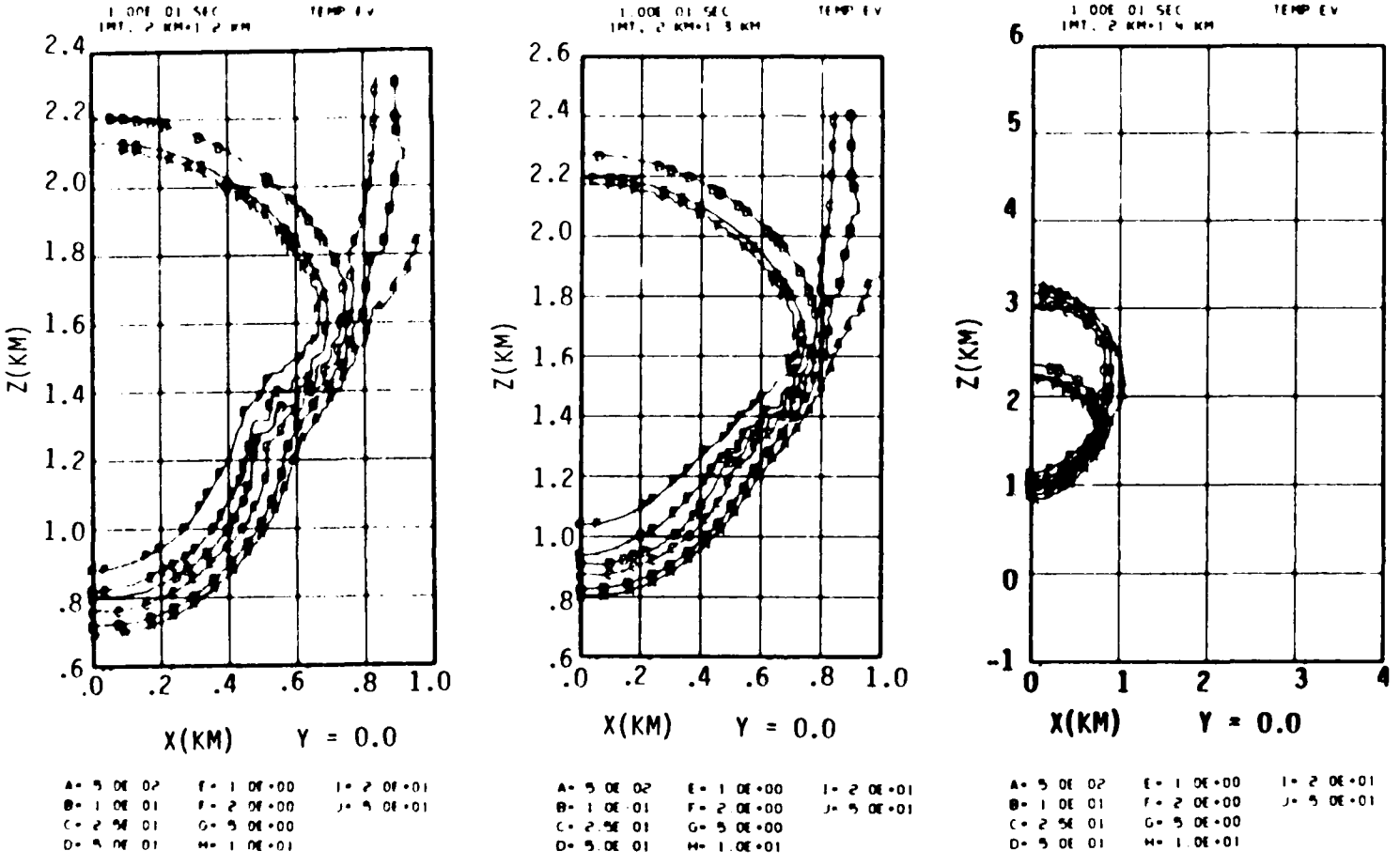

Figure 16. Distribution of temperature at 0.1 seconds for Δz = 0.8, 0.7, and 0.6 km from left to right.

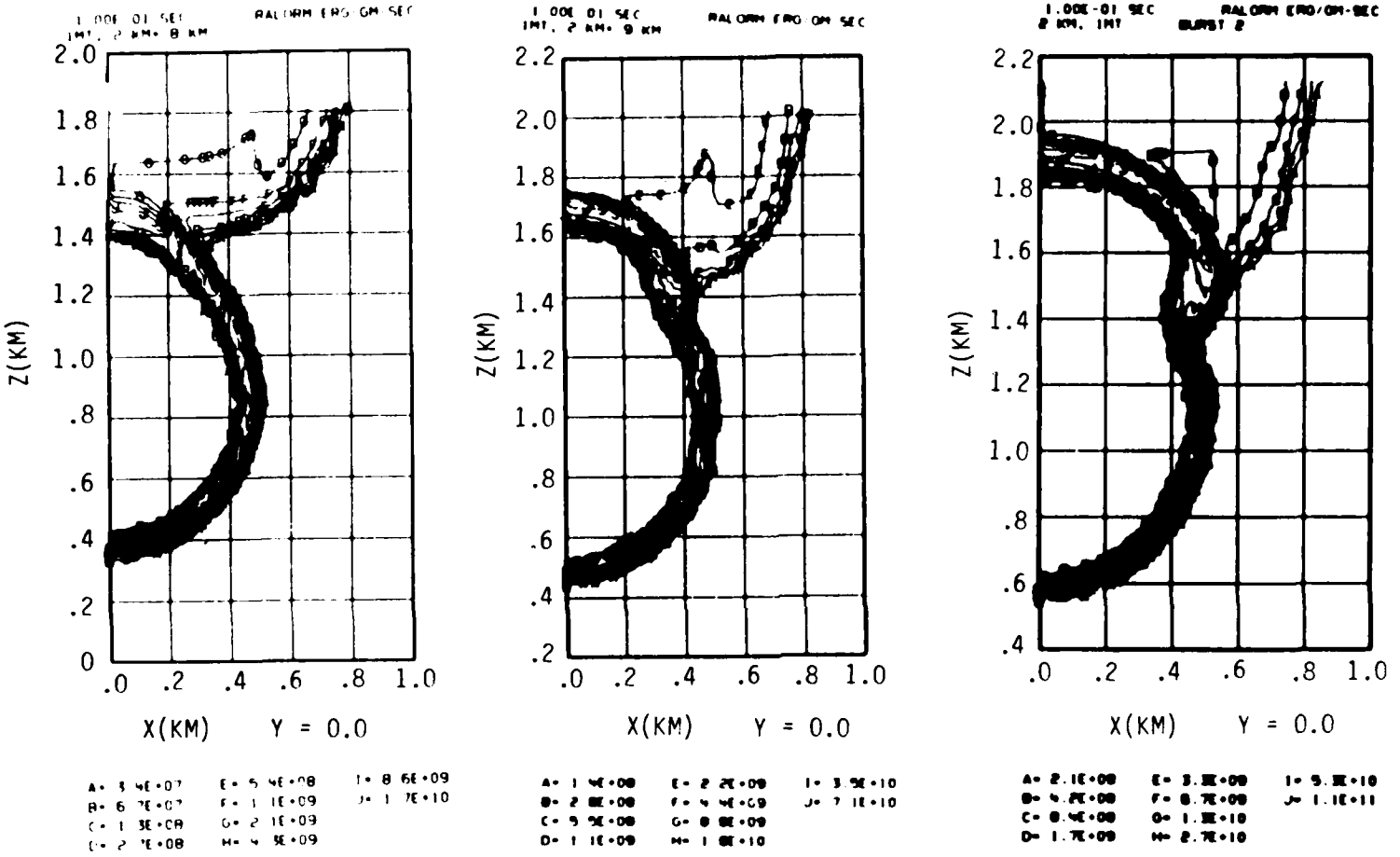

Figure 17. Distribution of cooling due to escaping radiation at 0.1 seconds for Δz = 1.2, 1.1, and 1.0 km from left to right.

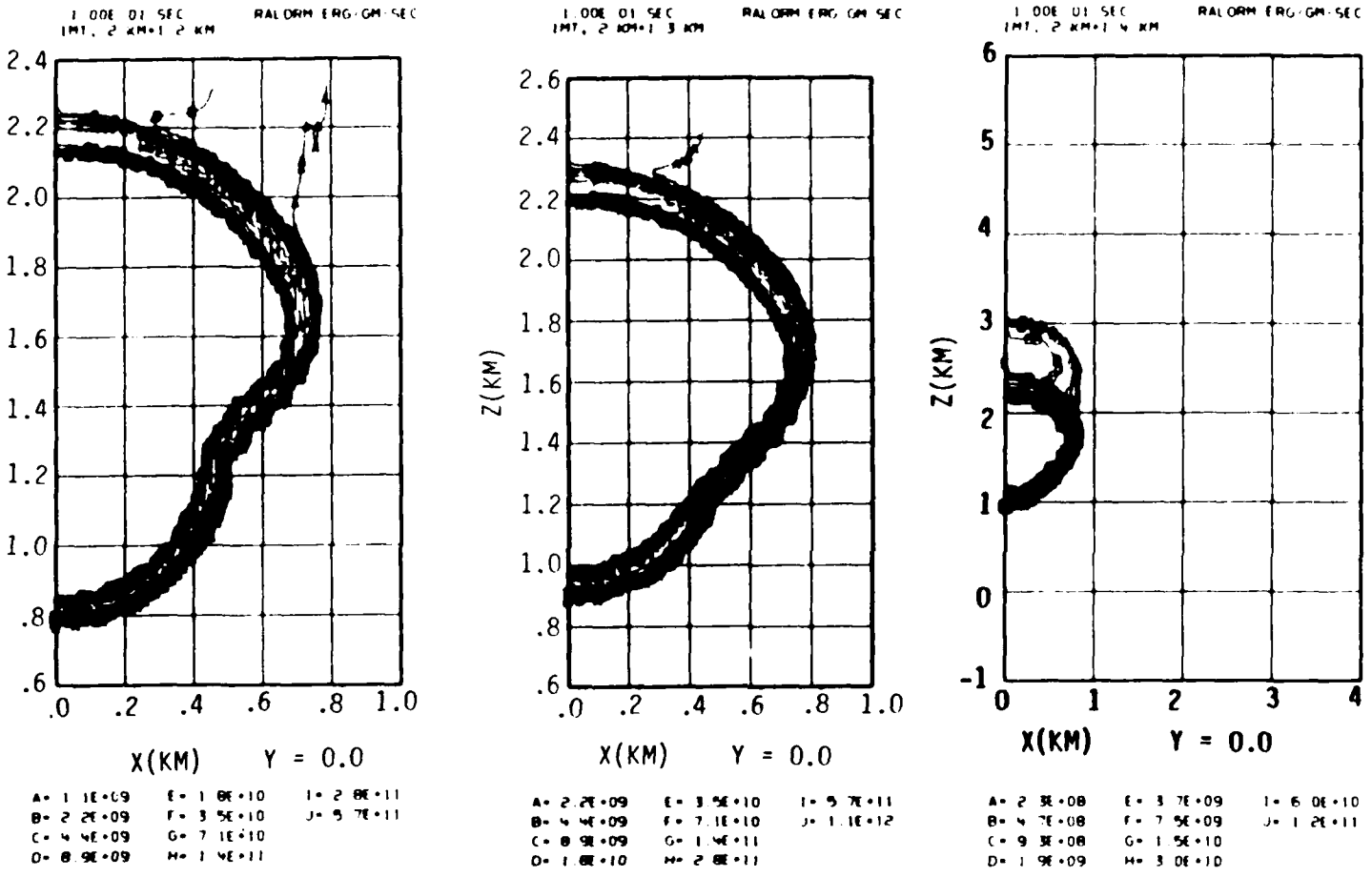

Figure 18. Distribution of cooling due to escaping radiation at 0.1 seconds for Δz = 0.8, 0.7, and 0.6 km from left to right. Note that the contours for Δz = 0.6 are plotted at a different scale than for the other separations.

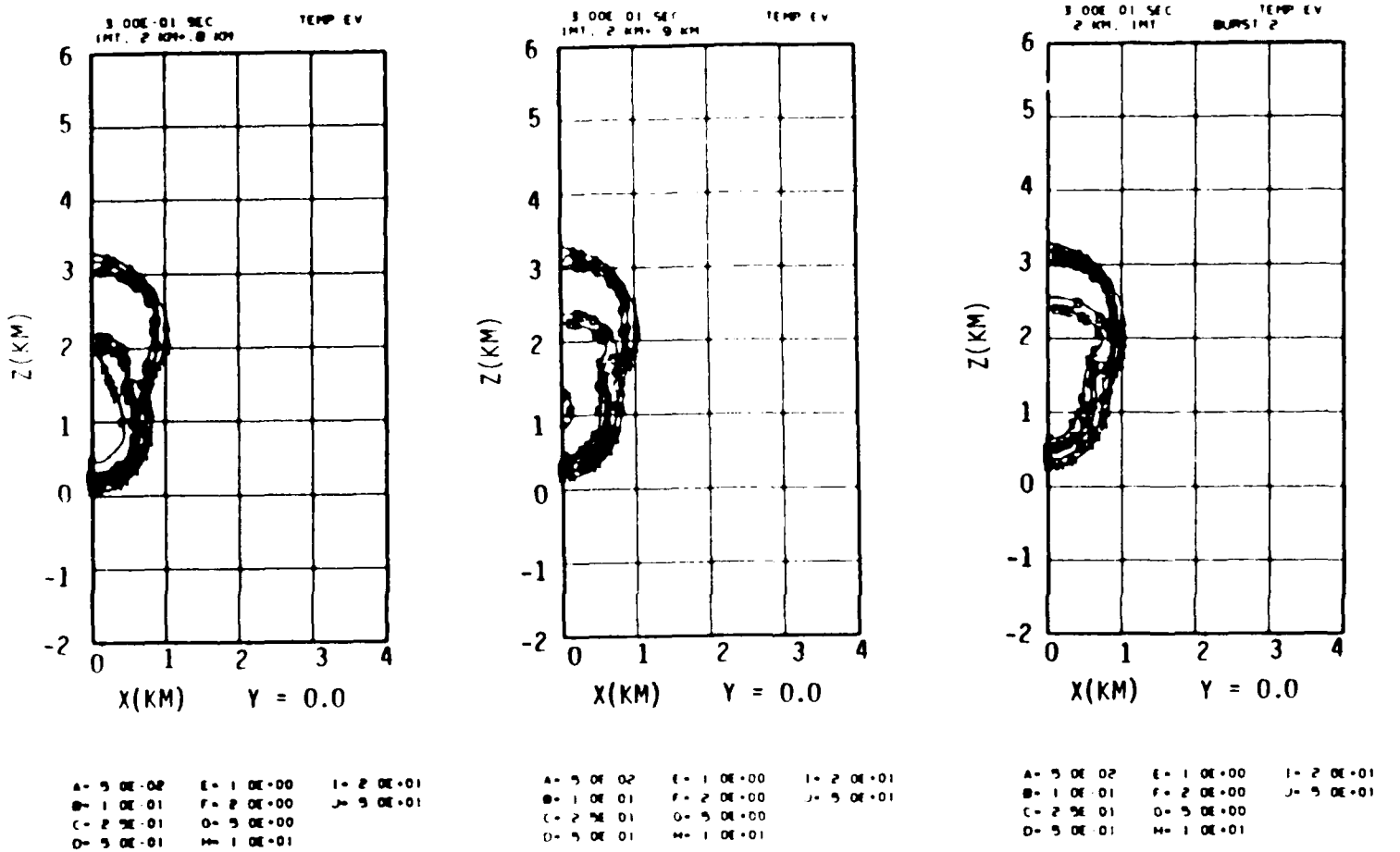

Figure 19. Distribution of temperature at 0.3 seconds for Δz = 1.2, 1.1, and 1.0 km from left to right.

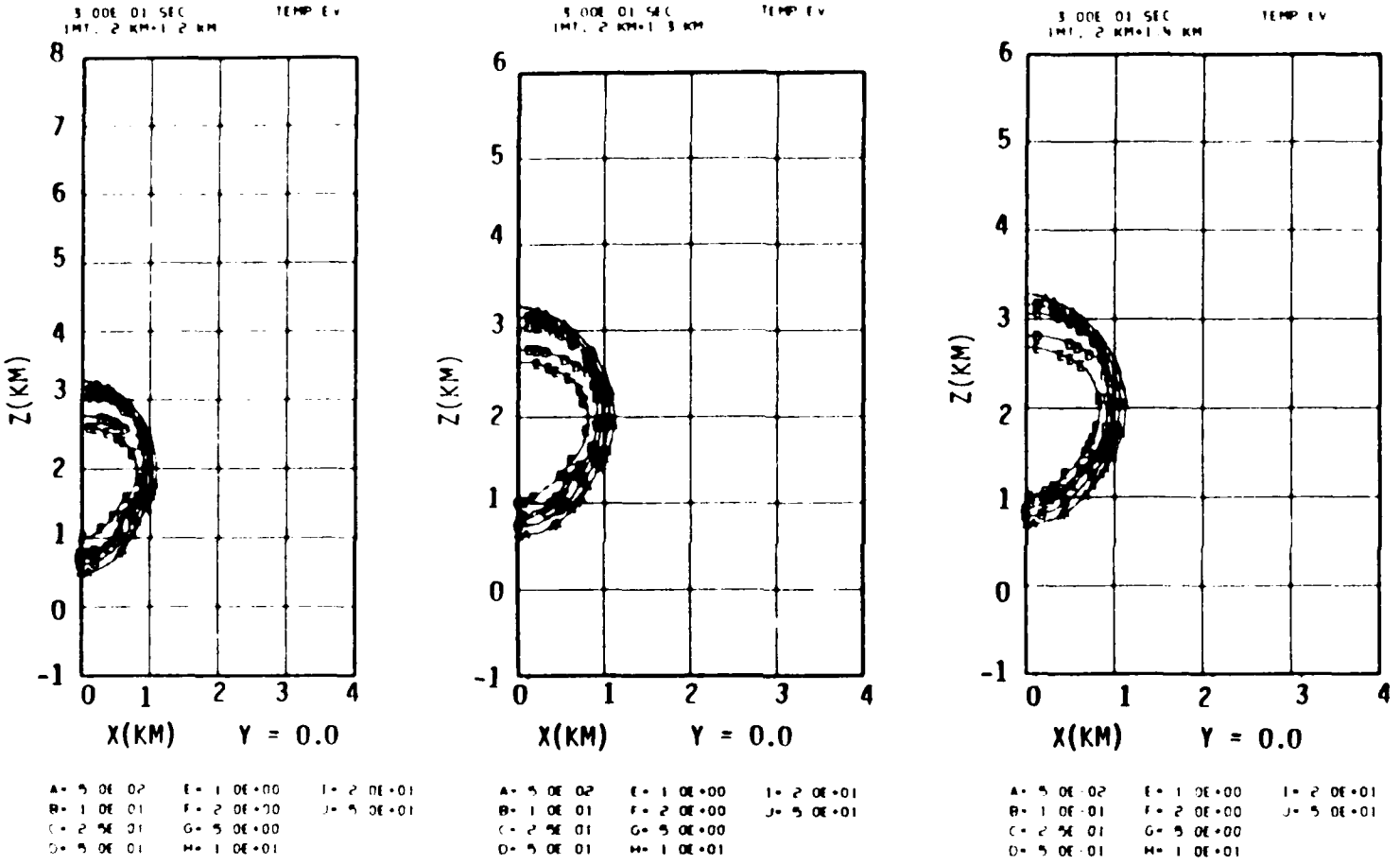

Figure 20. Distribution of temperature at 0.3 seconds for Δz = 0.8, 0.7, and 0.6 km from left to right.

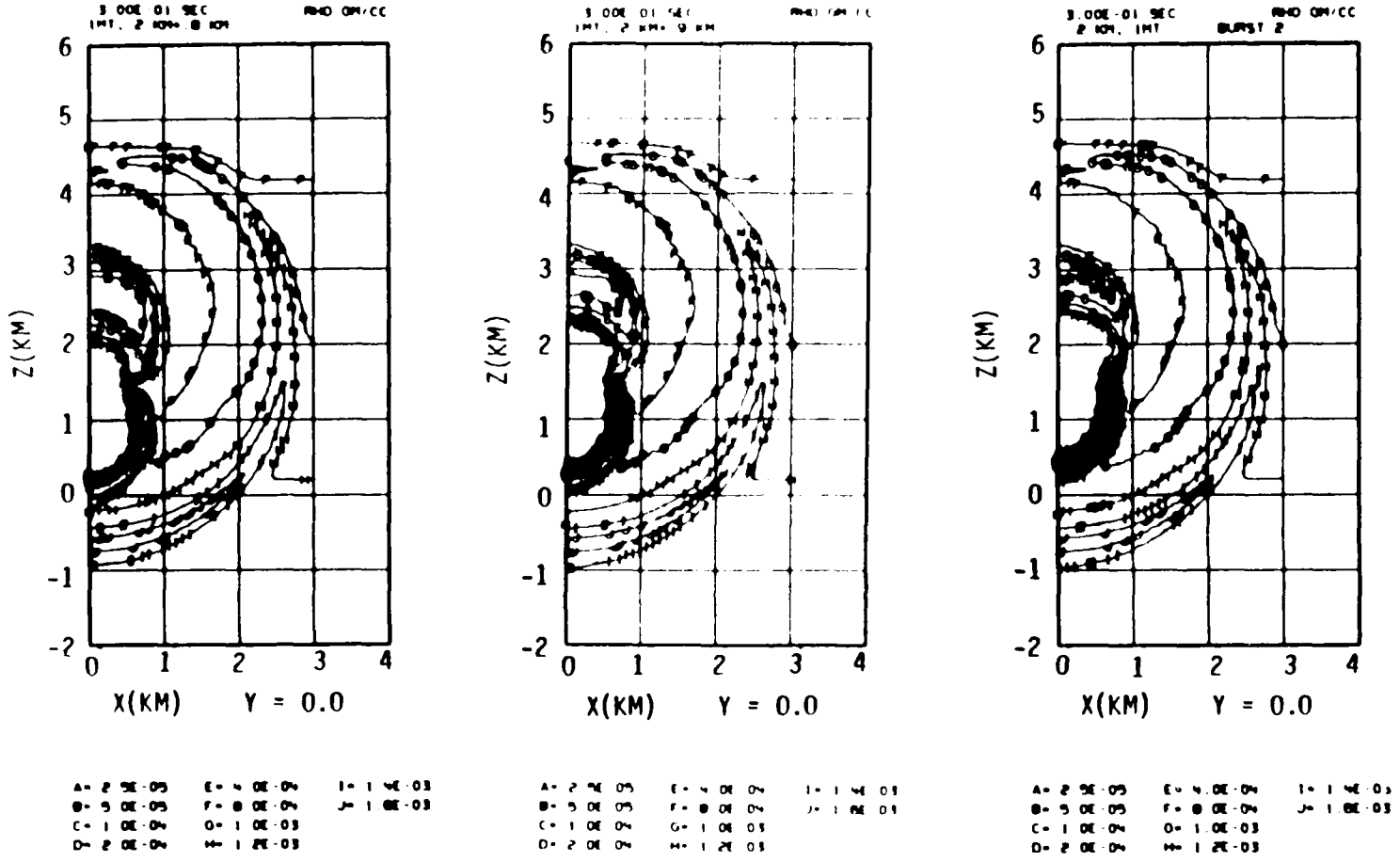

Figure 21. Distribution of density at 0.3 seconds for Δz = 1.2, 1.1, and 1.0 km from left to right.

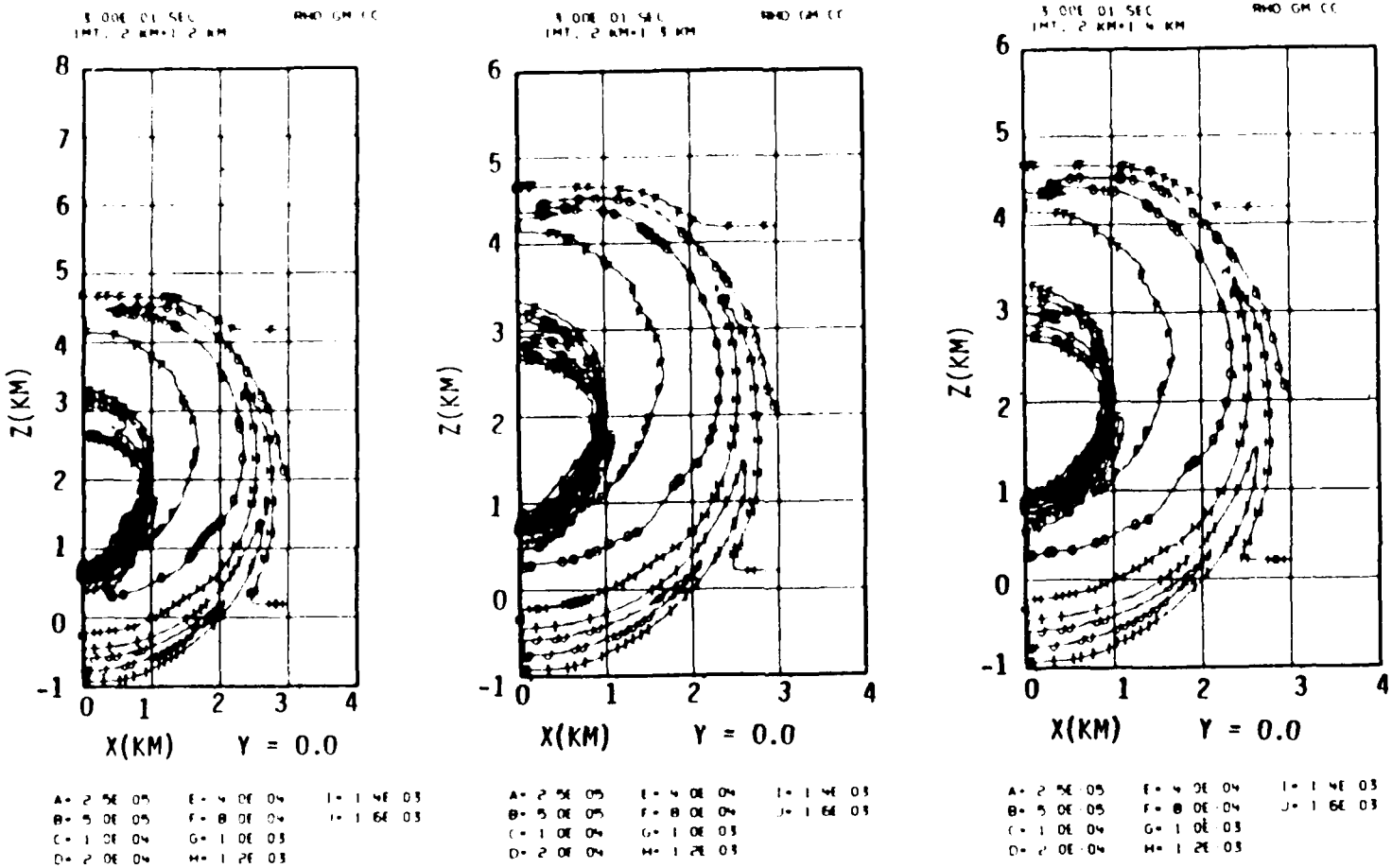

Figure 22. Distribution of density at 0.3 seconds for Δz = 0.8, 0.7, and 0.6 km from left to right.

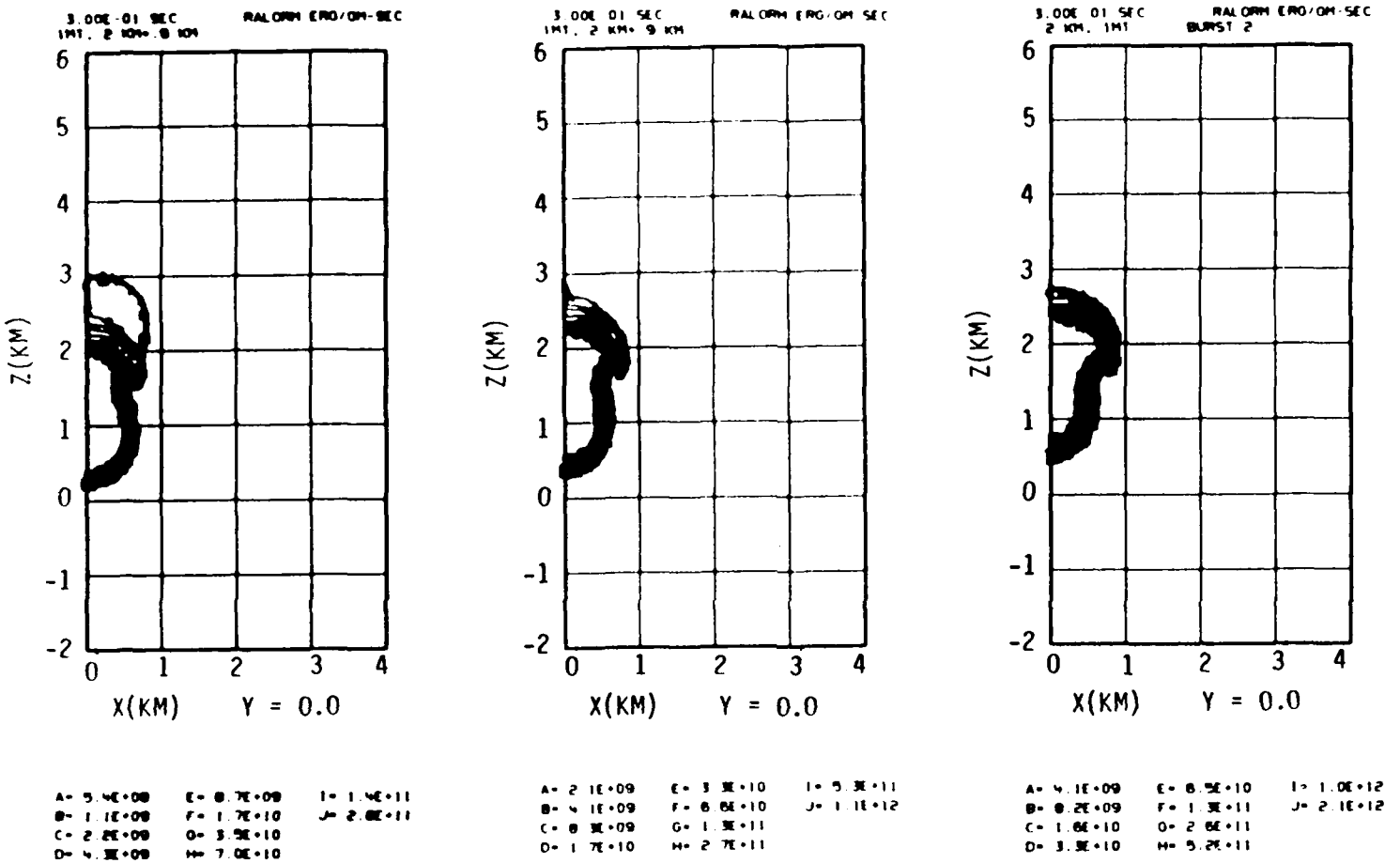

Figure 23. Distribution of cooling due to escaping radiation at 0.3 seconds for Δz = 1.2, 1.1, and 1.0 km from left to right.

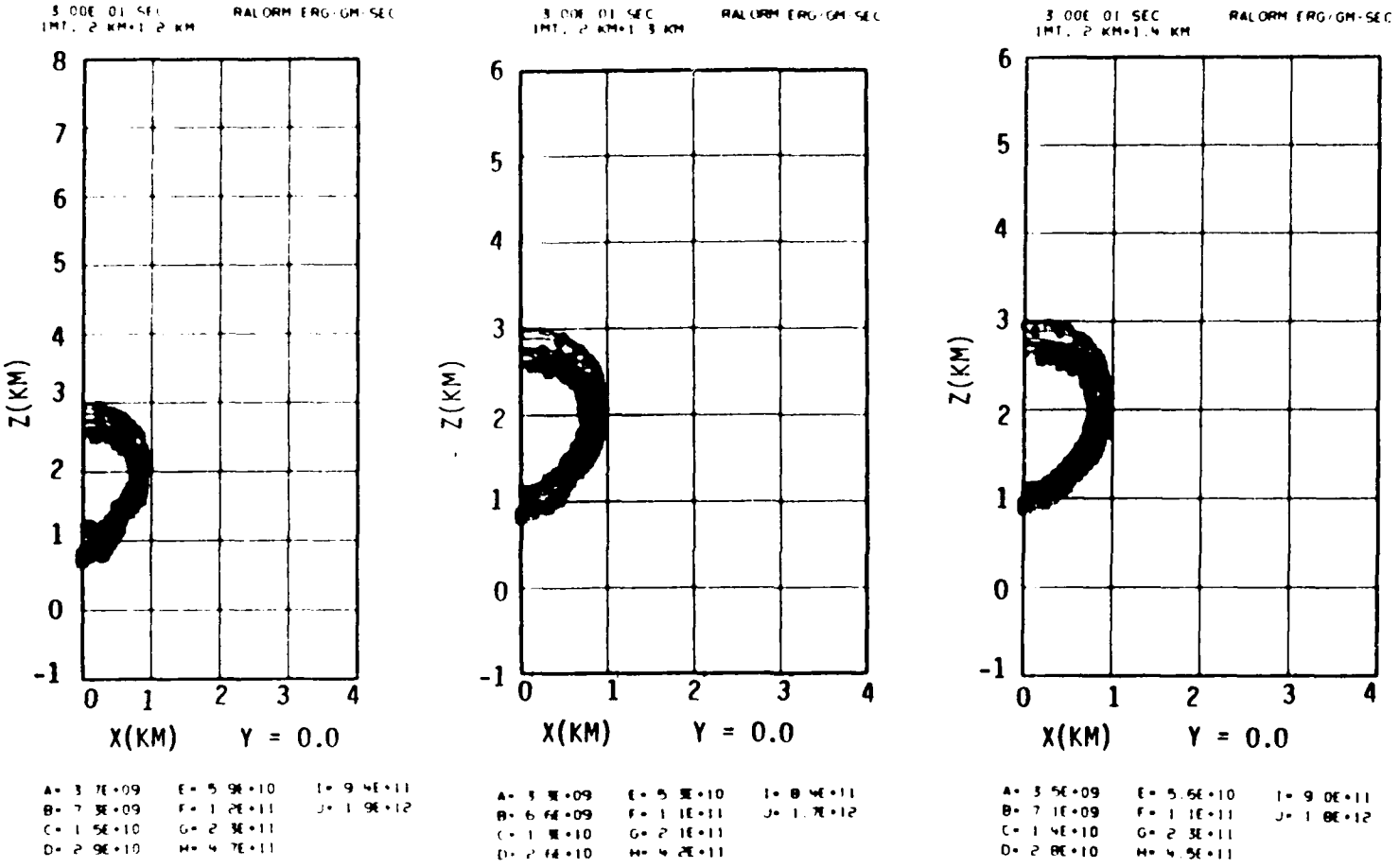

Figure 24. Distribution of cooling due to escaping radiation at 0.3 seconds for Δz = 0.8, 0.7, and 0.6 km from left to right.

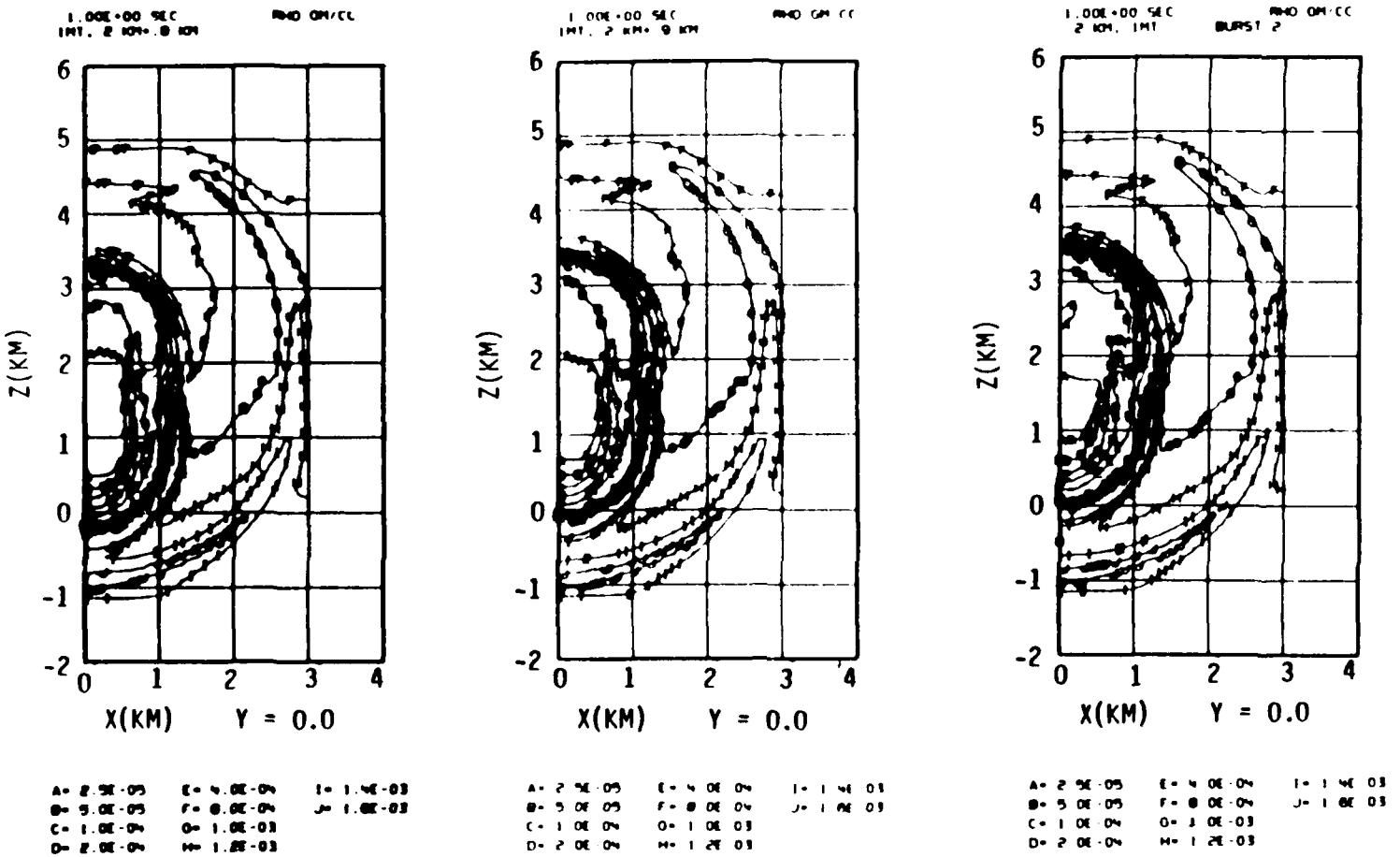

Figure 25. Distribution of density at 1.0 seconds for Δz = 1.2, 1.1, and 1.0 km from left to right.

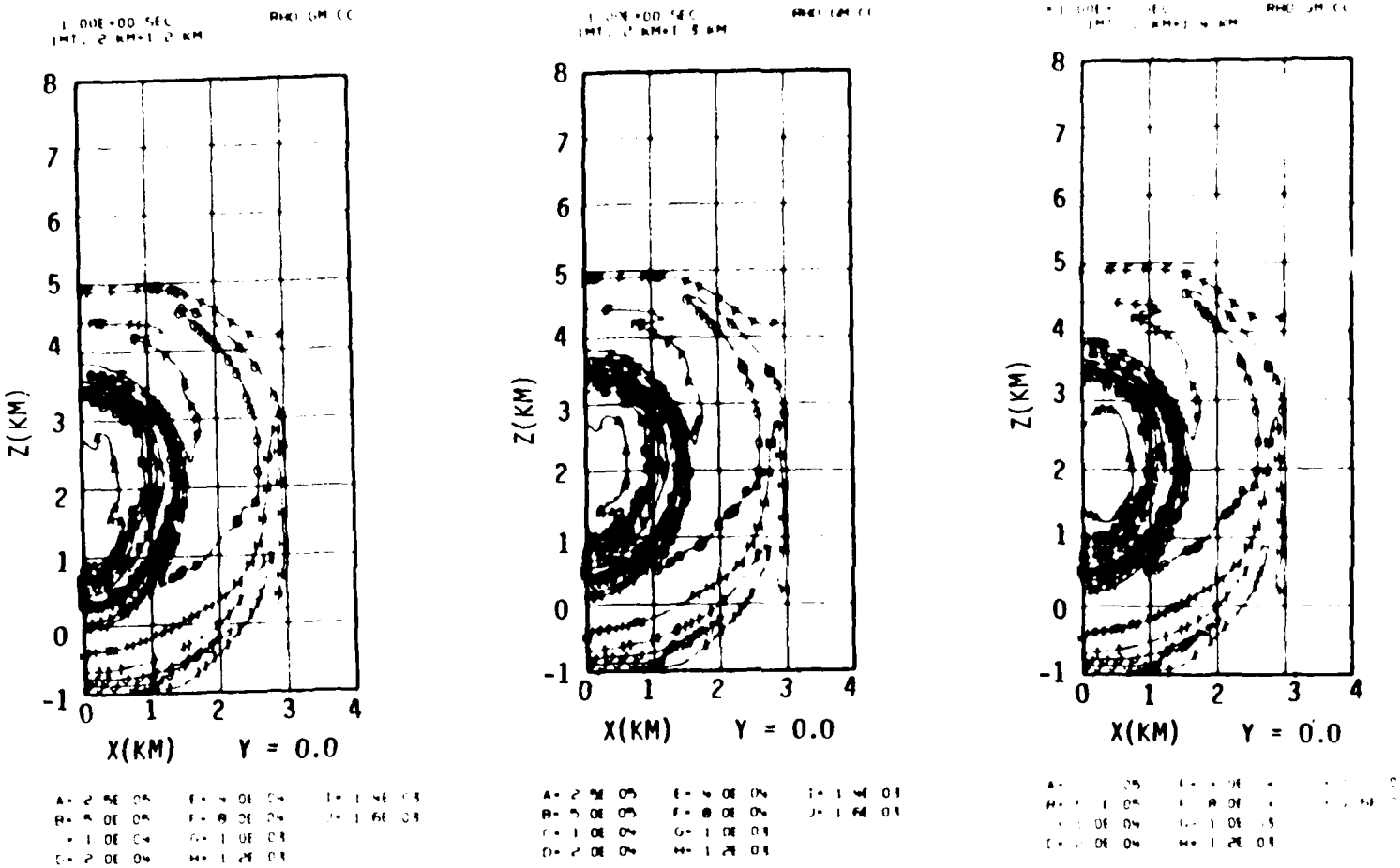

Figure 26. Distribution of density at 1.0 seconds for Δz = 0.8, 0.7, and 0.6 km from left to right.

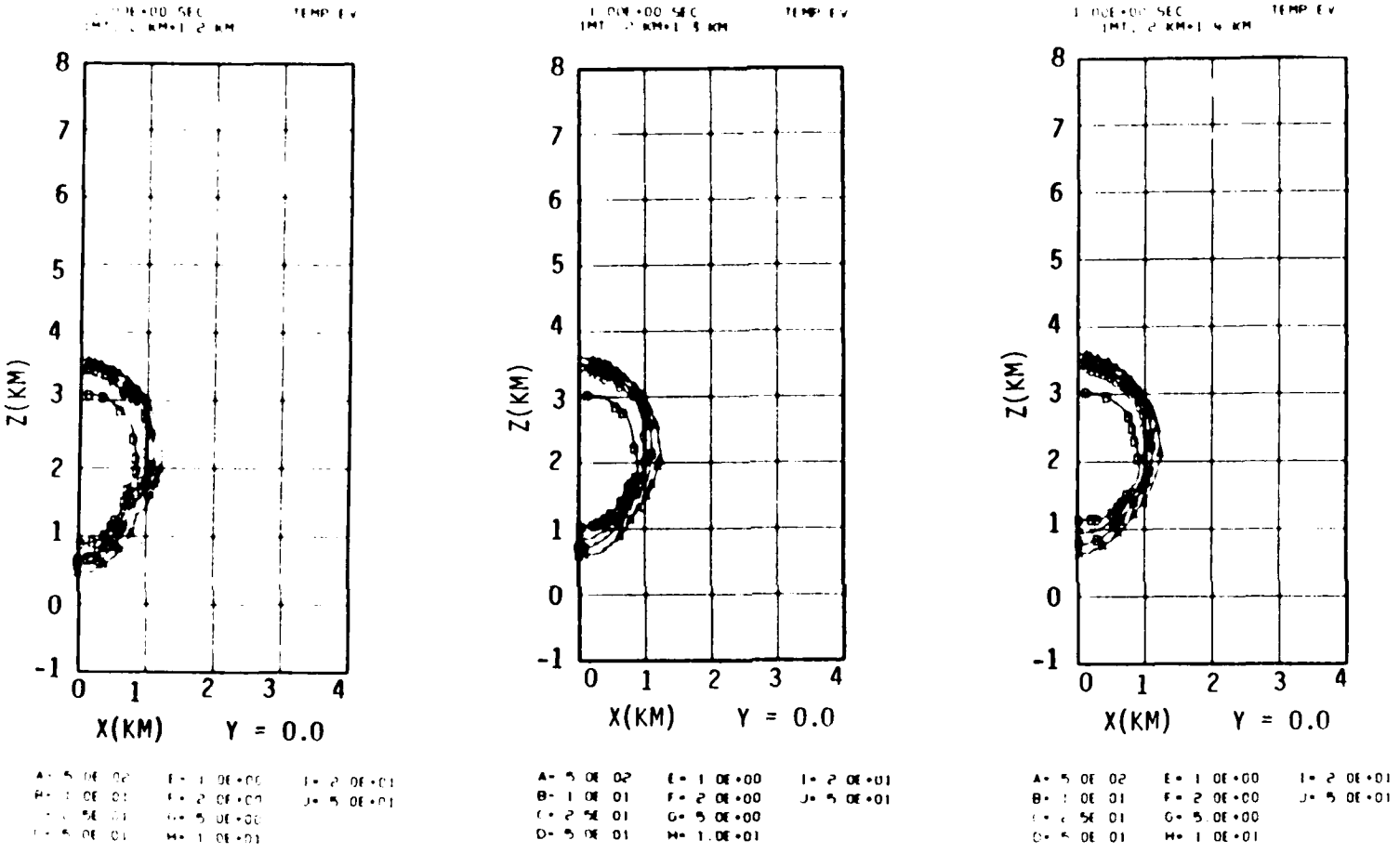

Figure 27. Distribution of temperature at 1.0 seconds for Δz = 0.8, 0.7, and 0.6 km from left to right.

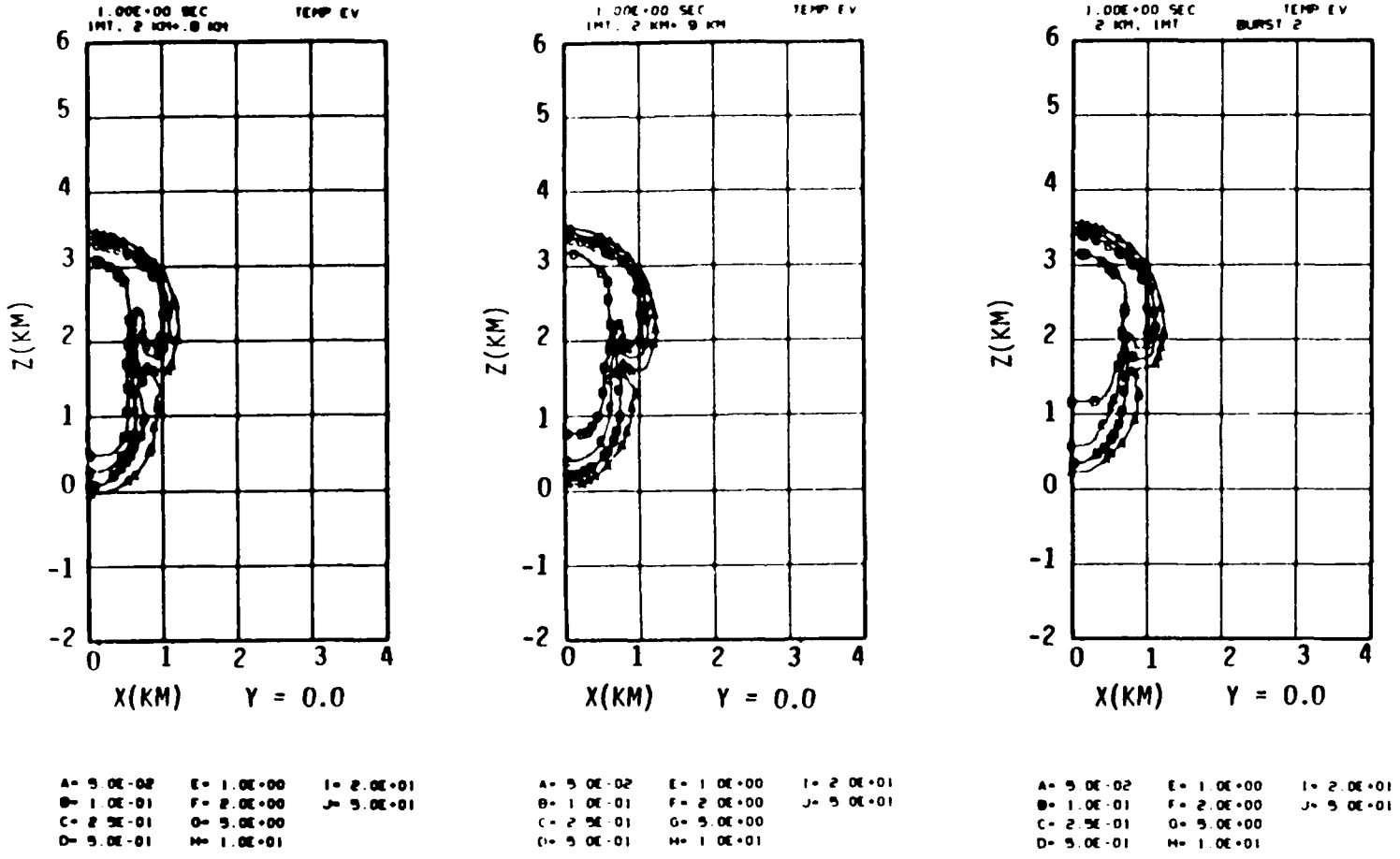

Figure 28. Distribution of temperature at 1.0 seconds for Δz = 1.2, 1.1, 1.0 km from left to right.

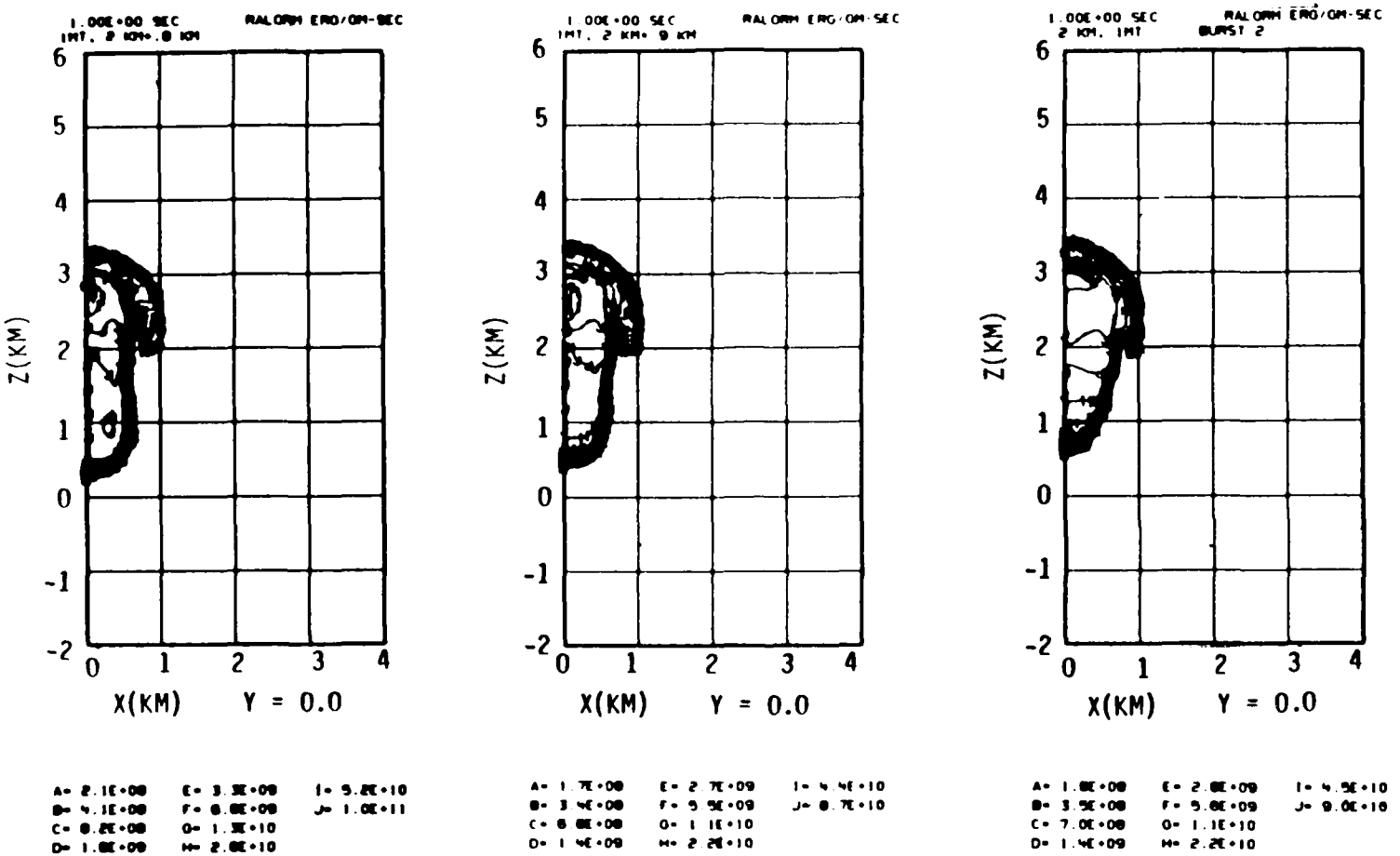

Figure 29. Distribution of cooling at 1.0 seconds due to escaping radiation for Δz = 1.2, 1.1, and 1.0 km from left to right.

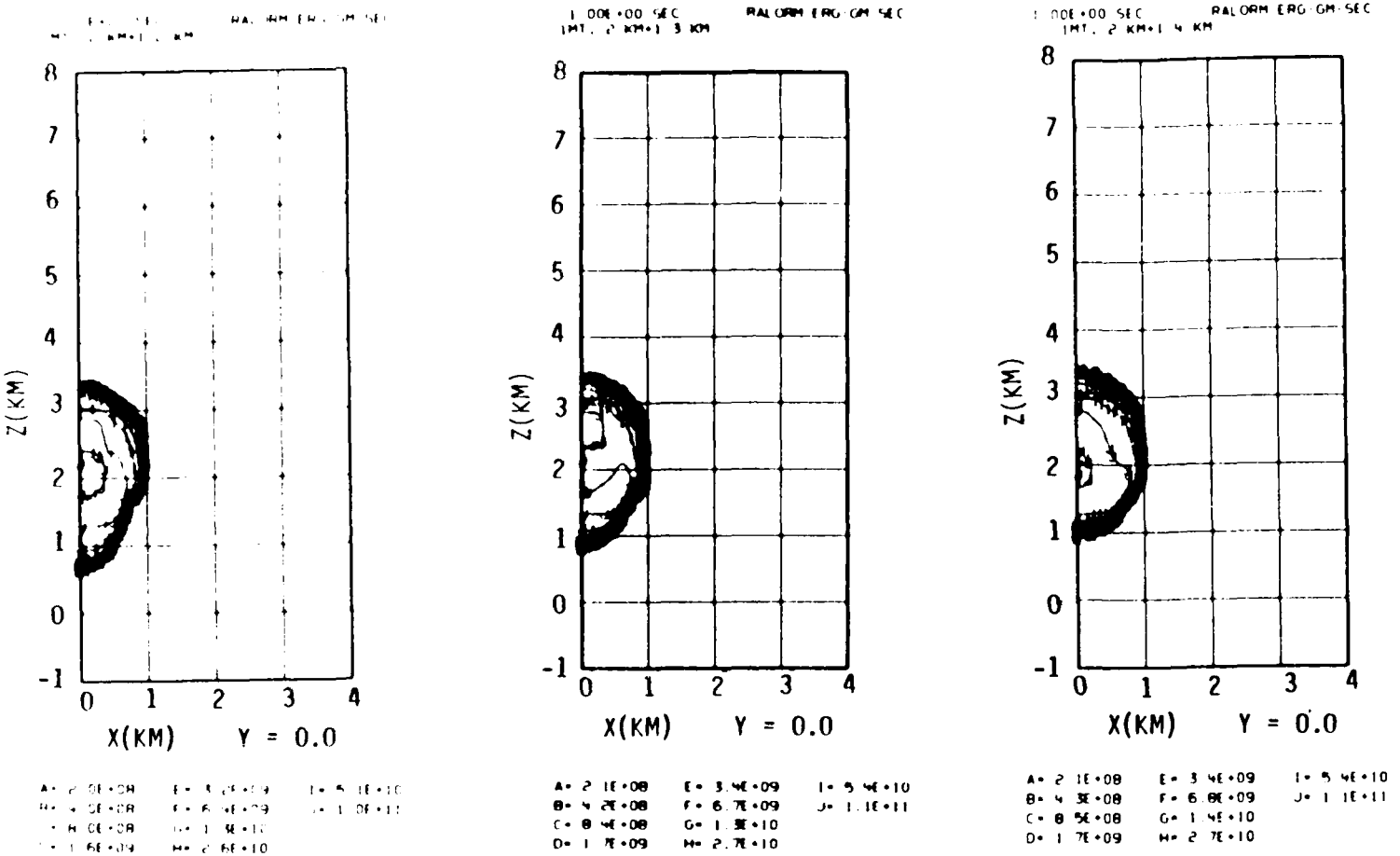

Figure 30. Distribution of cooling due to escaping radiation at 1.0 second for Δz = 0.8, 0.7, and 0.6 km from left to right.

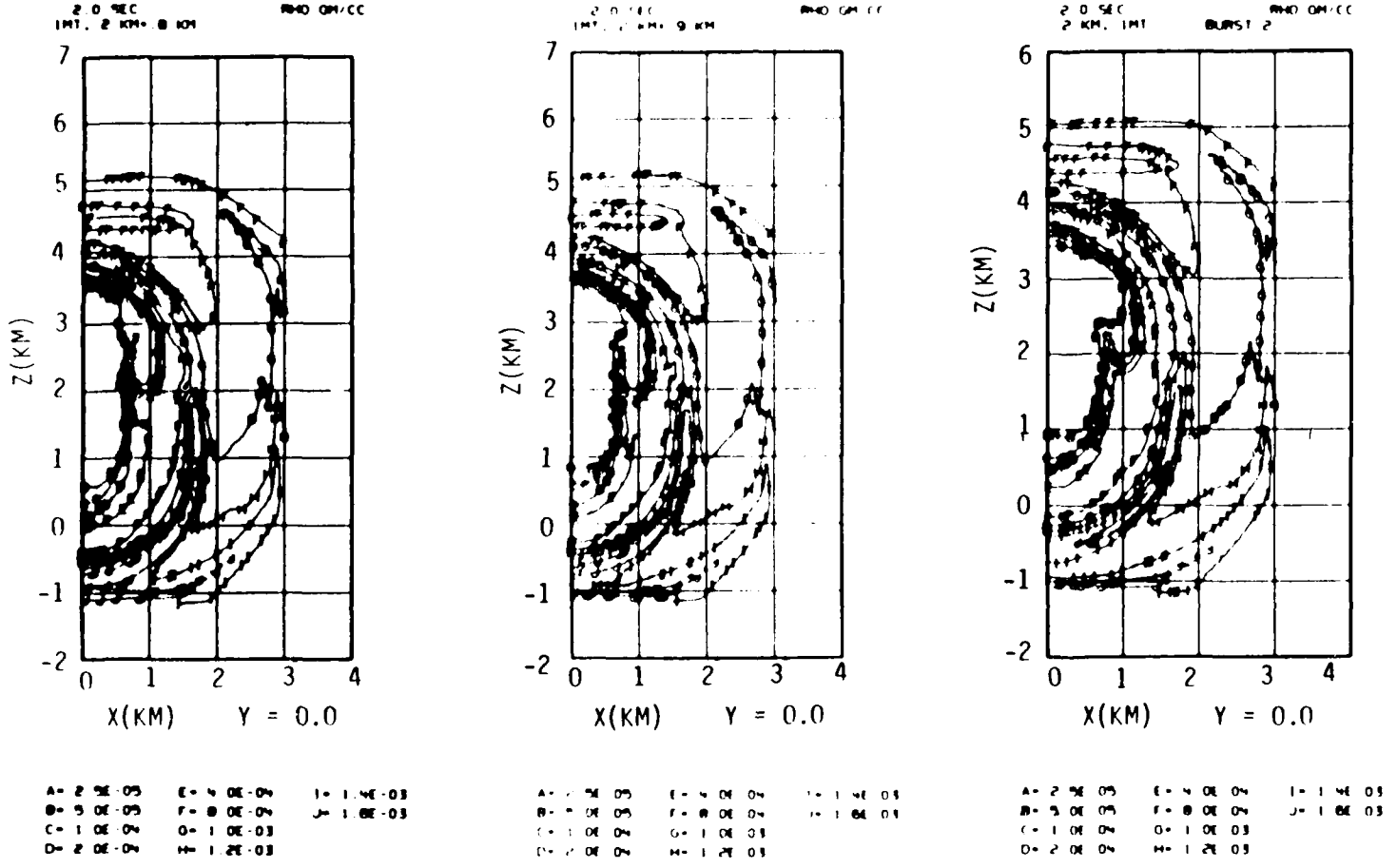

Figure 31. Distribution of density at 2.0 seconds for Δz = 1.2, 1.1, and 1.0 km from left to right.

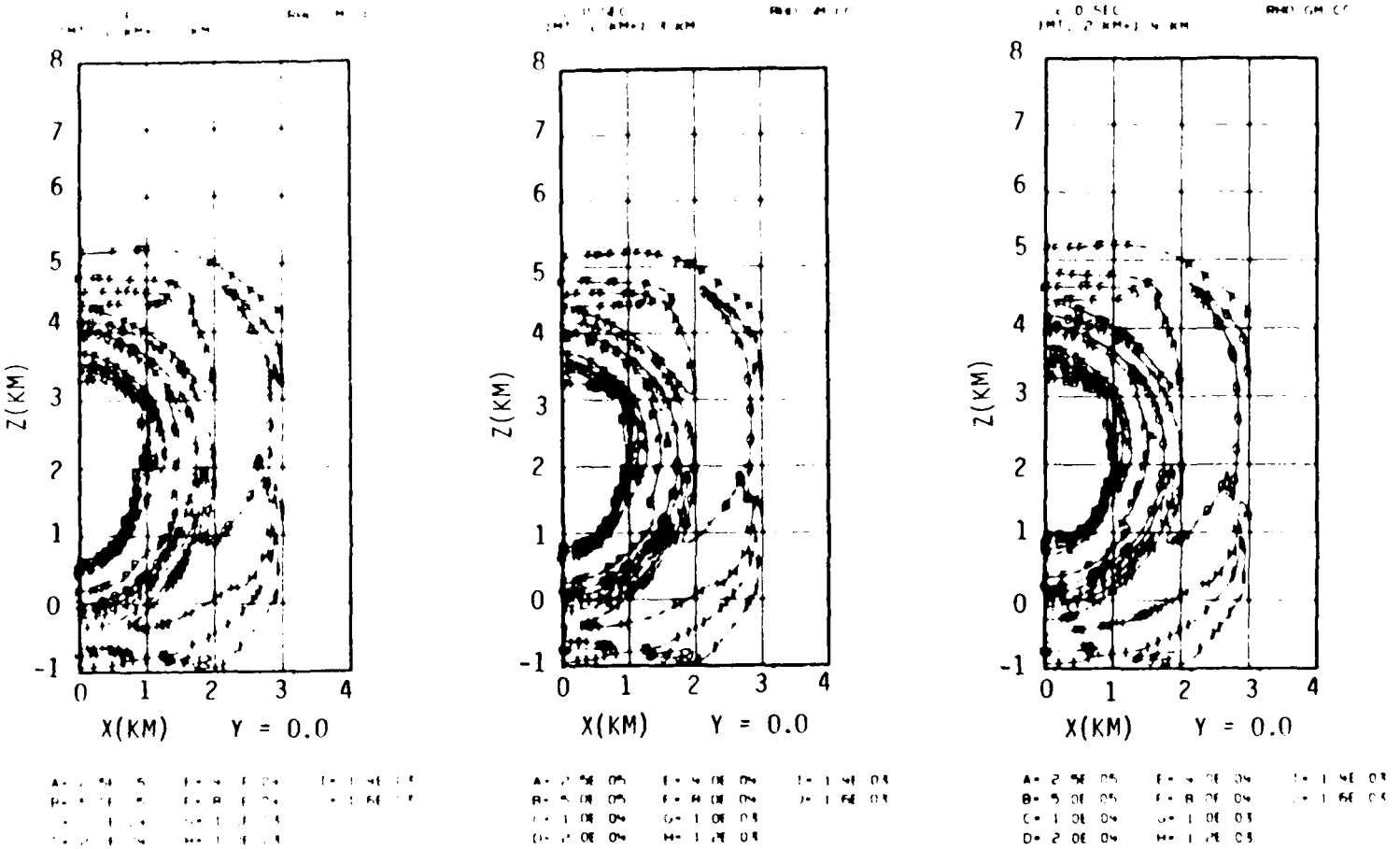

Figure 32. Distribution of density at 2.0 seconds for Δz = 0.8, 0.7, and 0.6 km from left to right.

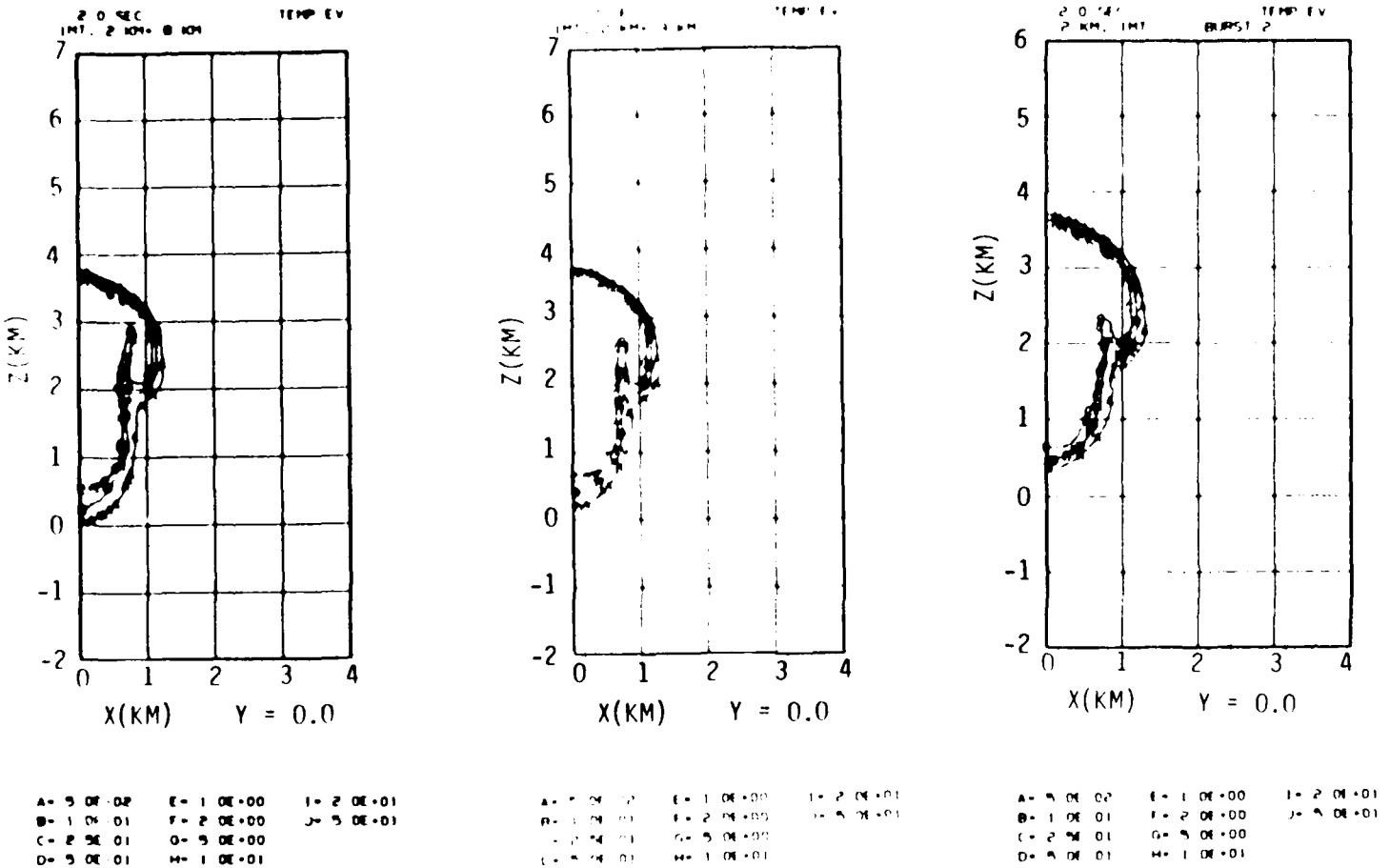

Figure 33. Distribution of temperature at 2.0 seconds for Δz = 1.2, 1.1, and 1.0 km from left to right.

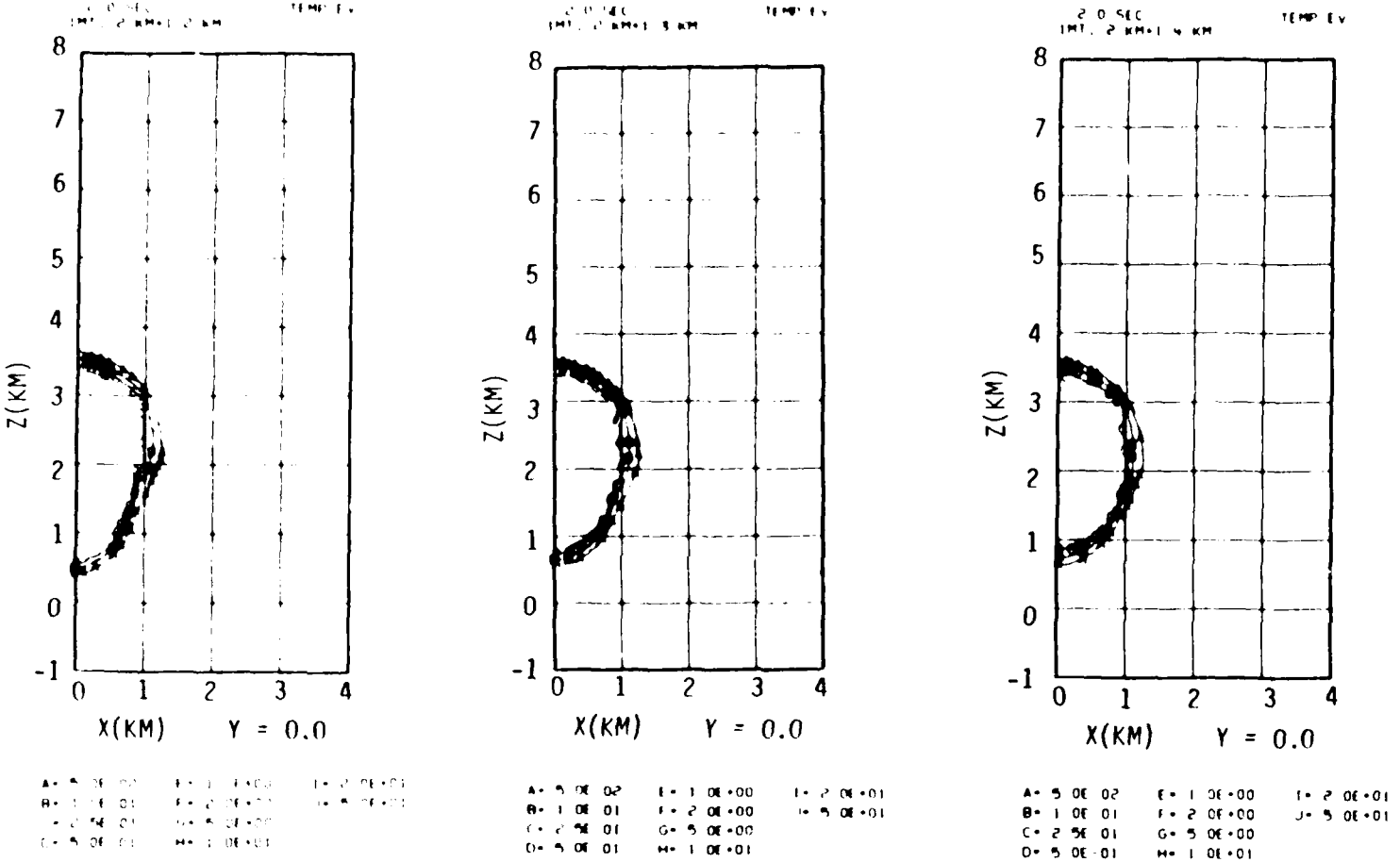

Figure 34. Distribution of temperature at 2.0 seconds for Δz = 0.8, 0.7, and 0.6 km from left to right.

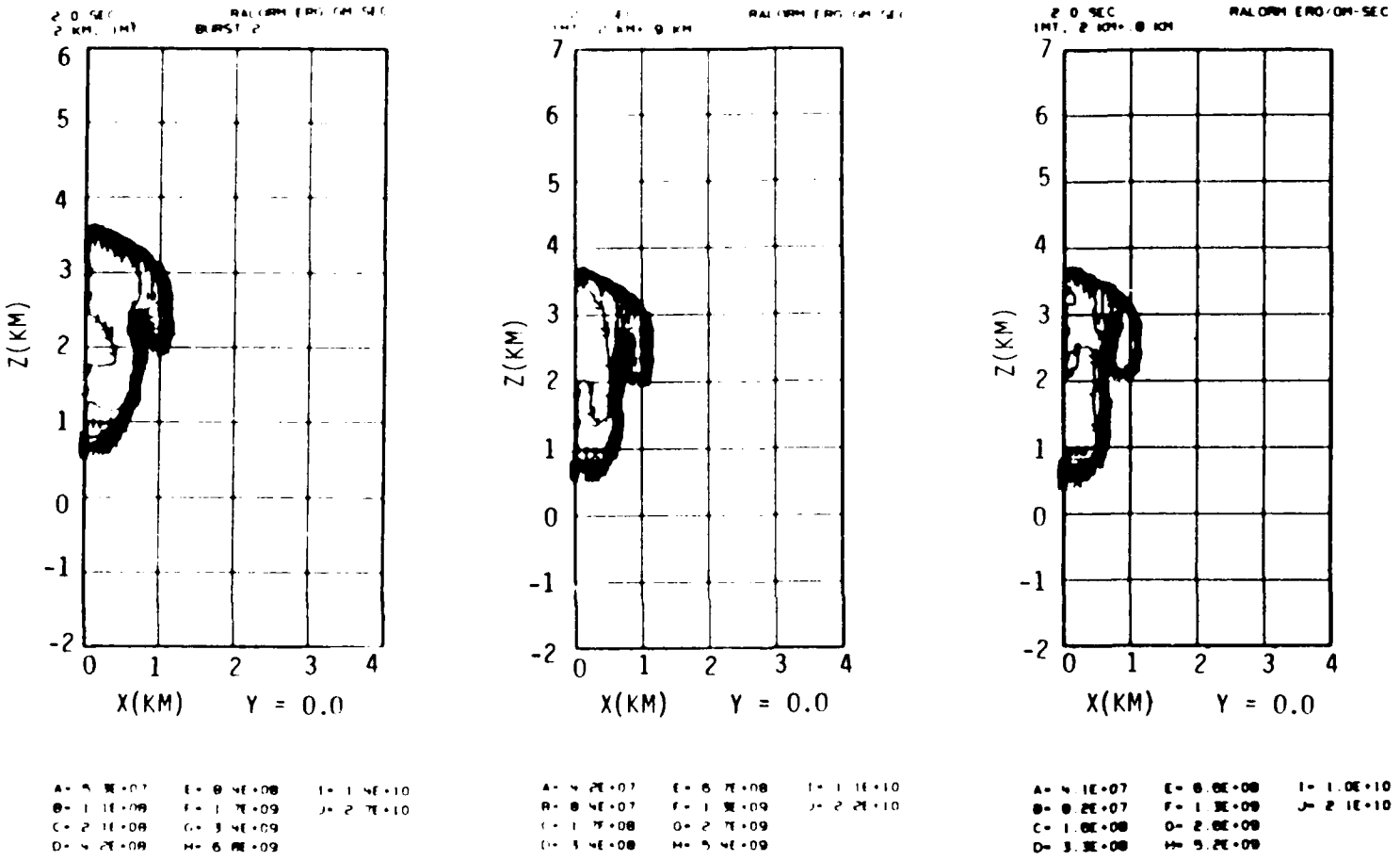

Figure 35. Distribution of cooling due to escaping radiation at 2.0 seconds for Δz = 1.0, 1.1, and 1.2 km from left to right.

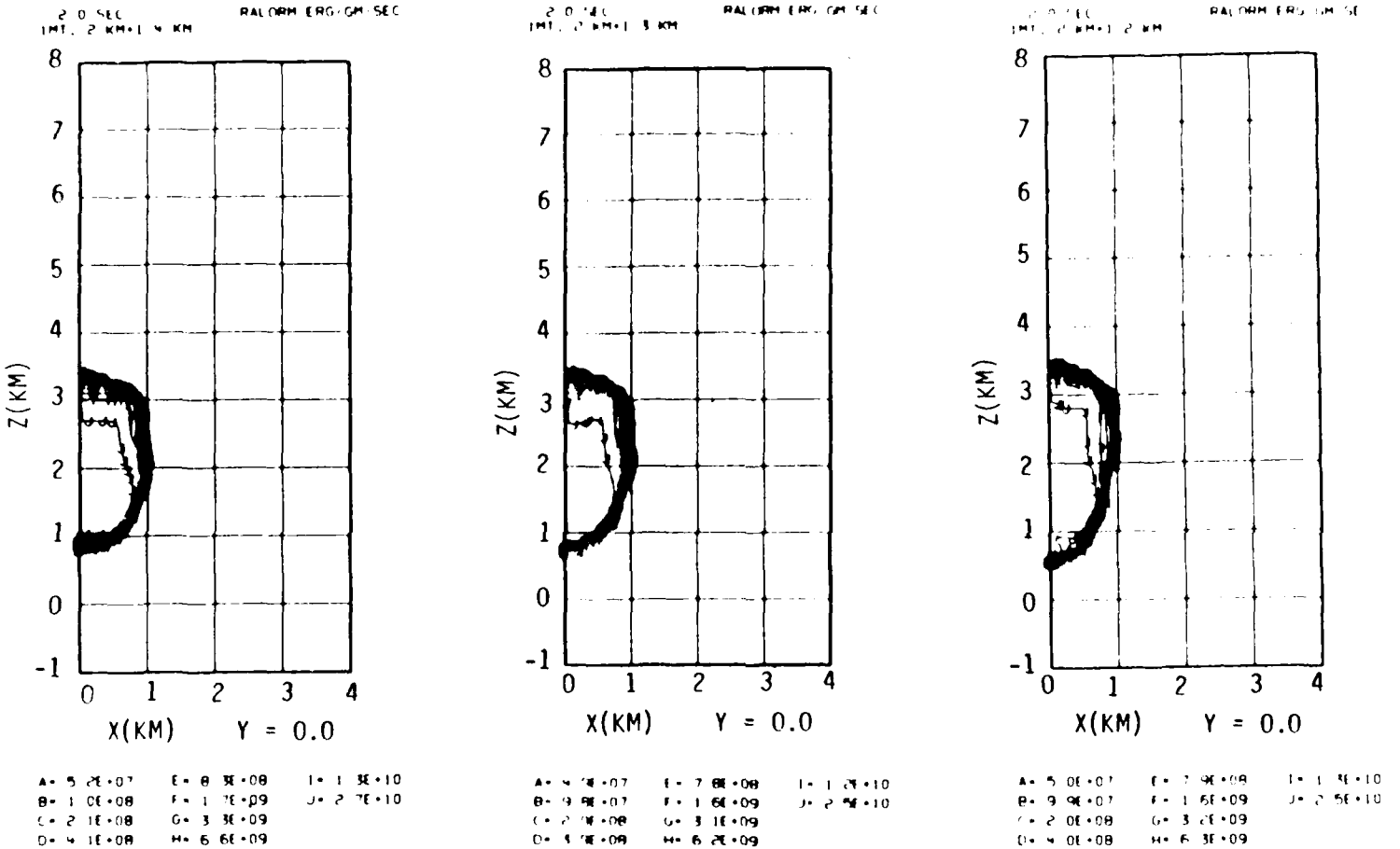

Figure 36. Distribution of cooling due to escaping radiation at 2.0 seconds for Δz = 0.6, 0.7, and 0.8 km from left to right.

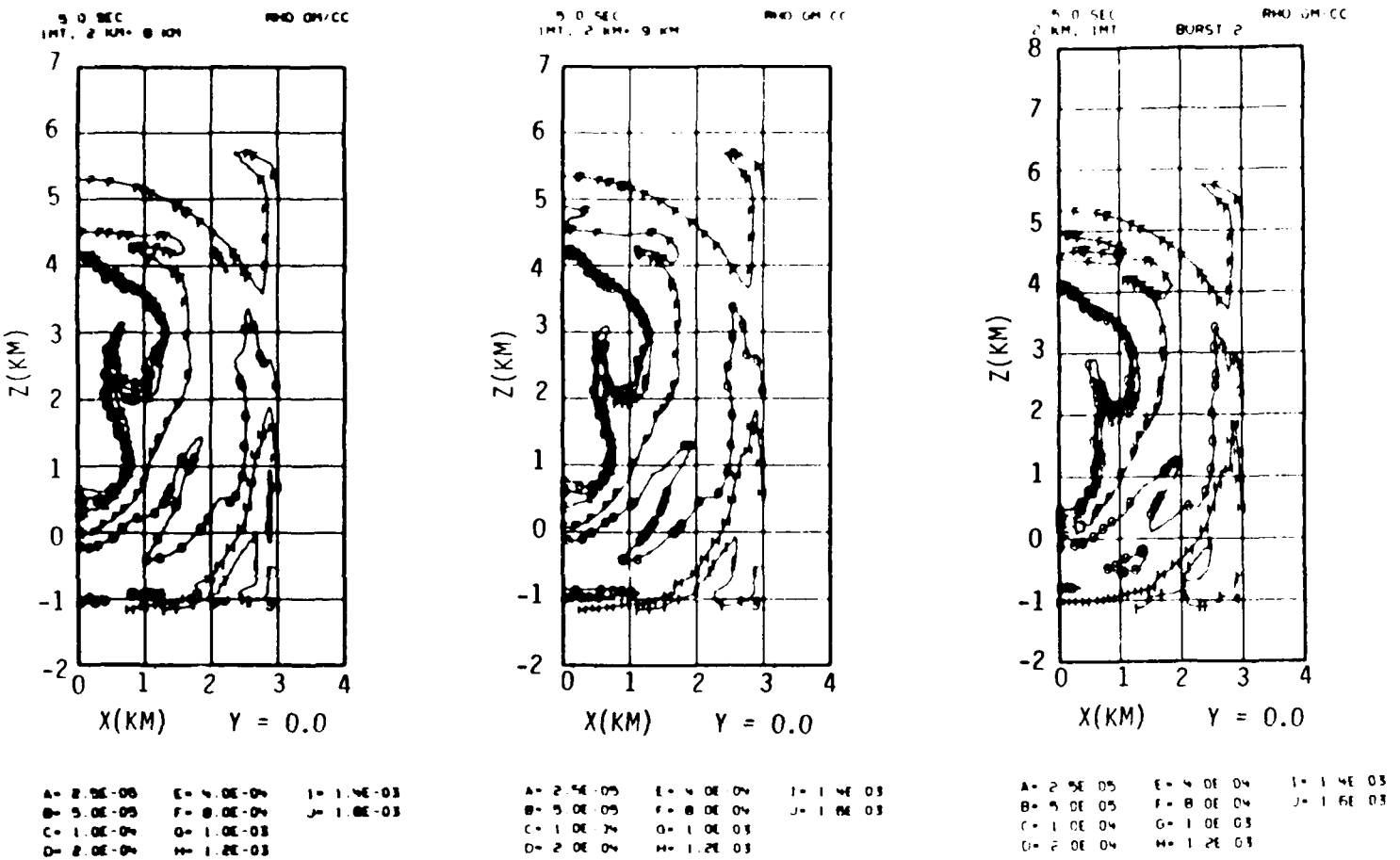

Figure 37. Distribution of density at 5.0 seconds for Δz = 1.2, 1.1, and 1.0 km from left to right.

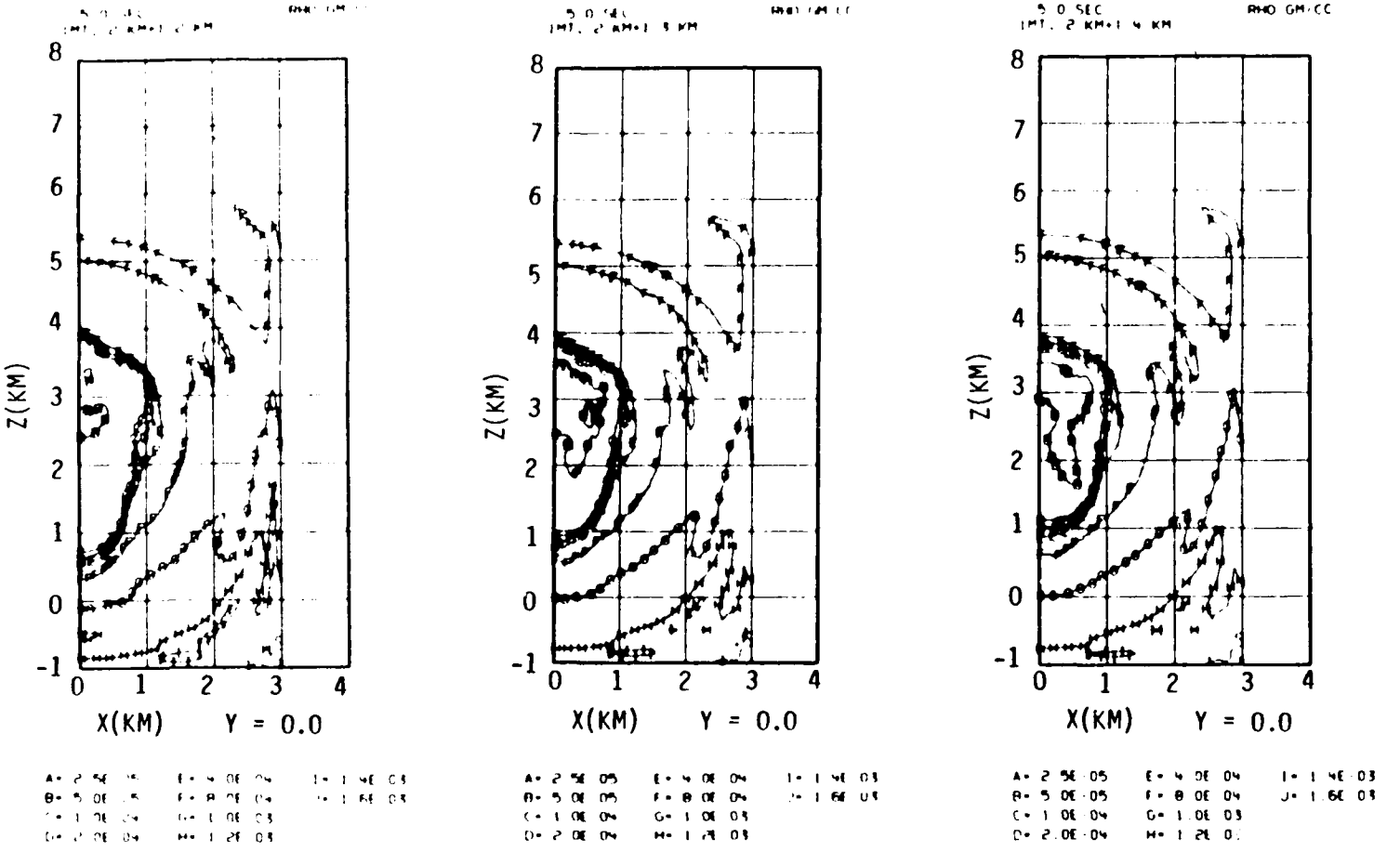

Figure 38. Distribution of density at 5.0 seconds for Δz = 0.8, 0.7, and 0.6 km from left to right.

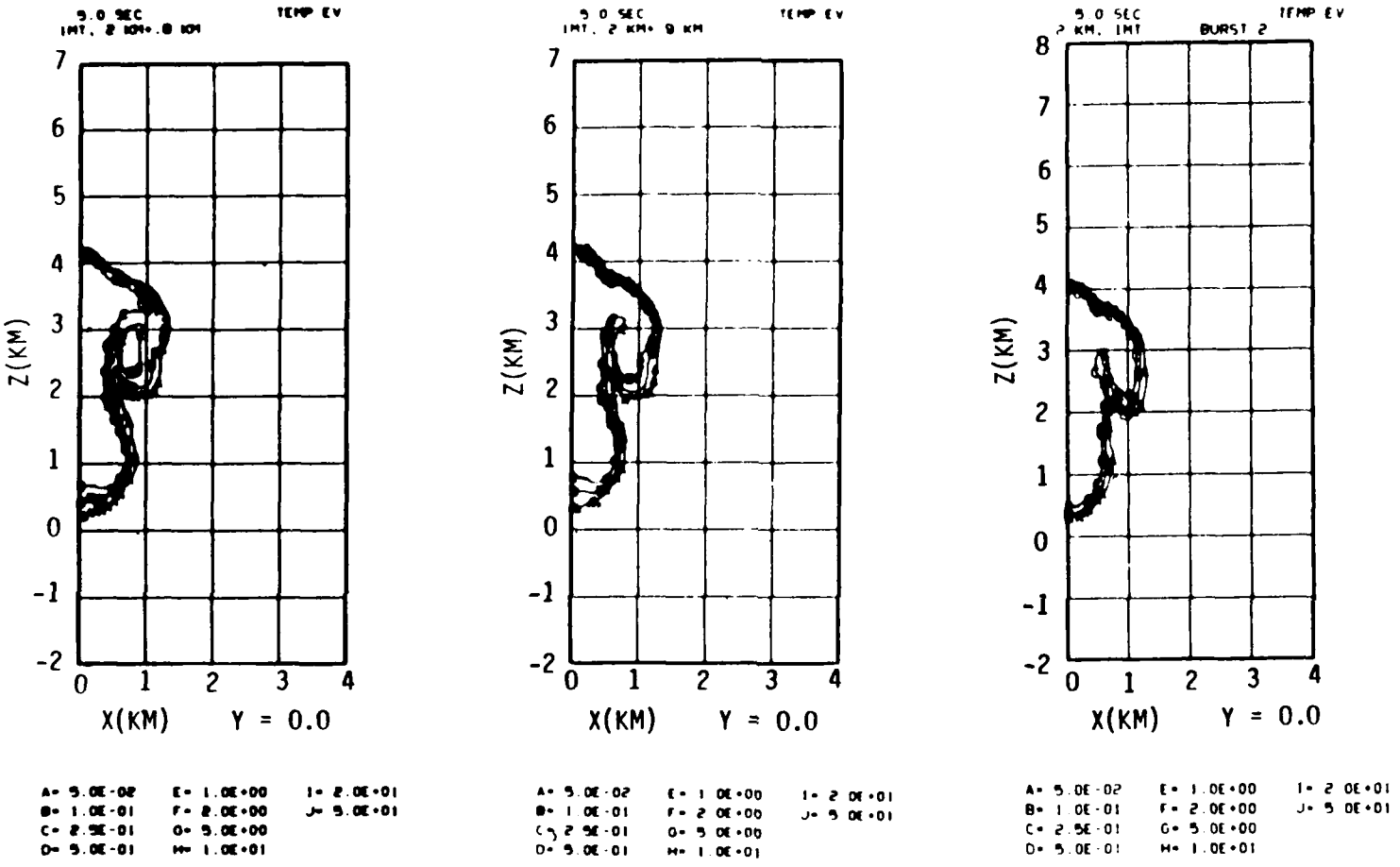

Figure 39. Distribution of temperature at 5.0 seconds for Δz = 1.2, 1.1, and 1.0 km from left to right.

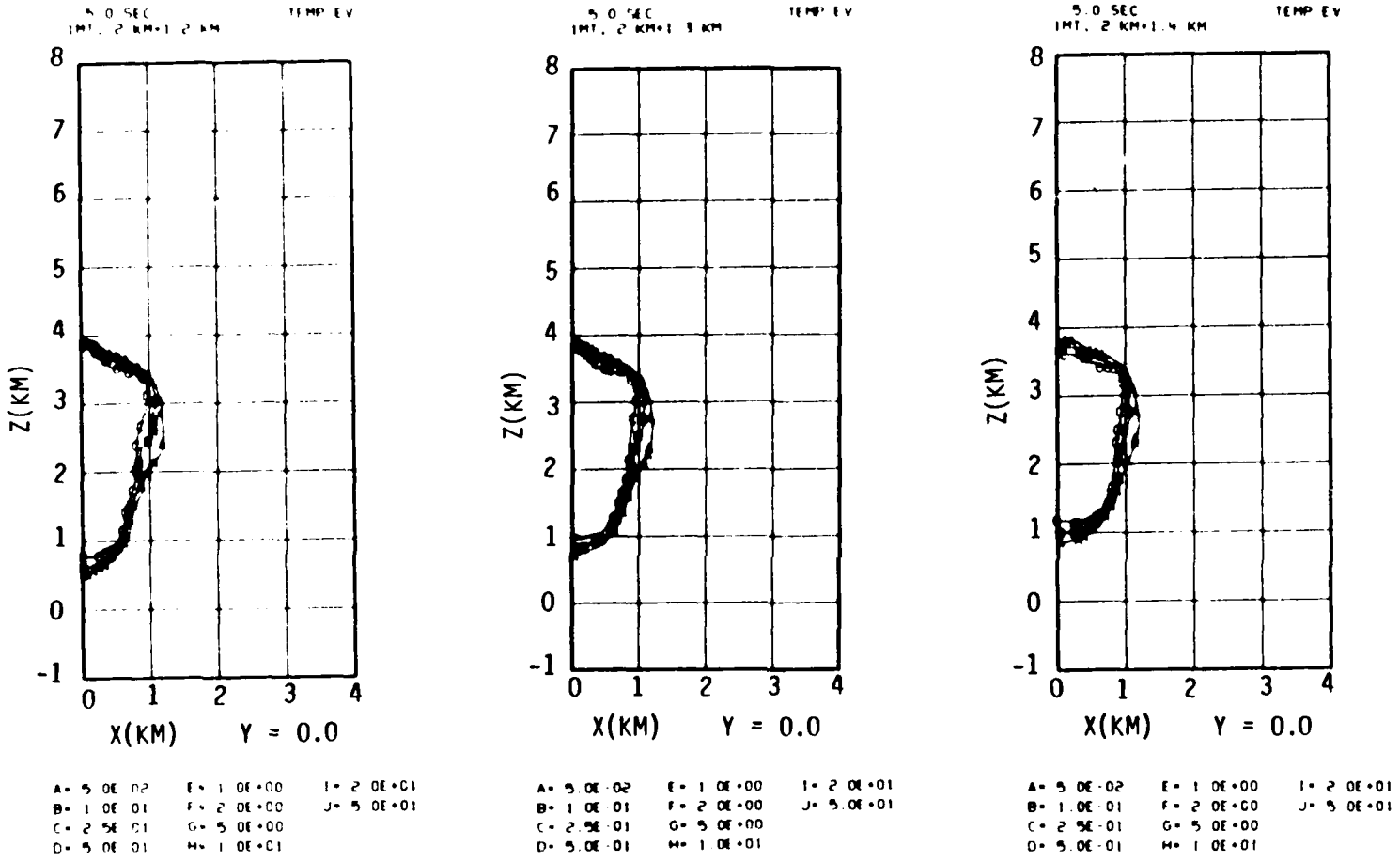

Figure 40. Distribution of temperature at 5.0 seconds for Δz = 0.8, 0.7, and 0.6 km from left to right.

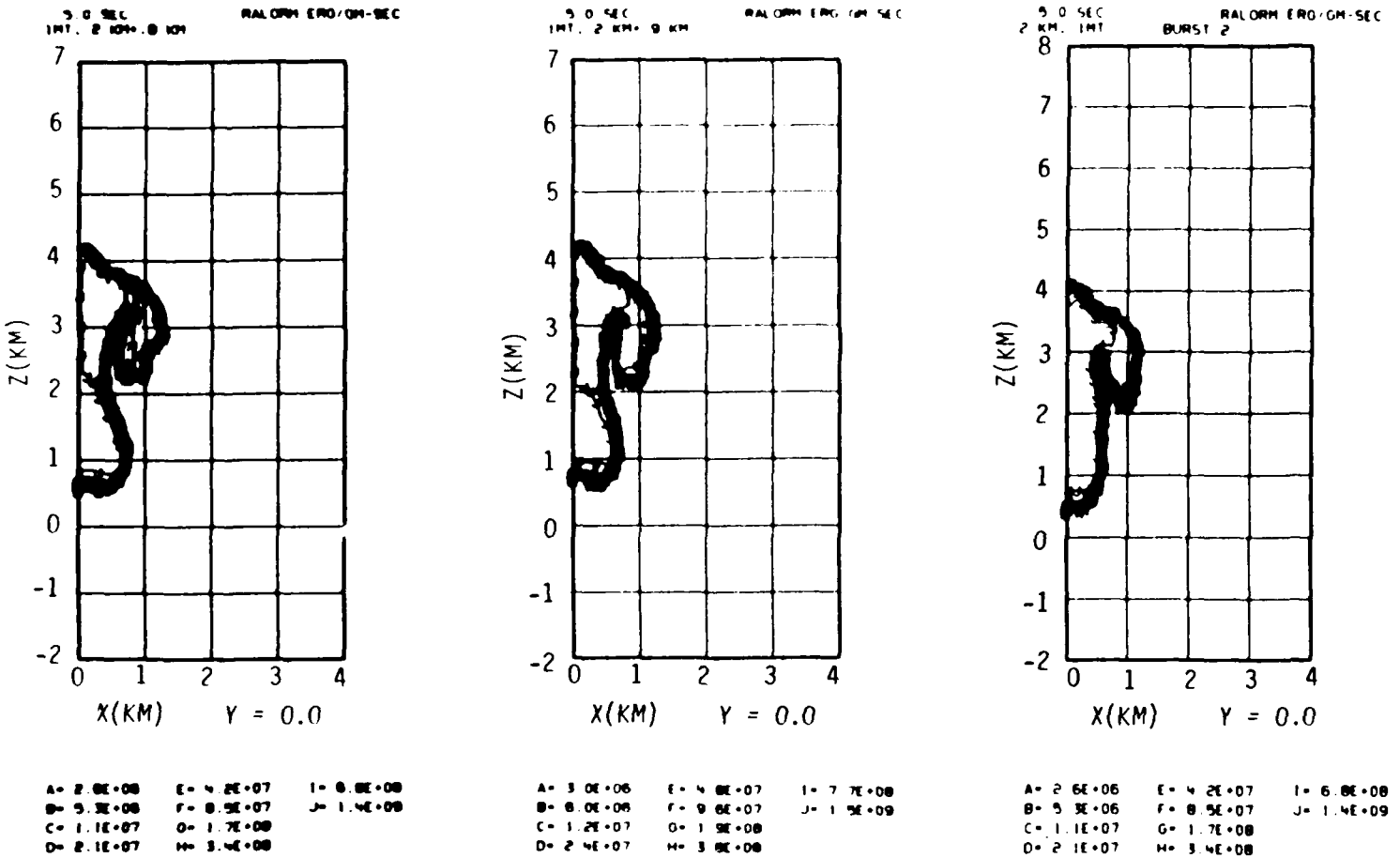

Figure 41. Distribution of cooling due to escaping radiation at 5.0 seconds for Δz = 1.2, 1.1, and 1.0 km from left to right.

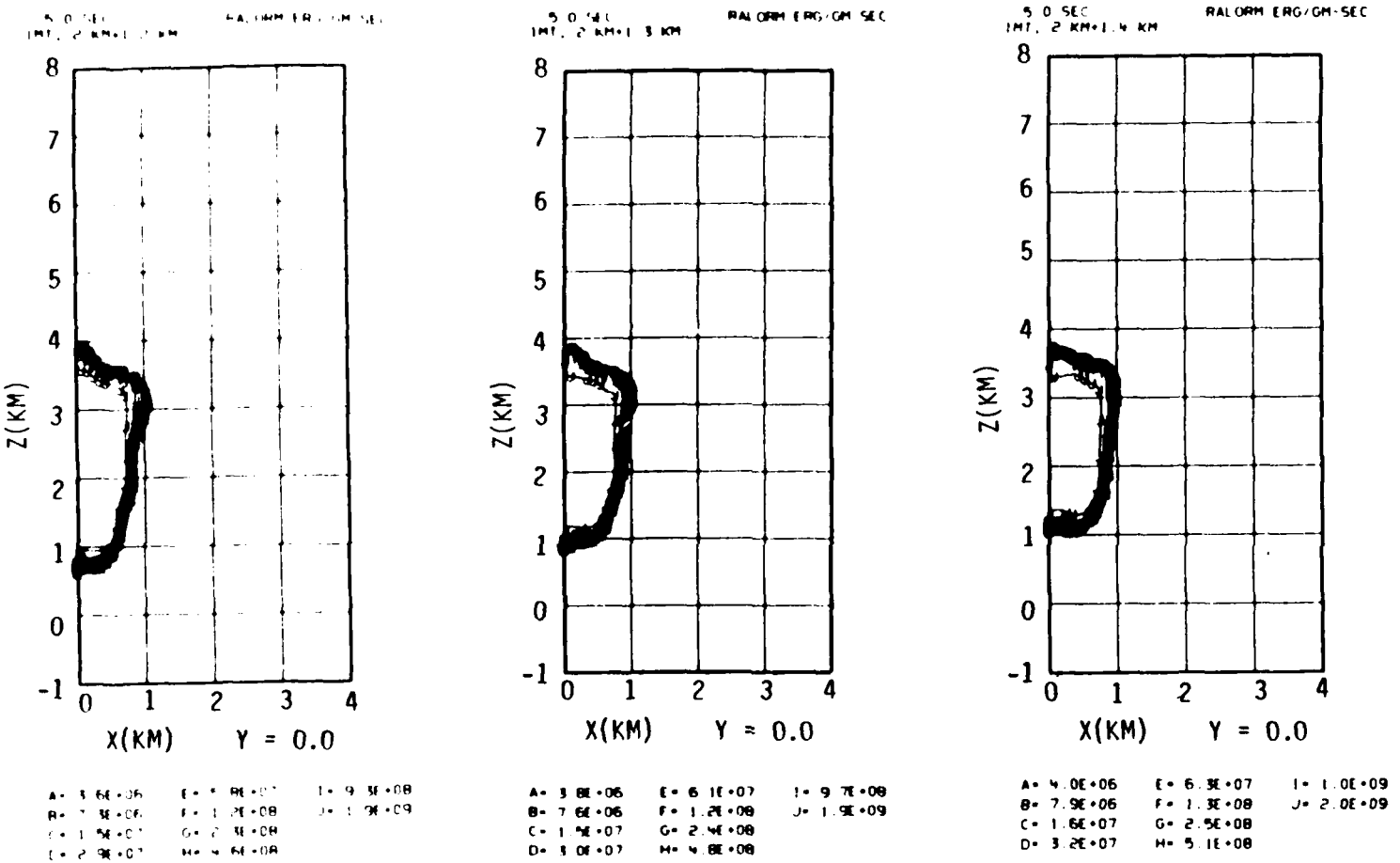

Figure 42. Distributions of cooling due to escaping radiation at 5.0 seconds for Δz = 0.8, 0.7, and 0.6 km from left to right.

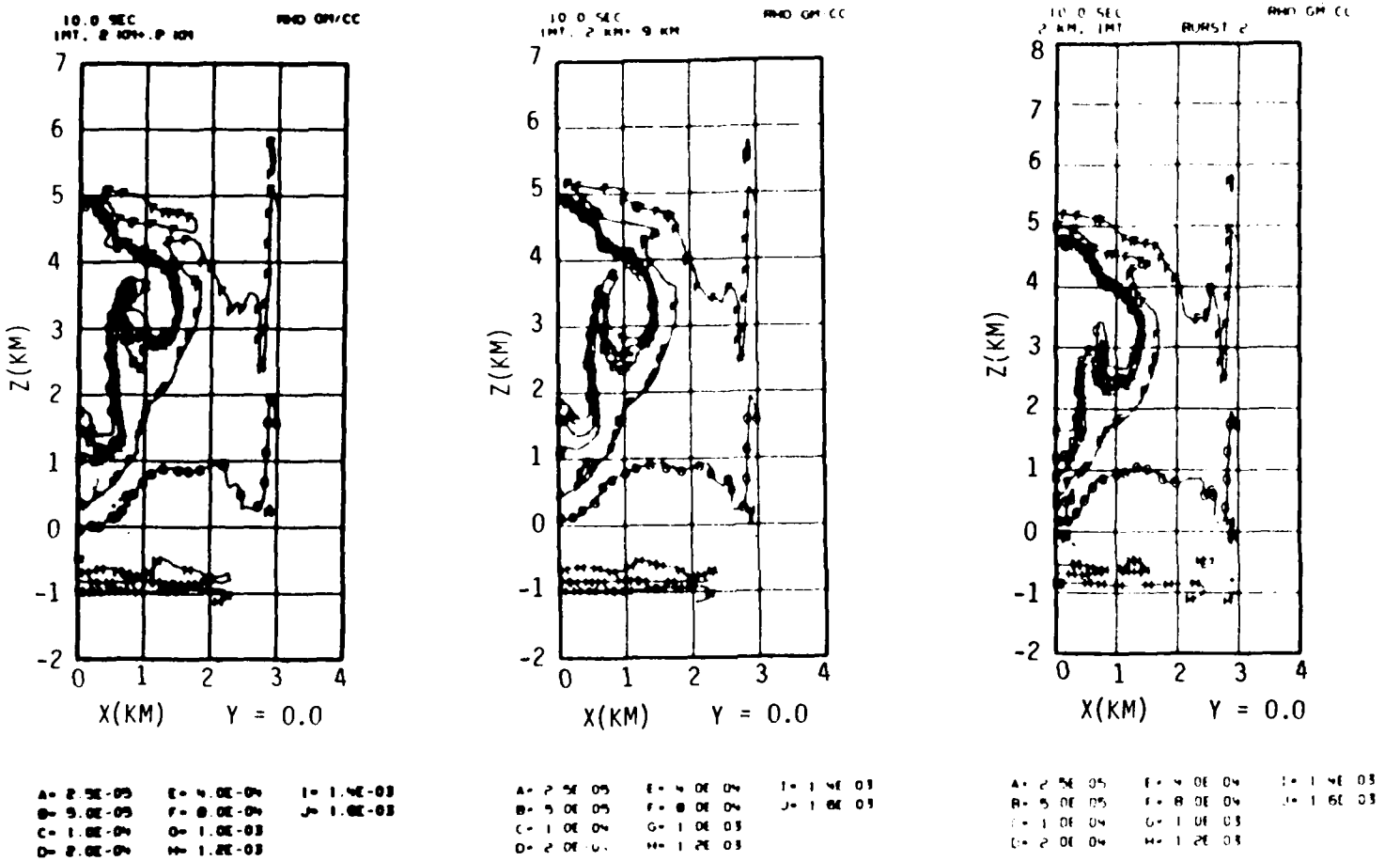

Figure 43. Distribution of density at 10.0 seconds for Δz = 1.2, 1.1, and 1.0 km from left to right.

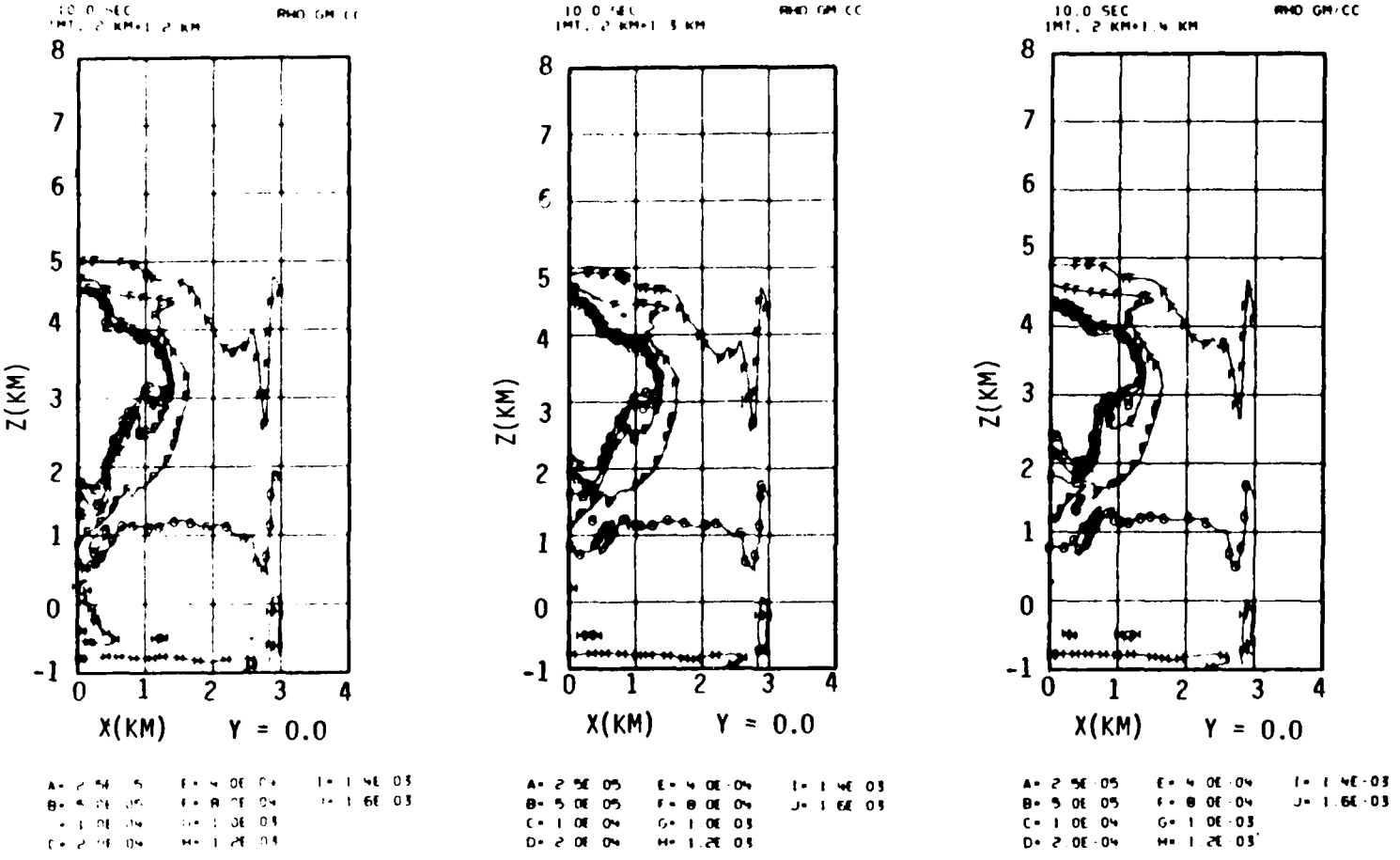

Figure 44. Distribution of density at 10.0 seconds for Δz = 0.8, 0.7, and 0.6 km from left to right.

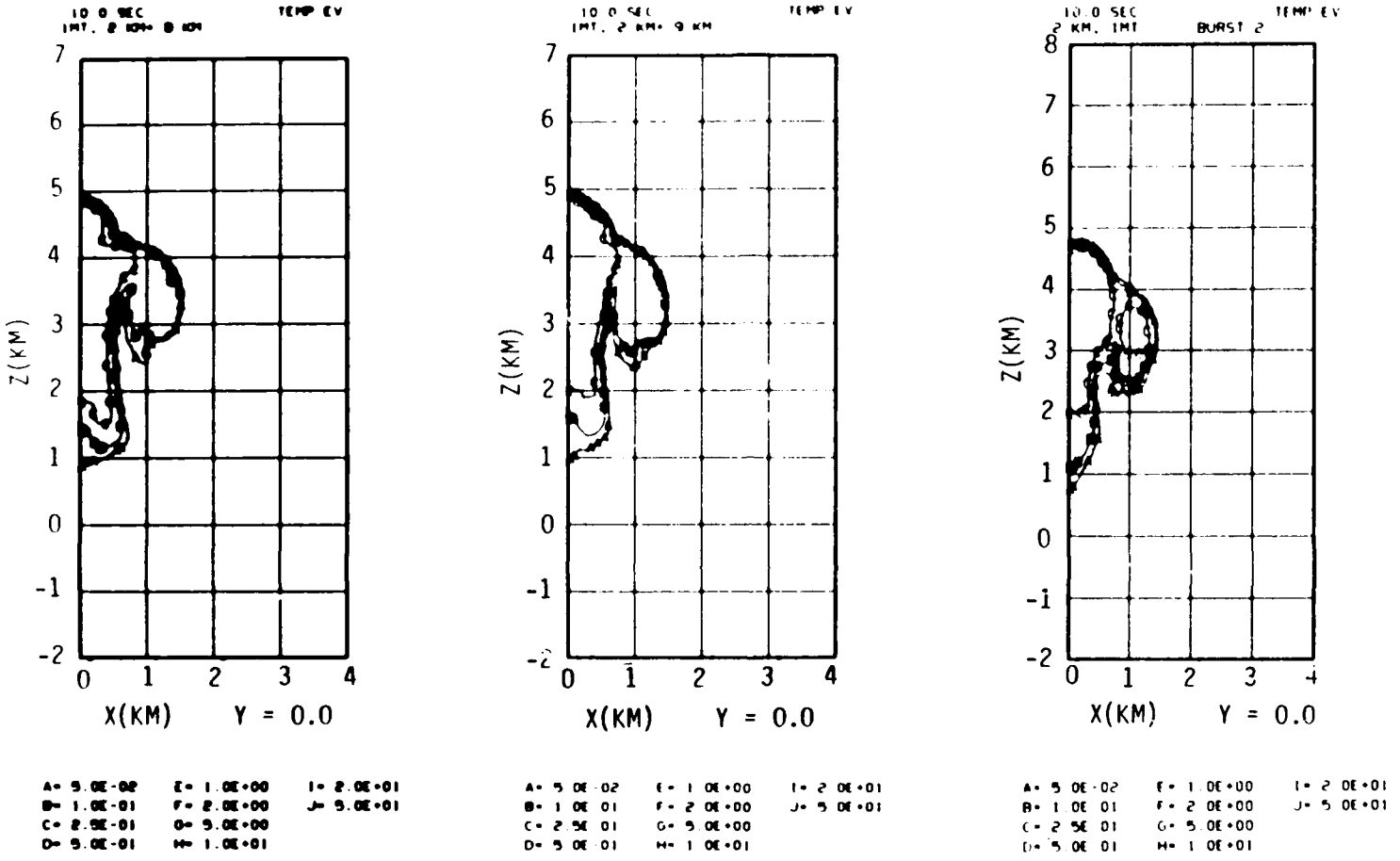

Figure 45. Distribution of temperature at 10.0 seconds for Δz = 1.2, 1.1, and 1.0 km from left to right.

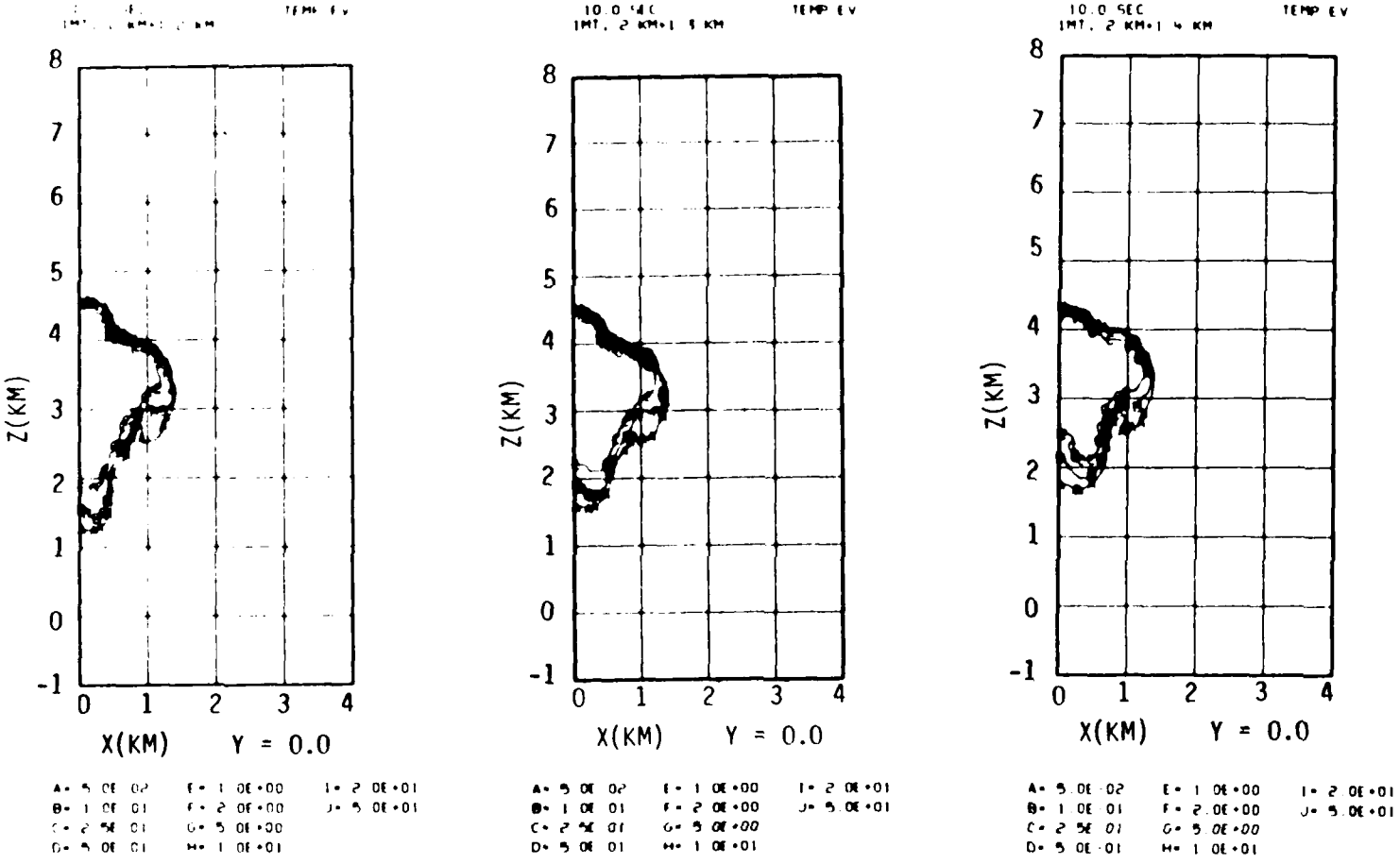

Figure 46. Distribution of temperature at 10.0 seconds for Δz = 0.8, 0.7, and 0.6 km from left to right.

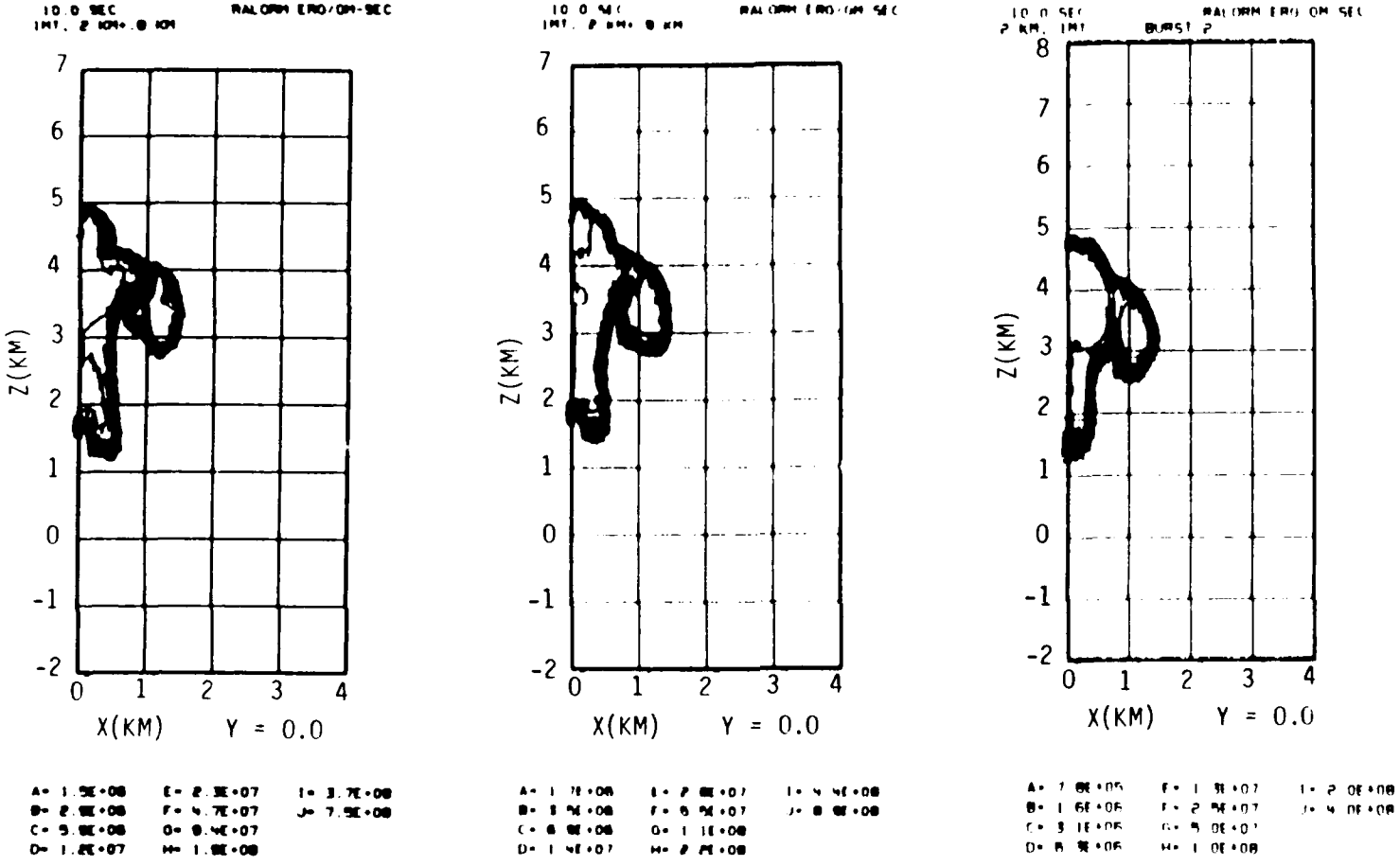

Figure 47. Distribution of cooling due to escaping radiation at 10.0 seconds for Δz = 1.2, 1.1, and 1.0 km from left to right.

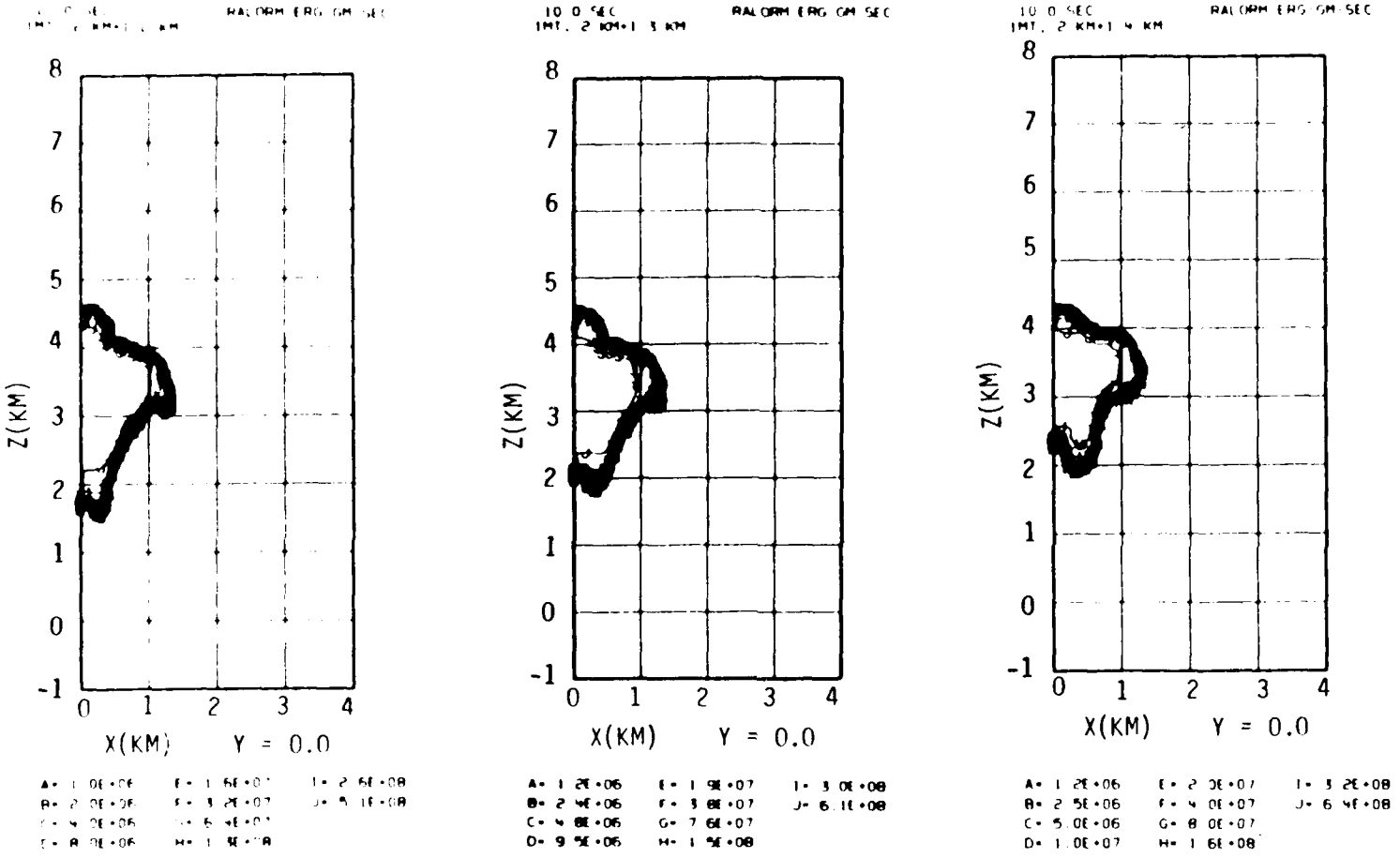

Figure 48. Distribution of cooling due to escaping radiation at 10.0 seconds for Δz = 0.8, 0.7, and 0.6 km from left to right.

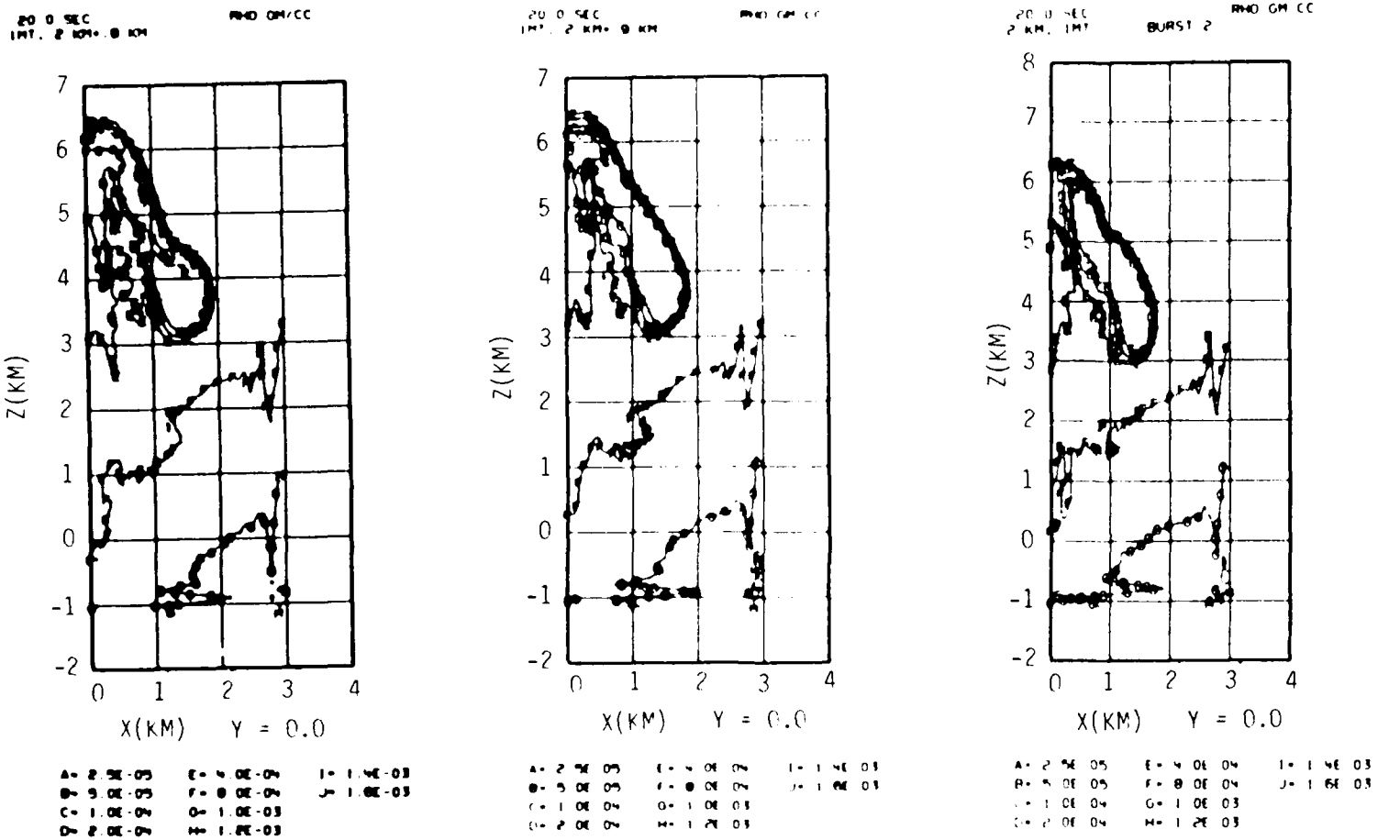

Figure 49. Distribution of density at 20.0 seconds for Δz = 1.2, 1.1, and 1.0 seconds from left to right.

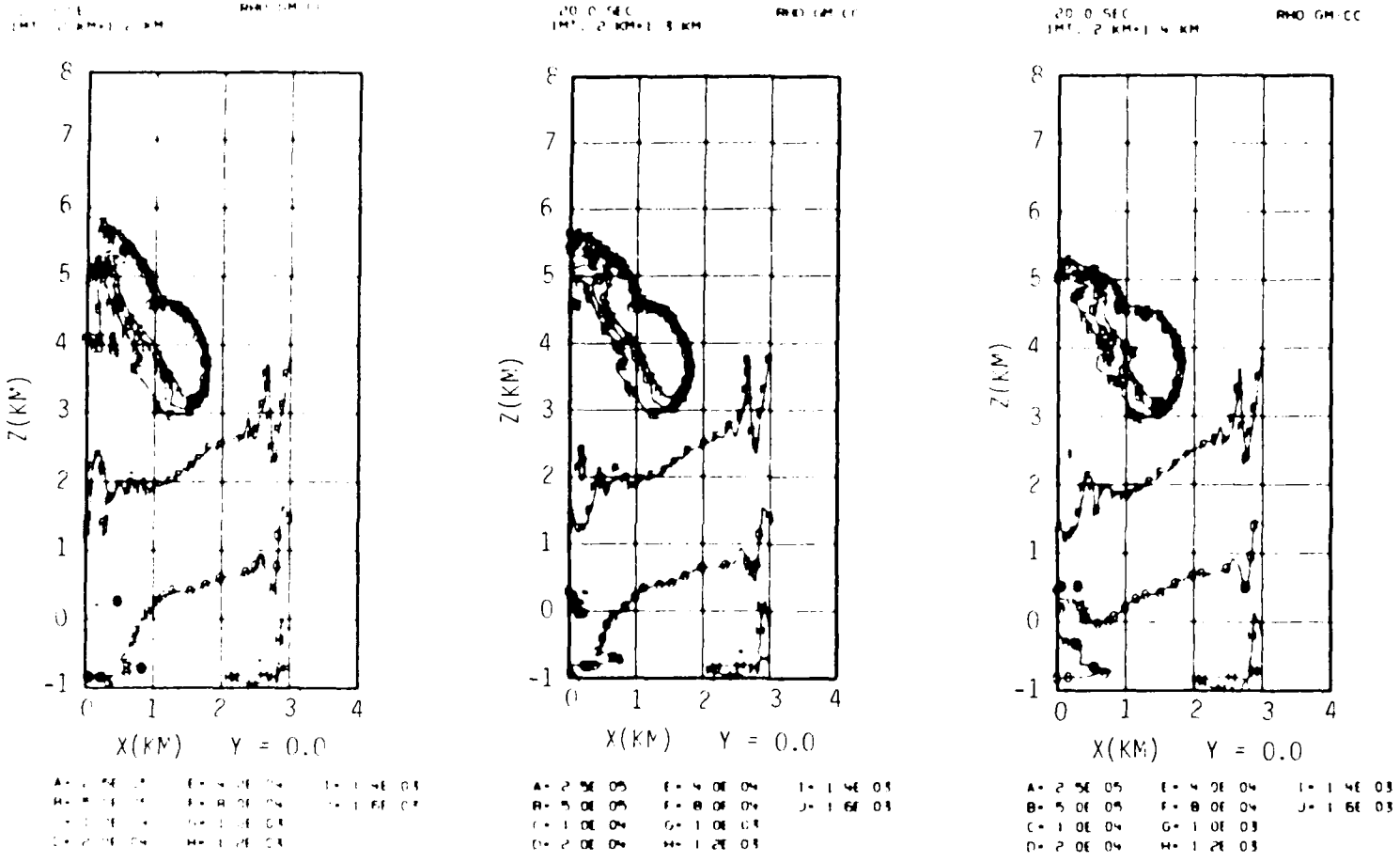

Figure 50. Distribution of density at 20.0 seconds for Δz = 0.8, 0.7, and 0.6 km from left to right.

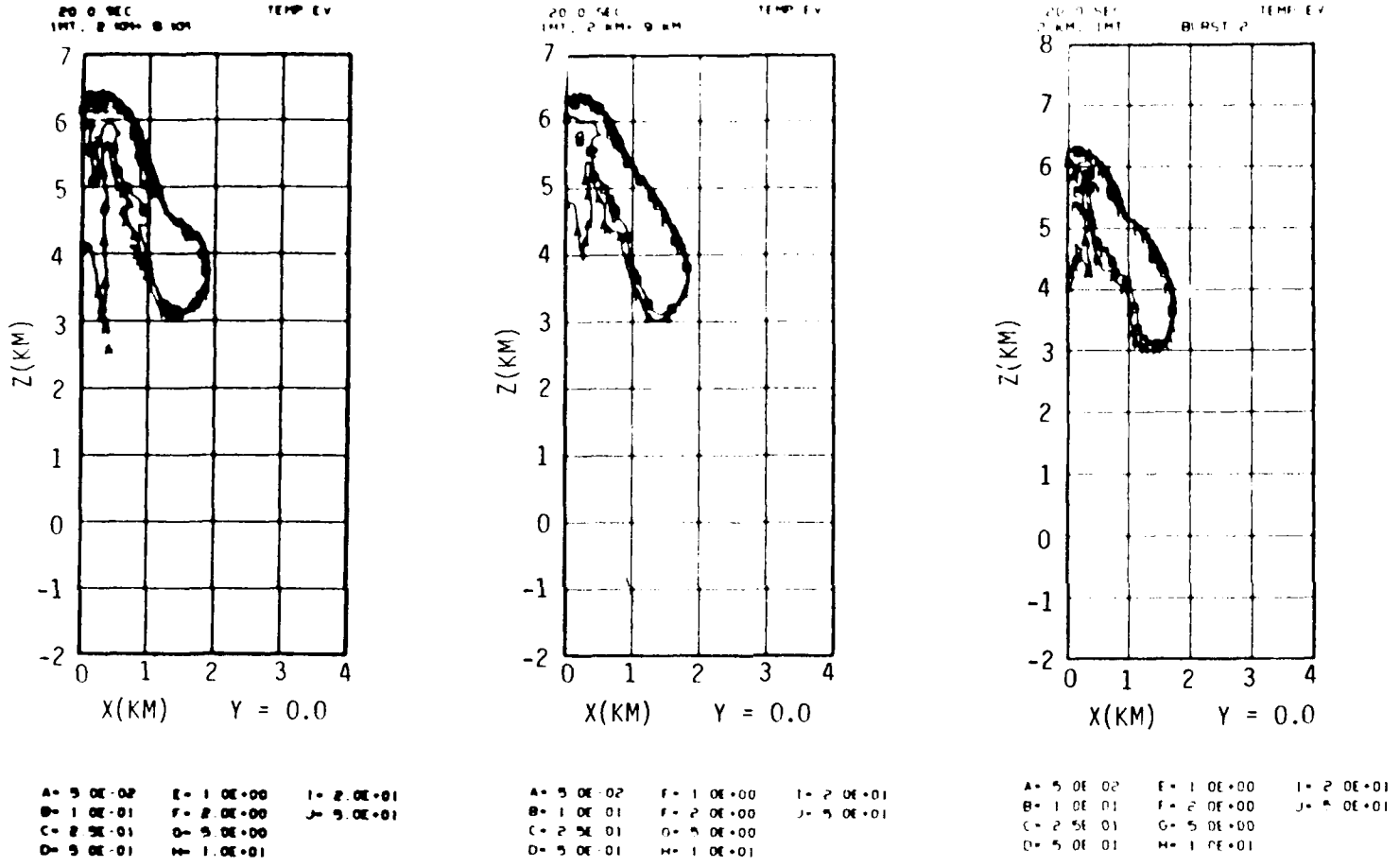

Figure 51. Distribution of temperature at 20.0 seconds for Δz = 1.2, 1.1, and 1.0 km from left to right.

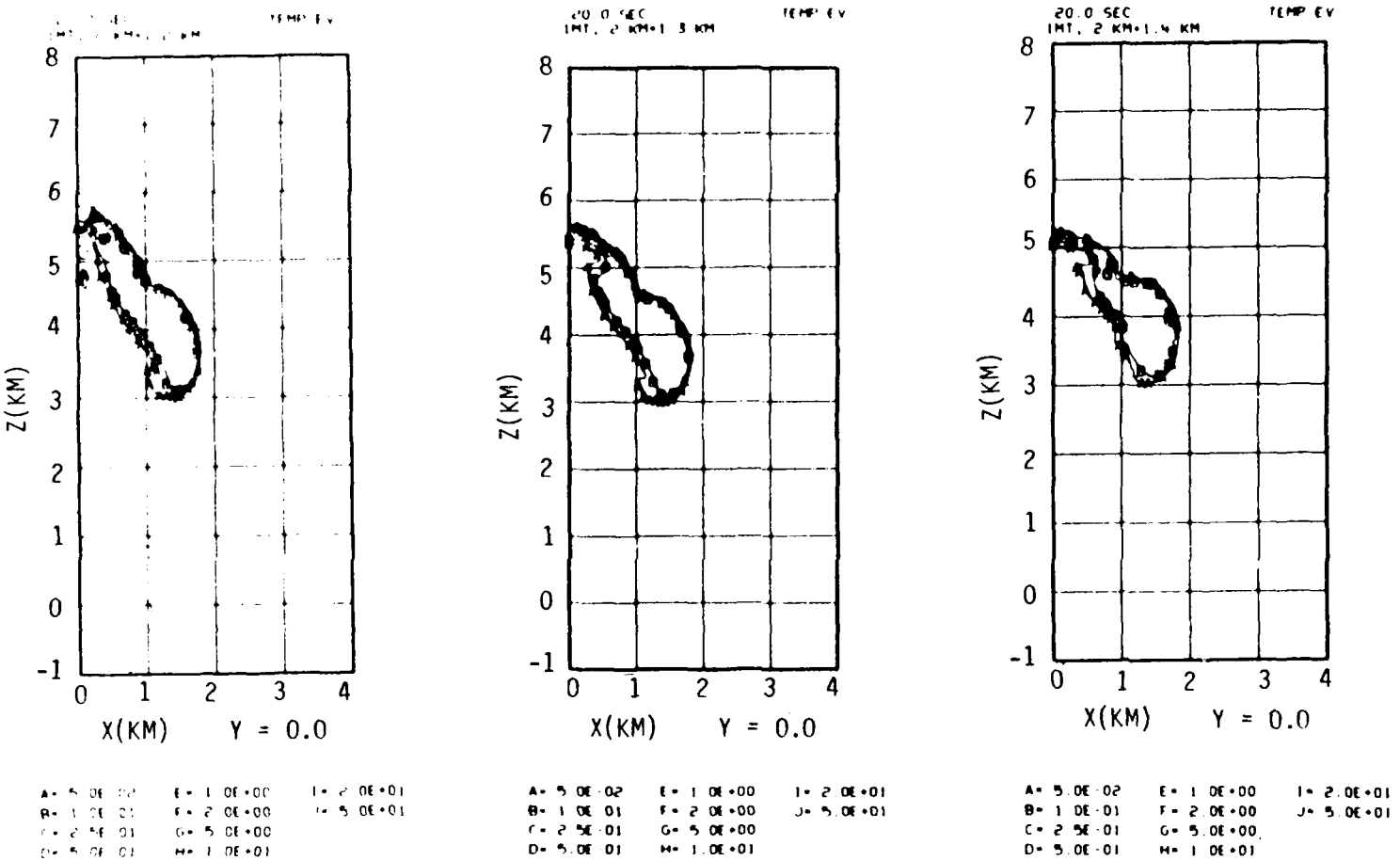

Figure 52. Distribution of temperature at 20.0 seconds for Δz = 0.8, 0.7, and 0.6 km from left to right.

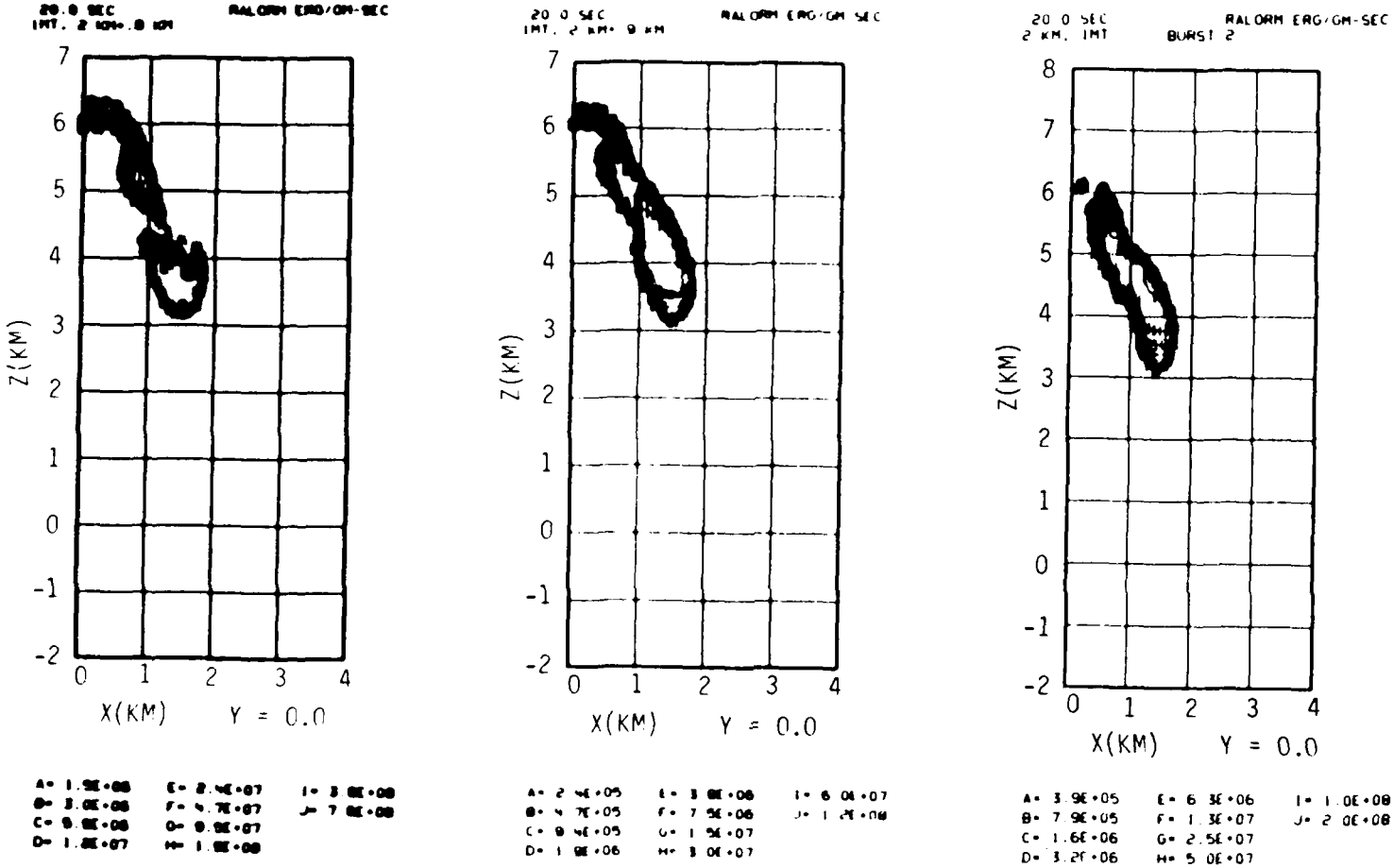

Figure 53. Distribution of cooling due to escaping radiation at 20.0 seconds for Δz = 1.2, 1.1, and 1.0 km from left to right.

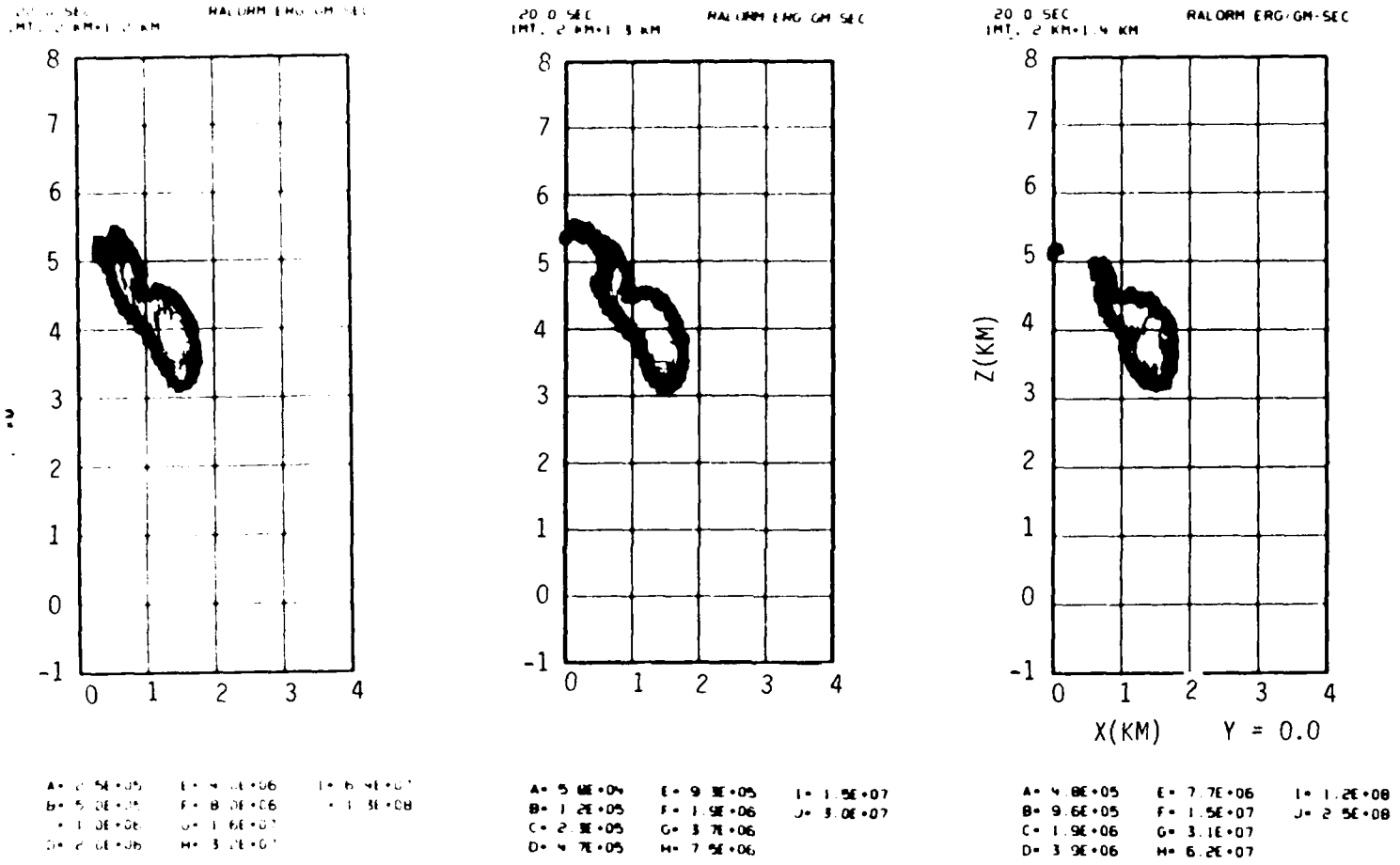

Figure 54. Distribution of cooling due to escaping radiation at 20 seconds for Δz = 0.8, 0.7, and 0.6 km from left to right.

REFERENCES

1. Cosner, K., "Mice Multiburst Calculations (U)," Unpublished.

2. Cosner, K., "Calculations of Multiple Concentric Bursts Near the Ground," MRC-R-758, May 1983 (U).

3. Jones, E. M., R. W. Whitaker, and J. W. Kodis, "Concentric Nuclear Explosions," LA-9688-MS, February 1983 (U).

4. Christian, R. H., R. E. Stoeckly, and W. A. Schlueter, "Two-Dimensional Dual Burst Results (U)," Unpublished.

DISTRIBUTION LIST

DEPARTMENT OF DEFENSE

Assistant to the Secy of Defense
Atomic Energy
ATTN: Executive Assistant

Defense Advanced Rsch Proj Agency
ATTN: GSD, R. Alewene
ATTN: STO, W. Kurowski

Defense Communications Agency
ATTN: Code 205
ATTN: Code 230
ATTN: J300 for Yen-Sun Fu

Defense Communications Engineer Center
ATTN: Code R410
ATTN: Code R123, Tech Lib
ATTN: Code R410, N. Jones

Defense Intelligence Agency
ATTN: DB, A. Wise
ATTN: DB-4C
ATTN: DT-1B
ATTN: Dir
ATTN: DC-7B

Defense Nuclear Agency
ATTN: RAAE, P. Lunn
ATTN: NATD
ATTN: STNA
ATTN: RAEE
ATTN: NAFD
ATTN: K. Schwartz
3 cys ATTN: RAAE
4 cys ATTN: STTI/CA

Defense Tech Info Center
12 cys ATTN: DD

Dep Under Secy of Defense
Comm, Cmd, Cont & Intell
ATTN: Dir of Intelligence Sys

Field Command
DNA, Det 1
Lawrence Livermore National Lab
ATTN: FC-1

Field Command
Defense Nuclear Agency
ATTN: FCTT, W. Summa
ATTN: FCTXE
ATTN: FCPR

Interservice Nuclear Weapons School
ATTN: TTV

Joint Chiefs of Staff
ATTN: C3S
ATTN: C3S, Evaluation Office, HD00

Joint Data System Support Ctr
ATTN: G510, G. Jones
ATTN: C-312, R. Mason
ATTN: C-500
ATTN: G510, P. Bird

DEPARTMENT OF DEFENSE (Continued)

Joint Strat Tgt Planning Staff
ATTN: JLK, DNA Rep
ATTN: JLAA
ATTN: JPPFD
ATTN: JPSS
ATTN: JLKS
ATTN: JPTM

National Security Agency
ATTN: W-36, O. Bartlett
ATTN: B-3, F. Leonard

Under Secy of Def for Rsch & Engrg
ATTN: Strat & Theater Nuc for, B. Stephan
ATTN: Strat & Space Sys (OS)

WWMCCS System Engineering Org
ATTN: R. Crawford

DEPARTMENT OF THE ARMY

Army Logistics Management Ctr
ATTN: DLSIE

Assistant Ch of Staff for Automation & Comm
ATTN: DAMO-C4, F. Kenny

Atmospheric Sciences Laboratory
ATTN: DELAS-EO, F. Niles

BMD Advanced Technology Center
ATTN: ATC-R, D. Russ
ATTN: ATC-R, W. Dickinson
ATTN: ATC-T, M. Capps
ATTN: ATC-O, W. Davies

BMD Systems Command
ATTN: BMDSC-HLE, R. Webb
2 cys ATTN: BMDSC-HW

Dep Ch of Staff for Ops & Plans
ATTN: DAMO-RQC, C2 Div

Harry Diamond Laboratories
ATTN: DELHD-NW-R, R. Williams
ATTN: Chief, Div 20000

US Army Chemical School
ATTN: ATZN-CM-CS

US Army Comm-Elec Engrg Instal Agency
ATTN: CC-CE-TP, W. Nair

US Army Communications Command
ATTN: CC-OPS-W
ATTN: CC-OPS-WR, H. Wilson

US Army Communications R&D Command
ATTN: DRDCO-COM-RY, W. Kesselman

US Army Foreign Science & Tech Ctr
ATTN: DRXST-SD

US Army Materiel Dev & Readiness Cmd
ATTN: DRCLDC, J. Bender

DEPARTMENT OF THE ARMY (Continued)

US Army Nuclear & Chemical Agency
ATTN: Library

US Army Satellite Comm Agency
ATTN: Doc Control

US Army TRADOC Sys Analysis Actvy
ATTN: ATAA-PL
ATTN: ATAA-TDC
ATTN: ATAA-TCC, F. Payan, Jr

US Army White Sands Missile Range
ATTN: STEWS-TN-N, K. Cummings

USA Missile Command
ATTN: DRSMI-YSO, J. Gamble

DEPARTMENT OF THE NAVY

Joint Cruise Missiles Proj Ofc
ATTN: JCMG-707

Naval Air Systems Command
ATTN: PMA 271

Naval Electronic Systems Command
ATTN: PME 106-4, S. Kearney
ATTN: PME 117-211, B. Kruger
ATTN: PME-106, F. Diederich
ATTN: PME-117-2013, G. Burnhart
ATTN: PME 117-20
ATTN: Code 501A
ATTN: Code 3101, T. Hughes

Naval Intelligence Support Ctr
ATTN: NISC-50

Naval Ocean Systems Center
ATTN: Code 532
ATTN: Code 5322, M. Paulson
ATTN: Code 5323, J. Ferguson

Naval Research Laboratory
ATTN: Code 4720, J. Davis
ATTN: Code 4700, S. Ossakow
ATTN: Code 4108, E. Szuszewicz
ATTN: Code 7500, B. Wald
ATTN: Code 6700
ATTN: Code 4700
ATTN: Code 4780
ATTN: Code 7950, J. Goodman
ATTN: Code 4187

Naval Space Surveillance System
ATTN: J. Burton

Naval Surface Weapons Center
ATTN: Code F31

Naval Telecommunications Command
ATTN: Code 341

Ofc of the Dep Ch of Naval Ops
ATTN: NOP 941D
ATTN: NOP 981N
ATTN: NOP 654, Strat Eval & Anal Br

Theater Nuclear Warfare Prj Ofc
ATTN: PM-23, D. Smith

DEPARTMENT OF THE NAVY (Continued)

Office of Naval Research
ATTN: Code 414, G. Joiner
ATTN: Code 412, W. Condell

Strategic Systems Project Office
ATTN: NSP-43, Tech Lib
ATTN: NSP-2141
ATTN: NSP-2722

DEPARTMENT OF THE AIR FORCE

Air Force Geophysics Laboratory
ATTN: LYD, K. Champion
ATTN: OPR-1
ATTN: R. Babcock
ATTN: CA, A. Stair
ATTN: OPR, H. Gardiner
ATTN: PHY, J. Buchau
ATTN: R. O'Neil

Air Force Satellite Ctrl Facility
ATTN: WE

Air Force Space Technology Ctr
ATTN: YH

Air Force Technical Applications Ctr
ATTN: TN

Air Force Weapons Laboratory
ATTN: SUL
ATTN: NTN

Air Force Wright Aeronautical Lab/AAAD
ATTN: W. Hunt
ATTN: A. Johnson

Air Logistics Command
ATTN: OO-ALC/MM

Air University Library
ATTN: AUL-LSE

Assistant Ch of Staff, Studies & Analysis
ATTN: AF/SASC, C. Rightmeyer

Ballistic Missile Office/DAA
ATTN: SYC, D. Kwan
ATTN: ENSN
ATTN: ENSN, W. Wilson

Dep Ch of Staff, Rsch, Dev & Acq
ATTN: AFRDQI
ATTN: AFRDS, Space Sys & C3 Dir

Dep Ch of Staff, Plans & Ops
ATTN: AFXOKCD
ATTN: AFXOKT
ATTN: AFXOKS

Electronic Systems Div
ATTN: ESD/SCTE, J. Clark
ATTN: SCS-2, G. Vinkels
ATTN: SCS-1E

Rome Air Development Center
ATTN: OCS, V. Coyne
ATTN: OCSA, R. Schneible
ATTN: TSLD

DEPARTMENT OF THE AIR FORCE (Continued)

Foreign Technology Division
ATTN: TQTD, B. Ballard
ATTN: NIIS, Library

Rome Air Development Center
ATTN: EEP, J. Rasmussen
ATTN: EEPS, P. Kossey

Space Command
ATTN: DC, T. Long

Strategic Air Command
ATTN: ADWA
ATTN: DCX
ATTN: XPQ
ATTN: XPFC
ATTN: DCZ
ATTN: NRI/STINFO Library
ATTN: XPFS

DEPARTMENT OF ENERGY

Department of Energy
GTN
ATTN: DP-233

NATO

NATO School, SHAPE
ATTN: US Documents Officer

OTHER GOVERNMENT AGENCIES

Bureau of Politico Military Affairs
ATTN: PM/STM

Central Intelligence Agency
ATTN: OSWR/NED
ATTN: OSWR/SSD for K. Feuerpfetl

National Bureau of Standards
ATTN: Sec Ofc for R. Moore

National Oceanic & Atmospheric Admin
ATTN: R. Grubb

Institute for Telecommunications Sciences
National Telecommunications & Info Admin
ATTN: A. Jean
ATTN: L. Berry
ATTN: W. Utlaut

DEPARTMENT OF ENERGY CONTRACTORS

EG&G, Inc
Attention Document Control for
ATTN: J. Colvin
ATTN: D. Wright

University of California
Lawrence Livermore National Lab
ATTN: L-31, R. Hager
ATTN: Tech Info Dept. Library

Sandia National Laboratories
ATTN: T. Cook
ATTN: B. Murphey
ATTN: A. Grossman

DEPARTMENT OF ENERGY CONTRACTORS (Continued)

Los Alamos National Laboratory
ATTN: T. Kunkle, ESS-5
ATTN: D. Simons
ATTN: MS 664, J. Zinn
ATTN: MS 670, J. Hopkins
ATTN: R. Jeffries
ATTN: J. Wolcott
ATTN: P. Keaton
ATTN: D. Sappenfield
ATTN: E. Jones

Sandia National Laboratories
ATTN: Org 1250, W. Brown
ATTN: Org 4231, T. Wright
ATTN: Space Project Div
ATTN: D. Thornbrough
ATTN: Tech Lib 3141
ATTN: D. Dahlgren
ATTN: R. Backstrom

DEPARTMENT OF DEFENSE CONTRACTORS

Aerospace Corp
ATTN: I. Garfunkel
ATTN: D. Olsen
ATTN: J. Kluck
ATTN: D. Whelan
ATTN: J. Straus
ATTN: R. Slaughter
ATTN: K. Cho
ATTN: V. Josephson
ATTN: T. Salmi

Aerospace Corp
ATTN: S. Mewaters

Analytical Systems Engineering Corp
ATTN: Radio Sciences

Analytical Systems Engineering Corp
ATTN: Security

BDM Corp
ATTN: L. Jacobs
ATTN: T. Neighbors

Berkely Rsch Associates, Inc
ATTN: S. Brecht
ATTN: J. Workman
ATTN: C. Prettie

Boeing Co
ATTN: G. Hall

Boeing Co
ATTN: MS 8K-85, Dr S. Tashird
ATTN: MS/87-63, D. Clauson

BR Communications
ATTN: J. McLaughlin

University of California
ATTN: H. Booker

Charles Stark Draper Lab, Inc
ATTN: A. Tetewski
ATTN: D. Cox
ATTN: J. Gilmore

DEPARTMENT OF DEFENSE CONTRACTORS (Continued)

Communications Satellite Corp
ATTN: D. Fang
ATTN: G. Hyde

Computer Sciences Corp
ATTN: F. Eisenbarth

Cornell University
ATTN: D. Farley, Jr
ATTN: M. Kelly

California Research & Technology
ATTN: M. Rosenblatt

E-Systems, Inc
ATTN: R. Berezdivin

Electrospace Systems, Inc
ATTN: P. Phillips
ATTN: H. Logston

EOS Technologies, Inc
ATTN: W. Lelevier
ATTN: B. Gabbard

General Electric Co
ATTN: R. Juner
ATTN: A. Steinmayer
ATTN: C. Zierdt

General Electric Co
ATTN: G. Millman

General Research Corp
ATTN: B. Bennett
ATTN: R. Rein
ATTN: R. Williams

GEO Centers, Inc
ATTN: E. Marram

GTE Communications Products Corp
ATTN: R. Steinhoff

GTE Communications Products Corp
ATTN: A. Murphy
ATTN: H. Gelman

Harris Corp
ATTN: E. Knick

Honeywell, Inc
ATTN: G. Terry, Avionics Dept
ATTN: A. Kearns, MS924-3

Horizons Technology, Inc
ATTN: R. Kruger

HSS, Inc
ATTN: D. Hansen

IBM Corp
ATTN: H. Ulander

Institute for Defense Analyses
ATTN: H. Gates
ATTN: J. Aein
ATTN: E. Bauer
ATTN: H. Wolfhard

DEPARTMENT OF DEFENSE CONTRACTORS (Continued)

ITT Corp
ATTN: Tech Library

ITT Corp
ATTN: G. Wetmore

JAYCOR
ATTN: J. Sperling

JAYCOR
ATTN: H. Dickinson

Johns Hopkins University
ATTN: C. Meng
ATTN: K. Potocki
ATTN: J. Phillips
ATTN: T. Evans
ATTN: J. Newland
ATTN: P. Komiske

Kaman Sciences Corp
ATTN: E. Conrad

Kaman Tempo
ATTN: B. Gambill
ATTN: DASIAC
ATTN: W. Schuleter
ATTN: W. McNamara

Kaman Tempo
ATTN: DASIAC

Litton Systems, Inc
ATTN: B. Zimmer

Lockheed Missiles & Space Co, Inc
ATTN: R. Sears
ATTN: J. Kumer

Lockheed Missiles & Space Co, Inc
ATTN: Dept 60-12
2 cys ATTN: D. Churchill

M. I. T. Lincoln Lab
ATTN: N. Doherty
ATTN: V. Vitto
ATTN: D. Towle

M/A Com Linkabit Inc
ATTN: A. Viterbi
ATTN: H. Van Trees
ATTN: I. Jacobs

Magnavox Govt & Indus Electronics Co
ATTN: G. White

Maxim Technologies, Inc
ATTN: E. Tsui
ATTN: J. Marshall
ATTN: R. Morganstern

McDonnell Douglas Corp
ATTN: Tech Library Services
ATTN: R. Halprin
ATTN: W. Olson

Meteor Communications Corp
ATTN: R. Leader

DEPARTMENT OF DEFENSE CONTRACTORS (Continued)

Mission Research Corp
ATTN: R. Bigoni
ATTN: G. McCartor
ATTN: F. Guigliano
ATTN: F. Fajen
ATTN: D. Knepp
ATTN: Tech Library
ATTN: R. Kilb
ATTN: R. Bogusch
ATTN: R. Hendrick
ATTN: C. Lauer
ATTN: S. Gutsche
ATTN: R. Dana
2 cys ATTN: K. Cosner
5 cys ATTN: Document Control

Mitre Corp
ATTN: G. Harding
ATTN: A. Kymmel
ATTN: MS J104, M. Dresp
ATTN: C. Callahan

Mitre Corp
ATTN: W. Hall
ATTN: J. Wheeler
ATTN: W. Foster
ATTN: M. Horrocks

Pacific-Sierra Research Corp
ATTN: F. Thomas
ATTN: H. Brode, Chairman SAGE
ATTN: E. Field, Jr

Pennsylvania State University
ATTN: Ionospheric Research Lab

Photometrics, Inc
ATTN: I. Kofsky

Physical Dynamics, Inc
ATTN: J. Secan
ATTN: E. Fremouw

Physical Research, Inc
ATTN: R. Deliberis
ATTN: J. Devore
ATTN: T. Stephens
ATTN: J. Thompson

R&D Associates
ATTN: R. Turco
ATTN: M. Gantsweg
ATTN: C. Greifinger
ATTN: F. Gilmore
ATTN: H. Ory
ATTN: G. Stcyr
ATTN: W. Karzas
ATTN: W. Wright
ATTN: P. Haas

R&D Associates
ATTN: B. Yoon

R&D Associates
ATTN: G. Ganong

DEPARTMENT OF DEFENSE CONTRACTORS (Continued)

Rand Corp
ATTN: E. Bedrozian
ATTN: P. Davis
ATTN: C. Crain

Rand Corp
ATTN: B. Bennett

Riverside Research Institute
ATTN: V. Trapani

Rockwell International Corp
ATTN: R. Buckner

Rockwell International Corp
ATTN: S. Quilici

Science Applications, Inc
ATTN: D. Sachs
ATTN: C. Smith
ATTN: D. Hamlin
ATTN: L. Linson
ATTN: E. Straker

Science Applications, Inc
ATTN: J. Cockayne

Science Applications, Inc
ATTN: M. Cross

SRI International
ATTN: A. Burns
ATTN: G. Price
ATTN: R. Tsunoda
ATTN: J. Vickrey
ATTN: V. Gonzales
ATTN: D. Neilson
ATTN: J. Petrickes
ATTN: M. Baron
ATTN: R. Livingston
ATTN: D. McDaniels
ATTN: W. Chesnut
ATTN: G. Smith
ATTN: C. Rino
ATTN: W. Jaye
ATTN: R. Leadabrand

Steward Radiance Laboratory
ATTN: J. Ulwick

Swerling, Manasse & Smith, Inc
ATTN: R. Manasse

Technology International Corp
ATTN: W. Boquist

Toyon Research Corp
ATTN: J. Ise
ATTN: J. Garbarino

TRW Electronics & Defense Sector
ATTN: R. Plebuch

DEPARTMENT OF DEFENSE CONTRACTORS (Continued)

Utah State University
Attention Sec Control Ofc for
ATTN: A. Steed
ATTN: D. Burt
ATTN: K. Baker, Dir Atmos & Space Sci
ATTN: L. Jensen, Elec Eng Dept

DEPARTMENT OF DEFENSE CONTRACTORS (Continued)

Visidyne, Inc
ATTN: J. Carpenter
ATTN: W. Reidy
ATTN: O. Shepard
ATTN: C. Humphrey
ATTN: H. Smith

END

FILMED

2-85

DTIC